(353 G)
Special Course (III)

3rd year Geophysics

By:

Dr. Mohammed Omran Khalifa

Dr. Ismail Sayed Ahmed

Dr. Ahmed Mohammed Abdel Gawad

2022/2023

Part 1:

Introduction to Earthquake Seismology

By:

Dr. Mohammed Omran Khalifa

INTRODUCTION TO EARTHQUAKES SEISMOLOGY

What Are Seismic Waves?

Seismic waves are the waves of energy caused by the sudden breaking of rock within the earth or an explosion. They are the energy that travels through the earth and is recorded on seismographs.

Types of Seismic Waves

There are several different kinds of seismic waves, and they all move in different ways. The two main types of waves are **body waves** and **surface waves**. Body waves can travel through the earth's inner layers, but surface waves can only move along the surface of the planet like ripples on water. Earthquakes radiate seismic energy as both body and surface waves.

BODY WAVES

Traveling through the interior of the earth, **body waves** arrive before the surface waves emitted by an earthquake. These waves are of a higher frequency than surface waves.

P WAVES

The first kind of body wave is the **P wave** or **primary wave**. This is the fastest kind of seismic wave, and, consequently, the first to 'arrive' at a seismic station. The P wave can move through solid rock and fluids, like water or the liquid layers of the earth. It pushes and pulls the rock it moves through just like sound

waves push and pull the air. Have you ever heard a big clap of thunder and heard the windows rattle at the same time? The windows rattle because the sound waves were pushing and pulling on the window glass much like P waves push and pull on rock.

Sometimes animals can hear the P waves of an earthquake. Dogs, for instance, commonly begin barking hysterically just before an earthquake 'hits' (or more specifically, before the surface waves arrive). Usuallypeople can only feel the bump and rattle of these waves.

P waves are also known as **compressional waves**, because of the pushing and pulling they do. Subjected to a P wave, particles move in the same direction that the the wave is moving in, which is the direction that the energy is traveling in, and is sometimes called the 'direction of wave propagation'.

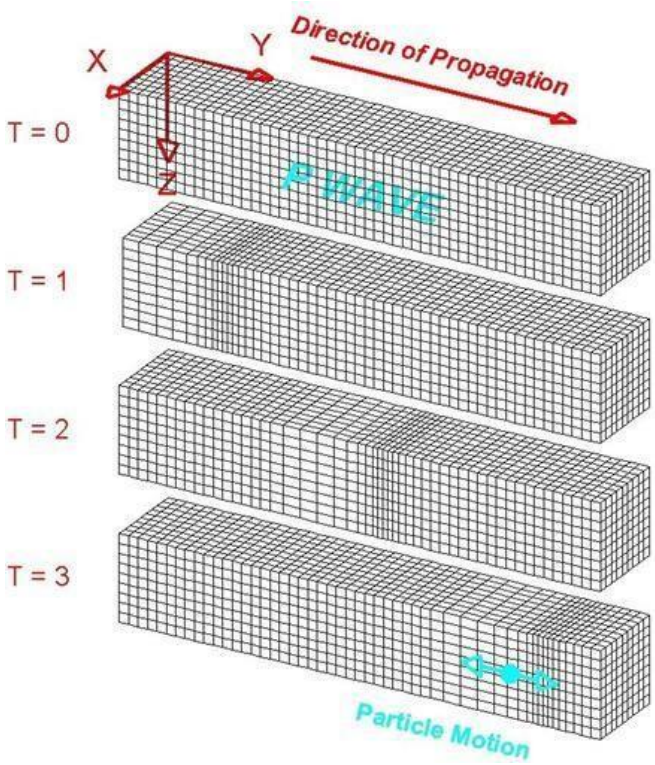

S WAVES

The second type of body wave is the **S wave** or **secondary wave**, which is the second wave you feel in an earthquake. An S wave is slower than a P wave and can only move through solid rock, not through any liquid medium. It is this property of S waves that led seismologists to conclude that the Earth's **outer core** is a liquid. S waves move rock particles up and down, or side-to-side--perpindicular to the direction that the wave is traveling in (the direction of wave propagation).

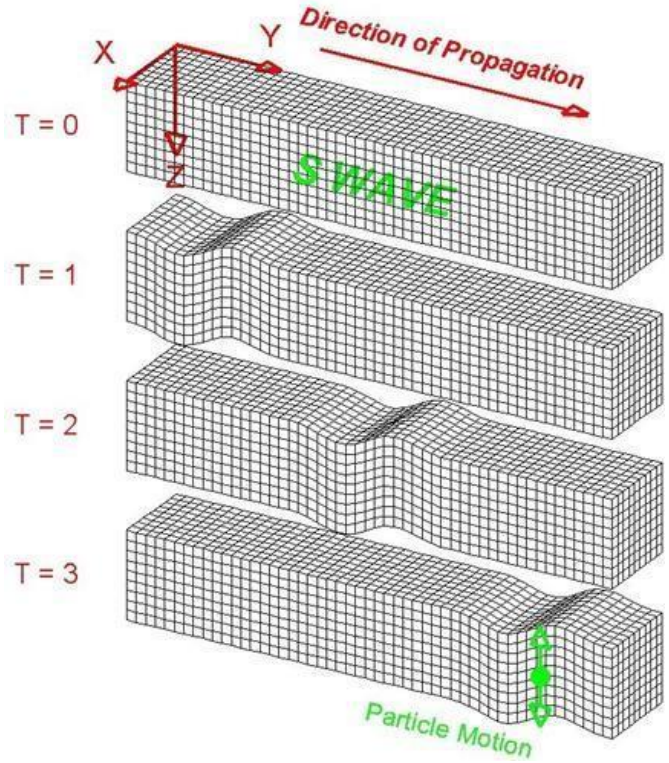

SURFACE WAVES

Travelling only through the crust, **surface waves** are of a lower frequency than body waves, and are easily distinguished on a seismogram as a result. Though they arrive after body waves, it is surface waves that are almost enitrely

responsible for the damage and destruction associated with earthquakes. This damage and the strength of the surface waves are reduced in deeper earthquakes.

LOVE WAVES

The first kind of surface wave is called a **Love wave**, named after A.E.H. Love,a British mathematician who worked out the mathematical model for this kind of wave in 1911. It's the fastest surface wave and moves the ground from side- to-side.

Confined to the surface of the crust, Love waves produce entirely horizontalmotion.

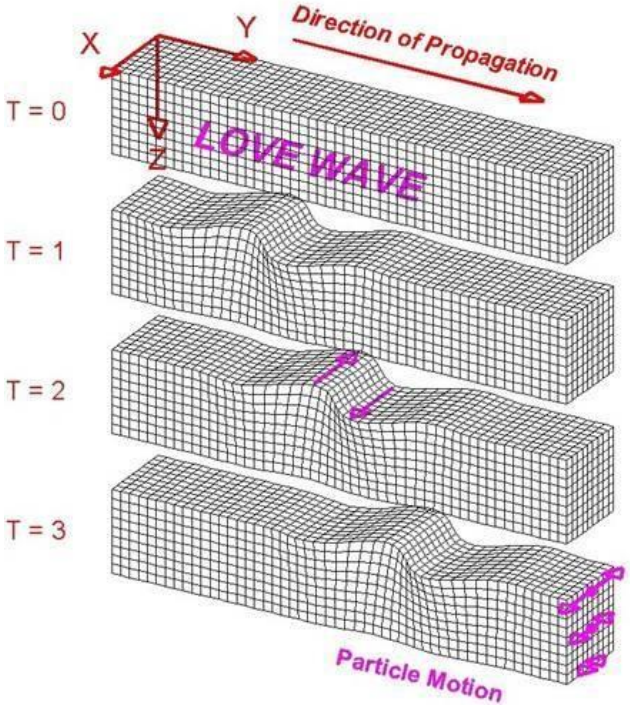

RAYLEIGH WAVES

The other kind of surface wave is the **Rayleigh wave**, named for John William

Strutt, Lord Rayleigh, who mathematically predicted the existence of this kind of wave in 1885. A Rayleigh wave rolls along the ground just like a wave rolls across a lake or an ocean. Because it rolls, it moves the ground up and down, andside-to-side in the same direction that the wave is moving. Most of the shaking felt from an earthquake is due to the Rayleigh wave, which can be much larger than the other waves

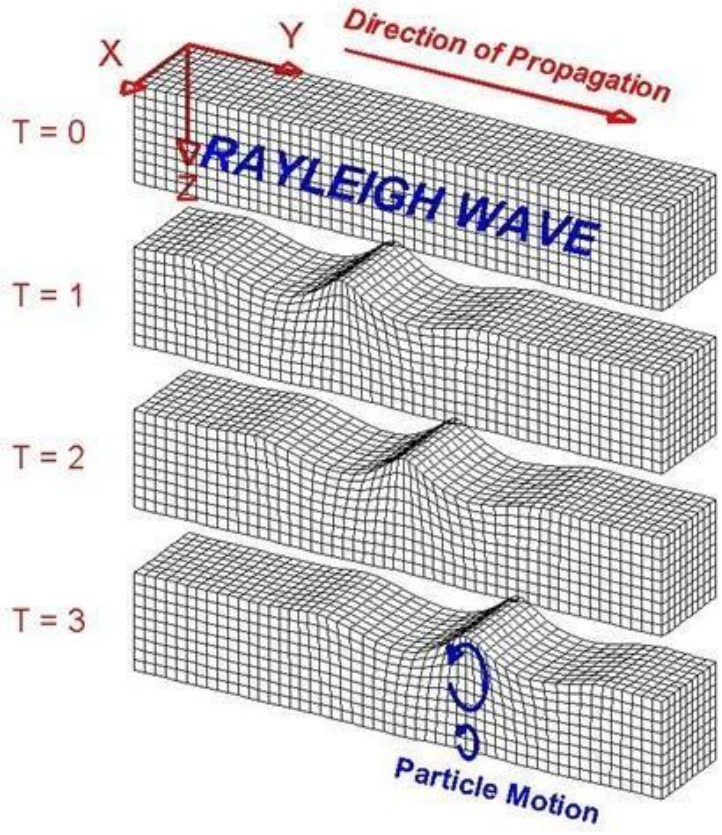

EARTHQUAKES

Earthquakes occur when energy stored in elastically strained rocks is suddenly released. This release of energy causes intense ground shaking in the area near the source of the earthquake and sends waves of elastic energy, called seismic waves, throughout the Earth. Earthquakes can be generated by bomb blasts, volcanic eruptions, sudden volume changes in minerals, and sudden slippage along faults. Earthquakes are definitely a geologic hazard for those living in earthquake prone areas, but the seismic waves generated by earthquakes are invaluable for studying the interior of the Earth.

In our discussion of earthquake we want to answer the following questions:

1. What causes earthquakes?
2. How are earthquakes studied?
3. What happens during an earthquake?
4. Where do earthquakes occur?
5. Can earthquakes be predicted?
6. Can humans be protected from earthquakes?
7. What can earthquakes tell us about the interior of the earth?

Causes of Earthquakes

Within the Earth rocks are constantly subjected to forces that tend to bend, twist, or fracture them. When rocks bend, twist or fracture they are said to deform. Strain is a change in shape, size, or volume. The forces that cause deformation are referred to as stresses. To understand the causes of earthquakes we must first explore stress and strain.

Stress and Strain

Recall that stress is a force applied over an area. A uniform stress is where the forces

act equally from all directions. Pressure is a uniform stress and is referred and is also called confining stress or hydrostatic stress. If stress is not equal from all directions then the stress is a differential stress.

Three kinds of differential stress occur.

1. ***Tensional stress (or extensional stress)***, which stretches rock;
2. ***Compressional stress***, which squeezes rock; and
3. ***Shear stress***, which result in slippage and translation.

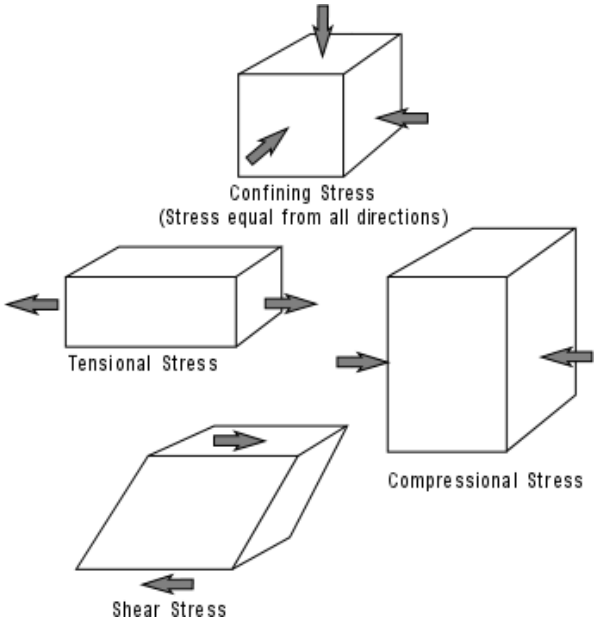

When a rock is subjected to increasing stress it changes its shape, size or volume. Such a change in shape, size or volume is referred to as ***strain***. When stress is applied to rock, the rock passes through 3 successive stages of deformation.

- ***Elastic Deformation*** -- wherein the strain is reversible.
- ***Ductile Deformation*** -- wherein the strain is irreversible.

Fracture -- irreversible strain wherein the material breaks.

We can divide materials into two classes that depend on their relative behavior under stress.

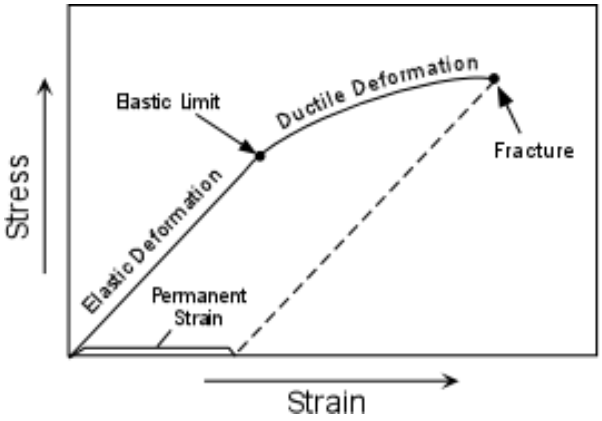

- ***Brittle materials*** have a small to large region of elastic behavior, but only a small region of ductile behavior before they fracture.
- ***Ductile materials*** have a small region of elastic behavior and a large region of ductile behavior before they fracture.

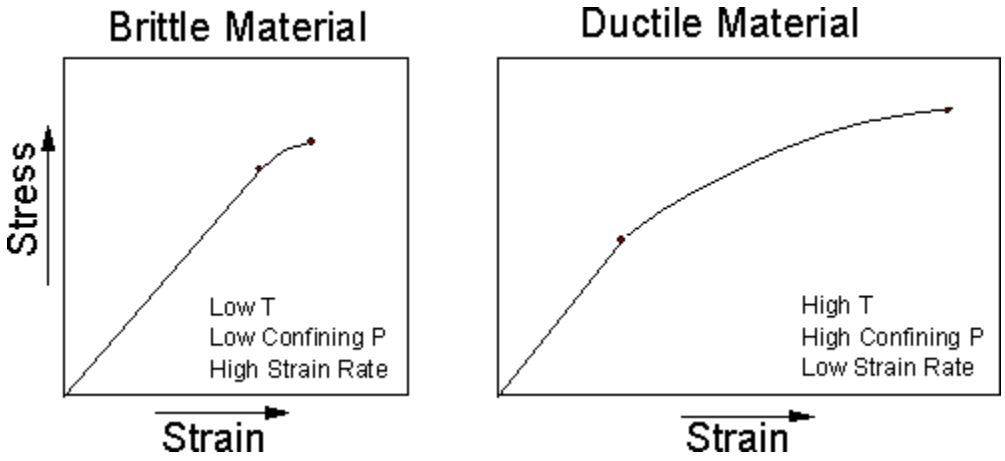

How a material behaves will depend on several factors. Among them are:

- Temperature - At high temperature molecules and their bonds can stretch and move, thus materials will behave in more ductile manner. At low Temperature, materials are brittle.

- Confining Pressure - At high confining pressure materials are less likely to fracture because the pressure of the surroundings tends to hinder the formation of fractures. At low confining stress, material will be brittle and tend to fracture sooner.

- Strain rate -- Strain rate refers to the rate at which the deformation occurs (strain divided by time). At high strain rates material tends to fracture. At low strain rates more time is available for individual atoms to move and therefore ductile behavior is favored.

- Composition -- Some minerals, like quartz, olivine, and feldspars are very brittle. Others, like clay minerals, micas, and calcite are more ductile. This is due to the chemical bond types that hold them together. Thus, the mineralogical composition of the rock will be a factor in determining the deformational behavior of the rock. Another aspect is presence or absence of water.

In general, rocks near the surface of the earth behave in a brittle fashion, unless they are deformed slowly. Thus, when they are acted upon by differential stress, they tend to fracture.

Faults

Most natural earthquakes are caused by sudden slippage along a fault. Faults occur when brittle rocks fracture and there is displacement of one side of the fracture relative to the other side. The amount of displacement in a single slippage event is rarely more that 10 to 20 m for large earthquakes, but after many events the displacement could be several hundred kilometers.

Types of Faults

Faults can be divided into several different types depending on the direction of relative displacement or slip on the fault. Most faults make an angle with the ground surface, and this angle is called the dip angle. If the dip angle is 90^{o} the fault plane is vertical. Faults can be divided into two major classes.

Dip Slip Faults - Dip slip faults are faults that have an inclined fault plane and along which the relative displacement or offset has occurred along the dip direction. Note that in looking at the displacement on any fault we don't know which side actually moved or if both sides moved, all we can determine is the relative sense of motion.

For any inclined fault plane we define the block above the fault as the ***hanging wall block*** and the block below the fault as the ***footwall block***

- ***Normal Faults -*** are faults that result from horizontal extensional stresses in brittle rocks and where the hanging-wall block has moved down relative to the footwall block.

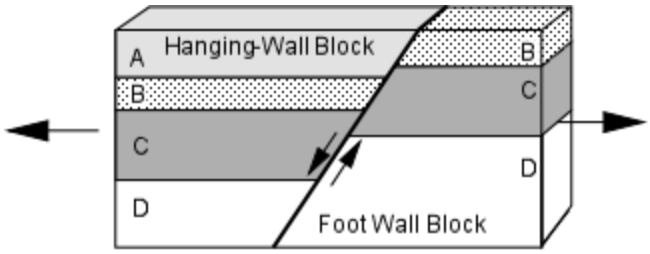

Normal Fault
Extensional Stress

- ***Reverse Faults*** - are faults that result from horizontal compressional stresses in brittle rocks, where the hanging-wall block has moved <u>up</u> relative the footwallblock.

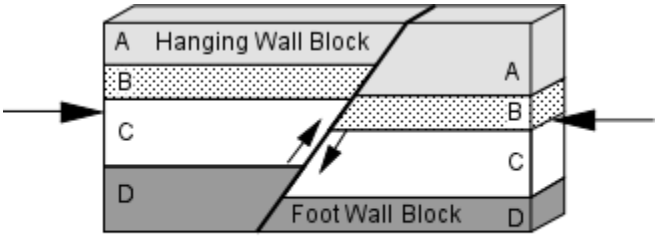

Reverse Fault
Compressional Stress

- A ***Thrust Fault*** is a special case of a reverse fault where the dip of the fault is less than 45^{o}. Thrust faults can have considerable displacement, measuring hundreds of kilometers, and can result in older strata overlying younger strata.

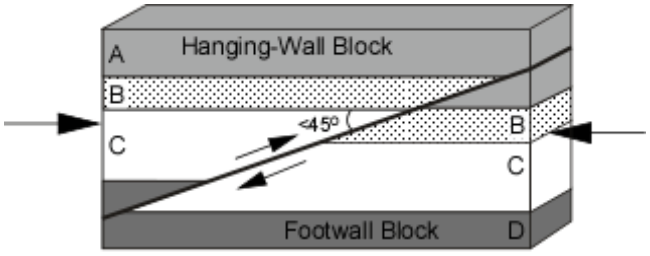

Thrust Fault
Compressional Stress

Strike Slip Faults - are faults where the displacement on the fault has taken place along a horizontal direction. Such faults result from shear stresses acting in the

crust. Strike slip faults can be of two varieties, depending on the sense of displacement. To an observer standing on one side of the fault and looking across the fault, if the block on the other side has moved to the left, we say that the fault is a left-lateral strike-slip fault. If the block on the other side has moved to the right, we say that the fault is a right-lateral strike-slip fault. The famous San Andreas Fault in California is an example of a right-lateral strike-slip fault. Displacements on the San Andreas fault are estimated at over 600 km.

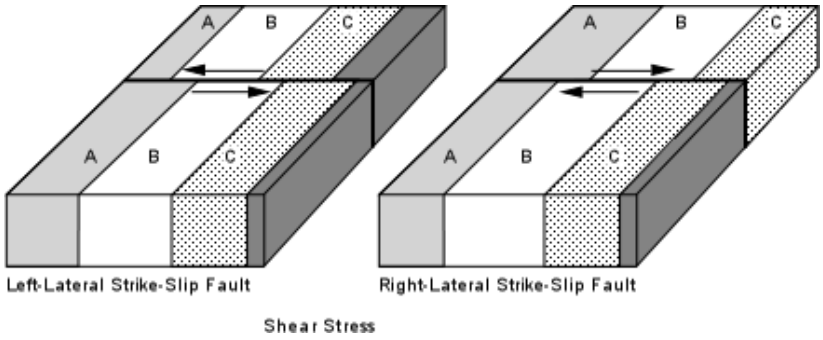

Oblique Slip Faults - If the displacement has both a vertical component and a horizontal component (i.e. a combination of dip slip and strike slip) it is called an oblique slip fault.

Blind Faults

A blind fault is one that does not break the surface of the earth. Rocks above the fault have behaved in ductile fashion and folded over the tip of the fault.

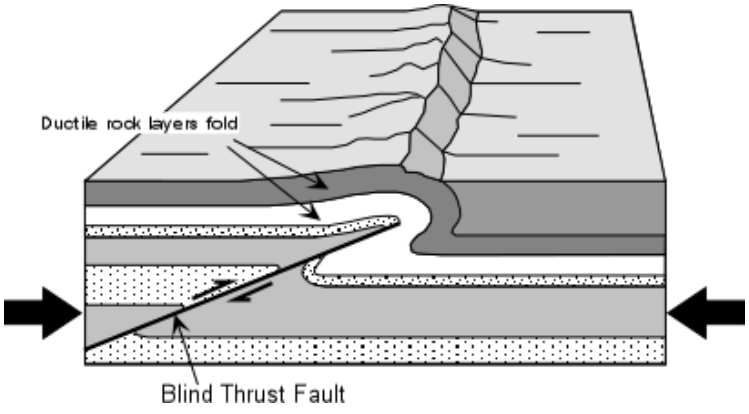

Active Faults

An active fault is one that has shown recent displacement and likely has thepotential to produce earthquakes. Since faulting is part of the deformation process,ancient faults can be found anywhere that deformation has taken place in thepast. Thus, not every fault one sees is necessarily an active fault.

Surface Expression of Faults

Where faults have broken the surface of the earth they can be delineated on maps and are called fault lines or fault zones. Recent ruptures of dip slip faults at the surface show a cliff that is called a fault scarp. Strike slip faults result in features like linear valleys, offset surface features (roads, stream channels, fences, etc.) or elongated ridges.

How Faults Develop

The ***elastic rebound theory*** suggests that if slippage along a fault is hindered such that elastic strain energy builds up in the deforming rocks on either side of the fault, when the slippage does occur, the energy released causes an earthquake.

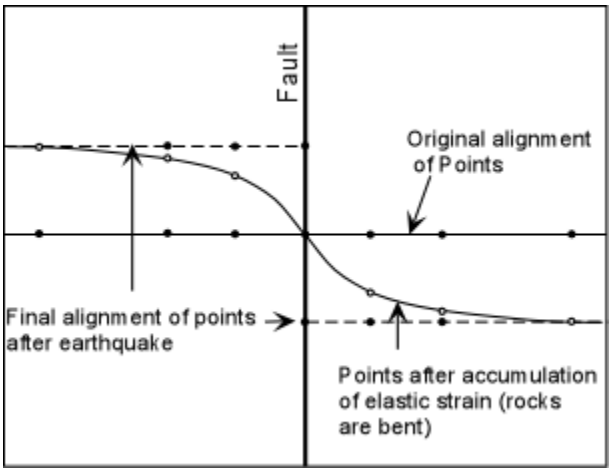

This theory was discovered by making measurements at a number of points across a fault. Prior to an earthquake it was noted that the rocks adjacent to the fault were bending. These bends disappeared

after an earthquake suggesting that the energy stored in bending the rocks was suddenly released during the earthquake.

Friction between the blocks then keeps the fault from moving again until enough strain has accumulated along the fault zone to overcome the friction and generate another earthquake. Once a fault forms, it becomes a zone of weakness in the crust, and so long as the tectonic stresses continue to be present more earthquakes are likely to occur on the fault. Thus faults move in spurts and this behavior is referred to as ***Stick Slip***. If the displacement during an earthquake is large, a large earthquake will be generated. Smaller displacements generate smallerearthquakes. Note that even for small displacements of only a millimeter per year,after 1 million years, the fault will accumulate 1 km of displacement.

Fault Creep - Some faults or parts of faults move continuously without generating earthquakes. This could occur if there is little friction on the fault and tectonic stresses are large enough to move the blocks in opposite directions. This is called fault creep. Note that if creep is occurring on one part of a fault, it is likely causing strain to build on other parts of the fault.

How Earthquakes Are Measured

When an earthquake occurs, the elastic energy is released and sends out vibrations that travel in all directions throughout the Earth. These vibrations are called seismic waves. The point within the earth where the fault rupture starts is called the ***focus or hypocenter***.

The ***epicenter*** is the point on the surface of the earth directly above the focus. Sometimes the media get these two terms confused.

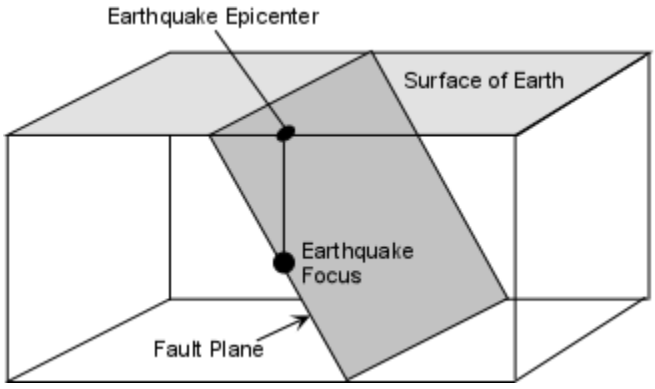

Seismic Waves

Seismic waves emanating from the focus can travel in several ways, and thus there are several different kinds of seismic waves.

Body Waves - emanate from the focus and travel in all directions through the body of the Earth. There are two types of body waves: P-waves and S waves.

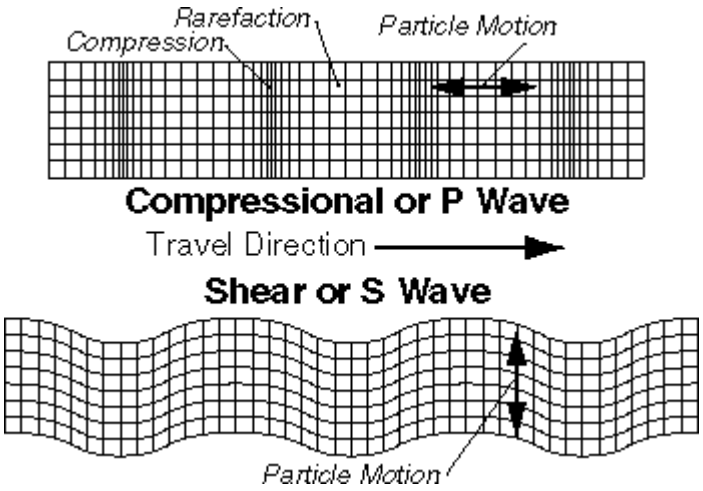

- ***P - waves*** - are Primary waves. They travel with a velocity that depends on the elastic properties of the rock through which they travel.

$$V_p = \sqrt{[(K+4/3\mu)/\rho]}$$

Where, V_p is the velocity of the P-wave, K is the incompressibility of the material, μ is the rigidity of the material, and ρ is the density of the material.

- P-waves are the same thing as sound waves. They move through the material by compressing it, but after it has been compressed it expands, so that the wave moves by compressing and expanding the material as it travels. Thus the velocity of the P-wave depends on how easily the material can be compressed (the

incompressibility), how rigid the material is (the rigidity), and the density of the material. P-waves have the highest velocity of all seismic waves and thus will reach all seismographs first.

- ***S-Waves*** - Secondary waves, also called shear waves. They travel with a velocity that depends only on the rigidity and density of the material through which they travel: $V_S = \sqrt{\mu / \rho}$
- S-waves travel through material by shearing it or changing its shape in the direction perpendicular to the direction of travel. The resistance to shearing of a material is the property called the rigidity. It is notable that liquids have no rigidity, so that the velocity of an S-wave is zero in a liquid. (This point will become important later). Note that S-waves travel slower than P-waves, so they will reach a seismograph after the P-wave.

Surface Waves - Surface waves differ from body waves in that they do not travel through the earth, but instead travel along paths nearly parallel to the surface of the earth. Surface waves behave like S-waves in that they cause up and down and side to side movement as they pass, but they travel slower than S-waves and do not travel through the body of the Earth. Love waves result in side to side motion and Rayleigh waves result in an up and down rolling motion. (see figure 10.10 in your text). Surface waves are responsible for much of the shaking that occurs during an earthquake.

The study of how seismic waves behave in the Earth is called ***seismology***.
Seismic waves are measured and recorded on instruments called seismometers.

Seismometers

Seismic waves travel through the earth as elastic vibrations. A ***seismometer*** is an instrument used to record these vibrations and the resulting graph that shows the vibrations is called a ***seismogram***.

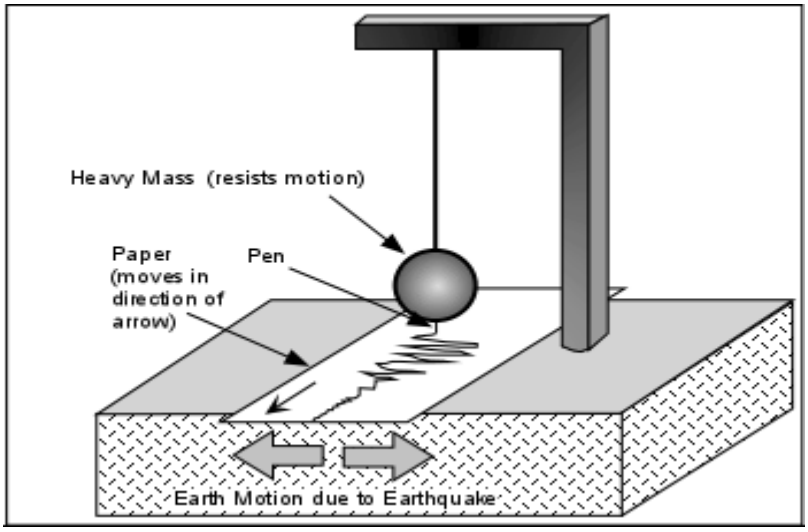

The seismometer must be able to move with the vibrations, yet part of it must remain nearly stationary. This is accomplished by isolating the recording device (like a pen) from the rest of the Earth using the principal of inertia. For example, if the pen is attached to a large mass suspended by a spring, the spring and the large mass move less than the paper which is attached to the Earth, and on which the record of the vibrations is made.

The record of an earthquake, a seismogram, as recorded by a seismometer, will be a plot of vibrations versus time. On the seismogram time is marked at regular intervals, so that we can determine the time of arrival of the first P-wave and the time of arrival of the first S-wave.

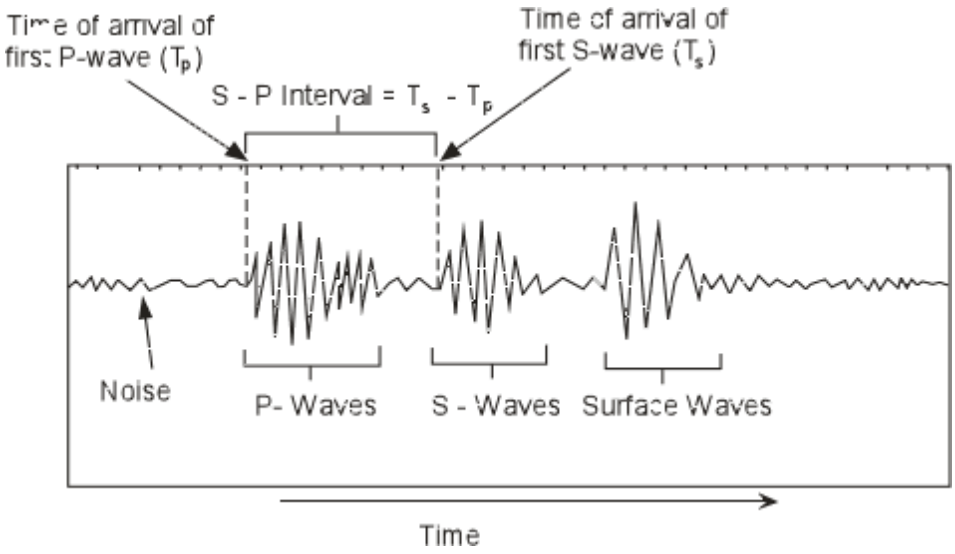

(Note again, that because P-waves have a higher velocity than S-waves, the P-waves arrive at the seismographic station before the S-waves).

Locating the Epicenter of an Earthquake

In order to determine the location of an earthquake, we need to have recorded a seismogram of the earthquake from at least three seismographic stations at different distances from the epicenter. In addition, we need one further piece of information - that is the time it takes for P-waves and S-waves to travel through the earth and arrive at a seismographic station. Such information has been collected over the last 100 or so years, and is available as travel time curves.

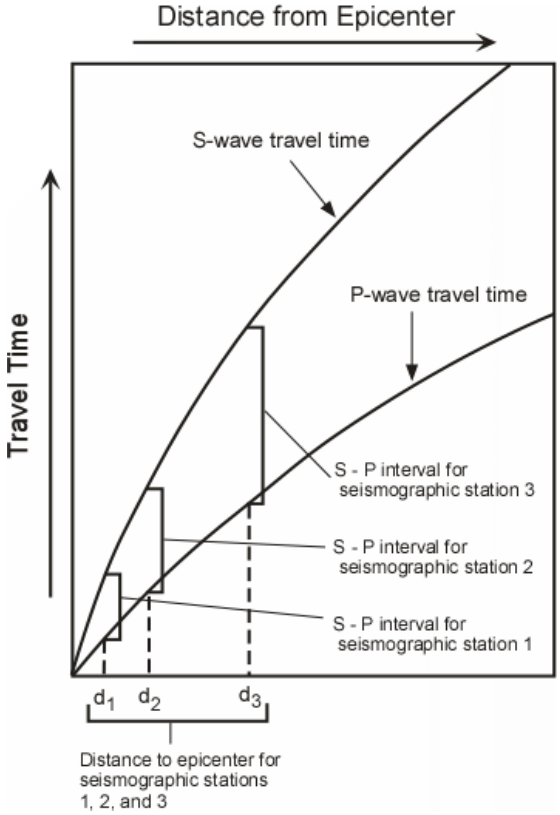

From the seismographs at each station one determines the S-P interval (the difference in the time of arrival of the first S-wave and the time of arrival of the first P-wave. Note that on the travel time curves, the S-P interval increases with increasing distance from the epicenter. Thus the S-P interval tells us the distance to the epicenter from the seismographic station where the earthquake was recorded.

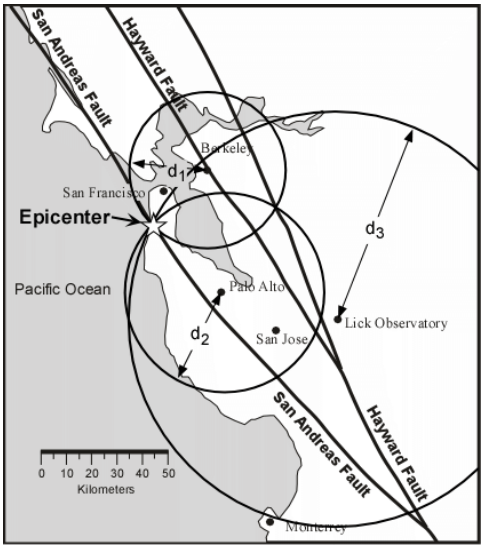

Thus, at each station we can draw a circle on a map that has a radius equal to the distance from the epicenter. Three such circles will intersect in a point that locates the epicenter of the earthquake.

Earthquake Size

Whenever a large destructive earthquake occurs in the world the press immediately wants to know where the earthquake occurred and how big the earthquake was (in California the question is usually - Was this the Big One?). The size of an earthquake is usually given in terms of a scale called the Richter Magnitude. Richter Magnitude is a scale of earthquake size developed by a seismologist named Charles F. Richter. The Richter Magnitude involves measuring the amplitude (height) of the largest recorded wave at a specific distance from the earthquake. While it is correct to say that for each increase in 1 in the Richter Magnitude, there is a tenfold increase in amplitude of the wave, it is **incorrect** to say that each increase of 1 in Richter Magnitude represents a tenfold increase in the size of the Earthquake (as is commonly incorrectly stated by the Press). A better measure of the size of an

earthquake is the amount of energy released by the earthquake. The amount of energy released is related to the Magnitude Scale by the following equation: Log E = 11.8 + 1.5 M

Where Log refers to the logarithm to the base 10, E is the energy released in ergs, and M is the Magnitude.

Anyone with a hand calculator can solve this equation by plugging in various values of M and solving for E, the energy released. I've done the calculation for you in the following table:

Magnitude	Energy (ergs)	Factor
1	2.0×10^{13}	31 x
2	6.3×10^{14}	
3	2.0×10^{16}	31 x
4	6.3×10^{17}	
5	2.0×10^{19}	31 x
6	6.3×10^{20}	
7	2.0×10^{22}	31 x
8	6.3×10^{23}	

From these calculations you can see that each increase in 1 in Magnitude represents a 31 fold increase in the amount of energy released. Thus, a magnitude 7 earthquake releases 31 times more energy than a magnitude 6 earthquake. A magnitude 8 earthquake releases 31 x 31 or 961 times more energy than a magnitude 6 earthquake.

Although the Richter Magnitude is the scale most commonly reported when referring to the size of an earthquake, it has been found that for larger earthquakes

a more accurate measurement of size is the ***moment magnitude, M_w.*** The moment magnitude is a measure of the amount of strain energy released by the earthquake as determined by measurements of the shear strength of the rock and the area of the rupture surface that slipped during the earthquake.

- Note that it usually takes more than one seismographic station to calculate the magnitude of an earthquake. Thus you will hear initial estimates of earthquake magnitude immediately after an earthquake and a final assigned magnitude for the same earthquake that may differ from initial estimates, but is assigned after seismologists have had time to evaluate the data from numerous seismographic stations.
- The moment magnitude for large earthquakes is usually greater than the Richter magnitude for the same earthquake. For example the Richter magnitude for the 1964 Alaska earthquake is usually reported as 8.6, whereas the moment magnitude for this earthquake is calculated at 9.2. The largest earthquake ever recorded was in Chile in 1960 with a moment magnitude of 9.5, The Summatra earthquake of 2004 had a moment magnitude of 9.0. Sometimes a magnitude is reported for an earthquake and no specification is given as to which magnitude (Richter or moment) is reported. This obviously can cause confusion. But, within the last few years, the tendency has been to report the moment magnitude rather than the Richter magnitude.
- The Hiroshima atomic bomb released an amount of energy equivalent to a moment magnitude 6 earthquake.
- Note that magnitude scales are open ended with no maximum or minimum. The largest earthquakes are probably limited by rock strength. Meteorite impacts could cause larger earthquakes than have ever been observed.

Frequency of Earthquakes of Different Magnitude Worldwide		
Magnitude	Number of arthquakes per Year	Description
> 8.5	0.3	Great
8.0 - 8.4	1	
7.5 - 7.9	3	Major
7.0 - 7.4	15	
6.6 - 6.9	56	
6.0 - 6.5	210	Destructive
5.0 - 5.9	800	Damaging
4.0 - 4.9	6,200	Minor
3.0 - 3.9	49,000	
2.0 - 2.9	300,000	
0 - 1.9	700,000	

Modified Mercalli Intensity Scale

Note that the Richter magnitude scale results in one number for the size of the earthquake. Maximum ground shaking will occur only in the area of the epicenter of the earthquake, but the earthquake may be felt over a much larger area. The Modified Mercalli Scale was developed in the late 1800s to assess the intensity of ground shaking and building damage over large areas.

- The scale is applied after the earthquake by conducting surveys of people's response to the intensity of ground shaking and destruction.

Modified Mercalli Intensity Scale

Intensity	Characteristic Effects	Richter Scale Equivalent
I	People do not feel any Earth movement	<3.4
II	A few people notice movement if at rest and/or on upper floors of tall buildings	
III	People indoors feel movement. Hanging objects swing back and forth. People outdoors might not realize that an earthquake is occurring	4.2
IV	People indoors feel movement. Hanging objects swing. Dishes, windows, and doors rattle. Feels like a heavy truck hitting walls. Some people outdoors may feel movement. Parked cars rock.	4.3 - 4.8
V	Almost everyone feels movement. Sleeping people are awakened. Doors swing open/close. Dishes break. Small objects move or are turned over. Trees shake. Liquids spill from open containers	4.9-5.4
VI	Everyone feels movement. People have trouble walking. Objects fall from shelves. Pictures fall off walls. Furniture moves. Plaster in walls may crack. Trees and bushes shake. Damage slight in poorly built buildings.	5.5 - 6.1
VII	People have difficulty standing. Drivers feel cars shaking. Furniture breaks. Loose bricks fall from buildings. Damage slight to moderate in well-built buildings; considerable in poorly built buildings.	5.5 - 6.1
VIII	Drivers have trouble steering. Houses not bolted down shift on foundations. Towers & chimneys twist and fall. Well-built buildings suffer slight damage. Poorly built structures severely damaged. Tree branches break. Hillsides crack if ground is wet. Water levels in wells change.	6.2 - 6.9
IX	Well-built buildings suffer considerable damage. Houses not bolted down move off foundations. Some underground pipes broken. Ground cracks. Serious damage to Reservoirs.	6.2 - 6.9
X	Most buildings & their foundations destroyed. Some bridges destroyed. Dams damaged. Large landslides occur. Water thrown on the banks of canals, rivers, lakes. Ground cracks in large areas. Railroad tracks bent slightly.	7.0 - 7.3
XI	Most buildings collapse. Some bridges destroyed. Large cracks appear in the ground. Underground pipelines destroyed. Railroad tracks badly bent.	7.4 - 7.9
XII	Almost everything is destroyed. Objects thrown into the air. Ground moves in waves or ripples. Large amounts of rock may move.	>8.0

- The Modified Mercalli Scale is shown in the table above. Note that correspondence between maximum intensity and Richter Scale magnitude **only applies in the area around the epicenter**.
- A given earthquake will have zones of different intensity all surrounding a zone of maximum intensity.
- The Mercalli Scale is very useful in examining the effects of an earthquake over a large area, because it will is responsive not only to the size of the earthquake as measured by the Richter scale for areas near the epicenter, but will also show the effects of the efficiency that seismic waves are transmitted through different types of material near the Earth's surface.
- The Mercalli Scale is also useful for determining the size of earthquakes that occurred before the modern seismographic network was available (before there were seismographic stations, it was not possible to assign a Magnitude).

What Happens During an Earthquake?

Earthquakes produce several effects that cause damage and destruction. Some of these effects are the direct result of the ground shaking produced by the arrival of seismic waves and others are secondary effects. Among these effects are the following:

Ground Shaking - Shaking of the ground caused by the passage of seismic waves near the epicenter of the earthquake is responsible for the collapse of most structures. The intensity of ground shaking depends on distance from the epicenter and on the type of bedrock underlying the area.

- In general, loose unconsolidated sediment is subject to more intense shaking than solid bedrock.
- Damage to structures from shaking depends on the type of construction. Concrete and masonry structures, because they are brittle are more susceptible to damage than wood and steel structures, which are more flexible.

Different kinds of shaking occur due to passage of different kinds of waves. As the P-waves arrive the ground will move up and down. The S-waves produce waves that both move the ground up and down and back and forth in the direction of wave motion. The Love waves shake the ground from side to side, and the Rayleigh waves create a rolling up and down motion (see figure 10.26 in your text).

Ground Rupture - Ground rupture only occurs along the fault zone that moves during the earthquake. Thus, structures that are built across fault zones may

collapse, whereas structures built adjacent to, but not crossing the fault maysurvive.

Fire - Fire is a secondary effect of earthquakes. Because power lines may be knocked down and because natural gas lines may rupture due to an earthquake, fires are often started closely following an earthquake. The problem is compounded if water lines are also broken during the earthquake since there will not be a supply of water to extinguish the fires once they have started. In the 1906 earthquake in San Francisco more than 90% of the damage to buildings was caused by fire.

Landslides and Debris/Rock Falls - In mountainous regions subjected to earthquakes ground shaking may trigger rapid mass-wasting events like landslides, rock and debris falls, slumps, and debris avalanches.

Liquefaction - ***Liquefaction*** is a processes that occurs in water-saturated unconsolidated sediment due to shaking. In areas underlain by such material, the ground shaking causes the grains to loose grain to grain contact, and thus the material tends to flow.

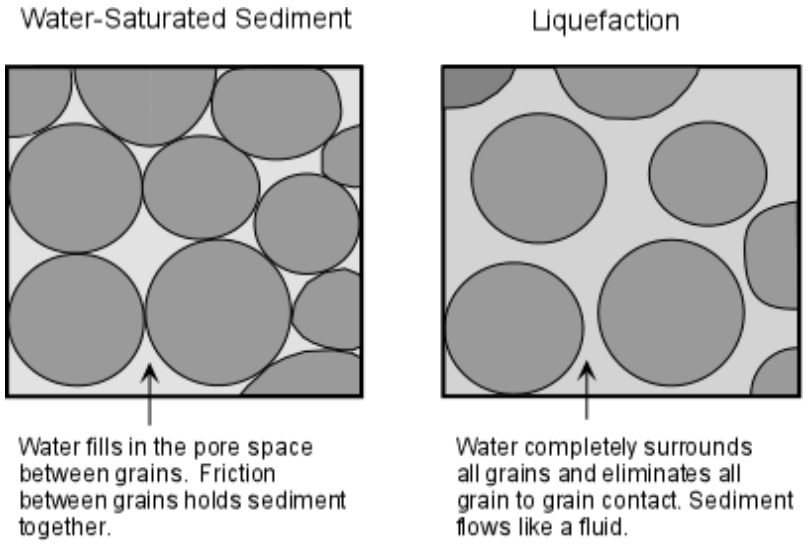

You can demonstrate this process to yourself next time your go the beach. Stand on the sand just after an incoming wave has passed. The sand will easily support your weight and you will not sink very deeply into the sand if you stand still. But, if you start to shake your body while standing on this wet sand, you will notice that the sand begins to flow as a result of liquefaction, and your feet will sink deeper into the sand.

Aftershocks - Earthquakes can change the stress state in rocks near the hypocenter and this may induce numerous earthquakes that occur after the main earthquake. These are almost always smaller earthquakes, but they can be numerous and last for many months after the main earthquake. Aftershocks are particularly dangerous because that can cause further damage to already damagedstructures and make it unsafe for rescue efforts to be pursued.

Tsunami - Tsunami are giant ocean waves that can rapidly travel across oceans. Earthquakes that occur along coastal areas can generate tsunami, which can cause damage thousands of kilometers away on the other side of the ocean.

Tsunami can be generated by anything that disturbs a body of water. This includes earthquakes that cause vertical offset of the sea floor, volcanic eruptions into a body of water, landslides into a body of water, underwater explosions, and meteorite impacts.

In general, the larger the earthquake, eruption, landslide, explosion or meteorite, the more likely it will be able to travel across an ocean. Smaller events may, however cause a tsunami that affect areas in the vicinity of the triggering event.

Tsunami waves have wavelengths and velocities much higher that wind driven ocean waves. Velocities are on the order of several hundred km/hr, similar to a jet airplane. They usually are more than one wave that hit the coastline tens of minutes to hours apart. Although wave heights are barely perceptible in the open ocean, the waves become amplified as the approach the shore and may build to several tens of meters. Thus, when the come ashore, the can flood areas far away from thecoast. Often the trough of a tsunami wave arrives before the crest. This produces a phenomenon called drawdown where the ocean recedes from the normal shoreline by as much as a kilometer.

Tsunami warning systems have been developed for the Pacific Ocean basin and, recently, the Indian Ocean where a tsunami killed over 250,000 people in 2004. But, such warning systems depend on the ability to detect and forecast a tsunami after an earthquake occurs and may take several hours to come up with an accurate forecast of wave heights and travel time.

Knowing something about these aspects of tsunami could save your life. It suggests that:

1. If you are near the beach and feel an earthquake immediately get to higher ground. Tsunami warnings require time and if you are near enough to the earthquake that generates a tsunami that you feel the earthquake, there may not

be enough time for a warning to be sounded, nor will there be enough time to get out of the way once you see the wave approaching.

2. If you are near the beach and see the ocean recede far offshore, immediately get to higher ground, as the receding ocean indicates that the trough of a tsunami wave has arrived and will be followed by the crest.

3. If you survive the first wave of a tsunami, don't go back to the coast assuming the event is over. Several waves are possible and any of them could be the largest of the waves. Wait for authorities to issue an "all clear signal".

4. Don't even consider "surfing the tsunami wave" or riding it out. The waves are so powerful and last such a long time, that you would have little chance of surviving.

Where do Earthquakes Occur?

The distribution and frequency of earthquakes is referred to as ***seismicity***. Most earthquakes occur along relatively narrow belts that coincide with plate boundaries (see figure 10.18 in your text).

This makes sense, since plate boundaries are zones along which lithospheric plates mover relative to one another. Earthquakes along these zones can be divided into shallow focus earthquakes that have focal depths less than about 70 km and deep focus earthquakes that have focal depths between 75 and 700 km.

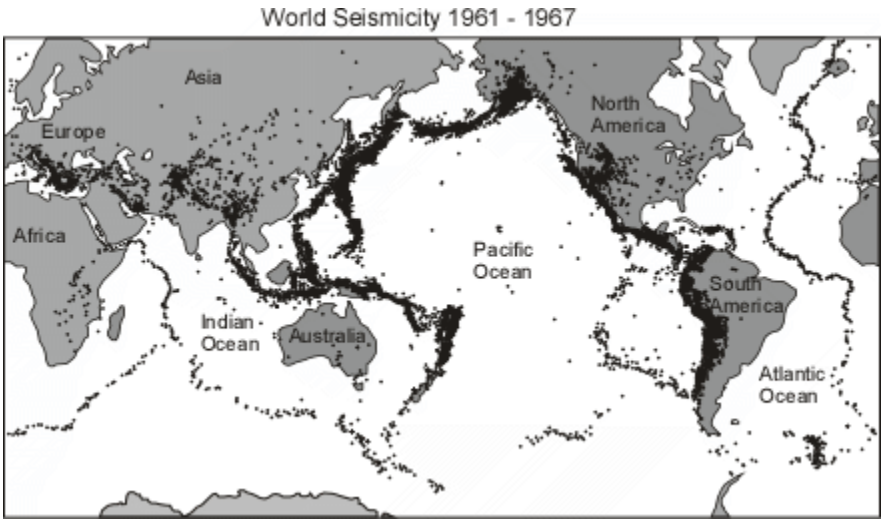

Earthquakes at Diverging Plate Boundaries

Diverging plate boundaries are zones where two plates move away from each other, such as at oceanic ridges. In such areas the lithosphere is in a state of tensional stress and thus normal faults and rift valleys occur. Earthquakes that occur along such boundaries show normal fault motion and tend to be shallow focus earthquakes,

with focal depths less than about 20 km. Such shallow focal depths indicate that the brittle lithosphere must be relatively thin along these diverging plate boundaries.

Earthquakes at Converging Plate Boundaries -

Convergent plate boundaries are boundaries where two plates run into each other. Thus, they tend to be zones where compressional stresses are active and thus reverse faults or thrust faults are common. There are two types of converging plate boundaries. (1) Subduction boundaries, where oceanic lithosphere is pushed beneath either oceanic or continental lithosphere; or (2) collision boundaries where two plates with continental lithosphere collide.

- **Subduction boundaries** -At subduction boundaries cold oceanic lithosphere is pushed back down into the mantle where two plates converge at an oceanic trench. Because the subducted lithosphere is cold, it remains brittle as it descends and thus can fracture under the compressional stress. When it fractures, it generates earthquakes that define a zone of earthquakes with increasing focal depths beneath the overriding plate. This zone of earthquakes is called the ***Benioff Zone***. Focal depths of earthquakes in the Benioff Zone can reach down to 700 km.

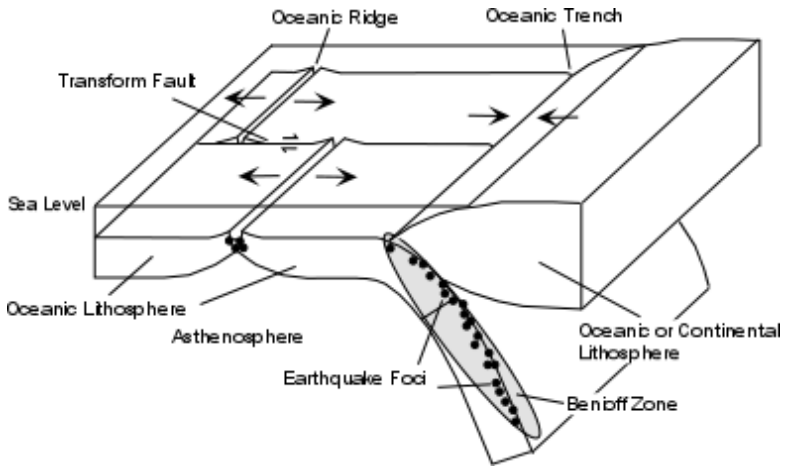

- **Collision boundaries** - At collisional boundaries two plates of continental lithosphere collide resulting in fold-thrust mountain belts. Earthquakes occur due to the thrust faulting and range in depth from shallow to about 200 km.

Earthquakes at Transform Fault Boundaries

Transform fault boundaries are plate boundaries where lithospheric plates slide past one another in a horizontal fashion. The San Andreas Fault of California is one of the longer transform fault boundaries known. Earthquakes along these boundaries show strike-slip motion on the faults and tend to be shallow focus earthquakes with depths usually less than about 50 km.

Intraplate Earthquakes - These are earthquakes that occur in the stable portions of continents that are not near plate boundaries. Many of them occur as a result of re-activation of ancient faults, although the causes of some intraplate earthquakesare not well understood.

- Examples - New Madrid Region, Central U.S., Charleston South Carolina, Along St. Lawrence River - U.S. - Canada Border.

Earthquake Risk

The risk that an earthquake will occur close to where you live depends on whether or not tectonic activity that causes deformation is occurring within the crust of that area. For the U.S., the risk is greatest in the most tectonically active area, that is near the plate margin in the Western U.S. Here, the San Andreas Fault which forms the margin between the Pacific Plate and the North American Plate, is responsible for about 1 magnitude 8 or greater earthquake per century. Also in the western U.S. is the Basin and Range Province where extensional stresses in the crust have created many normal faults that are still active. Historically, large earthquakes have also occurred in the area of New Madrid, Missouri; and Charleston, South Carolina. (See figure 10.39 in your text). Why earthquakes occur in these other areas is not well understood. If earthquakes have occurred before, they are expected to occur again.

Long-Term Forecasting

Long-term forecasting is based mainly on the knowledge of when and where earthquakes have occurred in the past. Thus, knowledge of present tectonic setting, historical records, and geological records are studied to determine locations and recurrence intervals of earthquakes. Two methods of earthquake forecasting are being employed - paleoseismology and seismic gaps.

- Paleoseismology - the study of prehistoric earthquakes. Through study of the offsets in sedimentary layers near fault zones, it is often possible to determine recurrence intervals of major earthquakes prior to historical records. If it is determined that earthquakes have recurrence intervals of say 1 every 100 years,

and there are no records of earthquakes in the last 100 years, then a long-term forecast can be made and efforts can be undertaken to reduce seismic risk.

- Seismic gaps - A seismic gap is a zone along a tectonically active area where no earthquakes have occurred recently, but it is known that elastic strain is building in the rocks. If a seismic gap can be identified, then it might be an area expected to have a large earthquake in the near future.

Short-Term Prediction

- Short-term predication involves monitoring of processes that occur in the vicinity of earthquake prone faults for activity that signify a coming earthquake.
- Anomalous events or processes that may precede an earthquake are called ***precursor events*** and might signal a coming earthquake.
  - Despite the array of possible precursor events that are possible to monitor, successful short-term earthquake prediction has so far been difficult to obtain. This is likely because: 1. the processes that cause earthquakes occur deep beneath the surface and are difficult to monitor, 2. earthquakes in different regions or along different faults all behave differently, thus no consistent patterns have so far been recognized

Among the precursor events that may be important are the following:

- ***Ground Uplift and Tilting*** - Measurements taken in the vicinity of active faults sometimes show that prior to an earthquake the ground is uplifted or tilts due to the swelling of rocks caused by strain building on the fault. This may lead to the

formation of numerous small cracks (called microcracks). This cracking in the rocks may lead to small earthquakes called foreshocks.

- ***Foreshocks*** - Prior to a 1975 earthquake in China, the observation of numerous foreshocks led to successful prediction of an earthquake and evacuation of the city of the Haicheng. The magnitude 7.3 earthquake that occurred, destroyed half of the city of about 100 million inhabitants, but resulted in only a few hundred deaths because of the successful evacuation.
- ***Water Level in Wells -*** As rocks become strained in the vicinity of a fault, changes in pressure of the groundwater (water existing in the pore spaces and fractures in rocks) occur. This may force the groundwater to move to higher or lower elevations, causing changes in the water levels in wells.

- ***Emission of Radon Gas*** - Radon is an inert gas that is produced by the radioactive decay of uranium and other elements in rocks. Because Radon is inert, it does not combine with other elements to form compounds, and thus remains in a crystal structure until some event forces it out. Deformation resulting from strain may force the Radon out and lead to emissions of Radon that show up in well water. Thenewly formed microcracks discussed above could serve as pathways for the Radon to escape into groundwater. Increases in the amount of radon emissions have been reported prior to some earthquakes

- ***Strange Animal Behavior*** - Prior to a magnitude 7.4 earthquake in Tanjin, China, zookeepers reported unusual animal behavior. Snakes refusing to go into their holes, swans refusing to go near water, pandas screaming, etc. This was the first systematic study of this phenomenon prior to an earthquake. Although other

attempts have been made to repeat a prediction based on animal behavior, there have been no other successful predictions.

Controlling Earthquakes

Although no attempts have yet been made to control earthquakes, earthquakes have been known to be induced by human interaction with the Earth. This suggests that in the future earthquake control may be possible.

Examples of human induced earthquakes

- For ten years after construction of the Hoover Dam in Nevada blocking the Colorado River to produce Lake Mead, over 600 earthquakes occurred, one with magnitude of 5 and 2 with magnitudes of 4.

- In the late 1960s toxic waste injected into hazardous waste disposal wells at Rocky Flats, near Denver apparently caused earthquakes to occur in a previously earthquake quiet area. The focal depths of the quakes ranged between 4 and 8 km, just below the 3.8 km-deep wells.

- Nuclear testing in Nevada set off thousands of aftershocks after the explosion of a 6.3 magnitude equivalent underground nuclear test. The largest aftershocks were about magnitude 5.

In the first two examples the increased seismicity was apparently due to increasing fluid pressure in the rocks which resulted in re-activating older faults by increasing strain.

The problem, however, is that of the energy involved. Remember that for every increase in earthquake magnitude there is about a 30 fold increase in the amount

of energy released. Thus, in order to release the same amount of energy as a magnitude 8 earthquake, 30 magnitude 7 earthquakes would be required. Since magnitude 7 earthquakes are still very destructive, we might consider generating smaller earthquakes. If we say that a magnitude 4 earthquake might be acceptable, how many magnitude 4 earthquakes are required to release the same amount of energy as a magnitude 8 earthquake? Answer 30 x 30 x 30 x 30 =810,000! Still, in the future it may be possible to control earthquakes either with explosions to gradually reduce the stress or by pumping fluids into the ground.

How Seismic Waves Help Understand Earth's Internal Structure

Much of what we know about the interior of the Earth comes from knowledge of seismic wave velocities and their variation with depth in the Earth. Recall that body wave velocities are as follows:

$$V_p = \sqrt{[(K+4/3\mu)/\rho]}$$

$$V_S = \sqrt{\mu/\rho}$$

Where K = incompressibility μ = rigidity ρ = density

If the properties of the earth, i.e. K,μ, and ρwhere the same throughout, then V_p and V_s would be constant throughout the Earth and seismic waves would travel along straight line paths through the Earth. We know however that density must change with depth in the Earth, because the density of the Earth is 5,200 kg/cubic meter and density of crustal rocks is about 2,500 kg/cubic meter. If the density were the only property to change, then we could make estimates of the density, and predict the arrival times or velocities of seismic waves at any point away from an earthquake. Observations do not follow the predictions, so, something else must be happening. In fact we know that K, μ, and ρ change due to changing temperatures, pressures and compositions of material. The job of seismology is, therefore, to use the observed seismic wave velocities to determine how K, μ, and ρ change with depth in the Earth, and then infer how pressure, temperature, and composition change with depth in the Earth. In other words to tell us something about the internal structure of the Earth.

Reflection and Refraction of Seismic Waves

If composition (or physical properties) change abruptly at some interface, then seismic wave will both reflect off the interface and refract (or bend) as they pass through the interface. Two cases of wave refraction can be recognized.

1. If the seismic wave velocity in the rock above an interface is less than the seismic wave velocity in the rock below the interface, the waves will be refracted or bent upward relative to their original path.

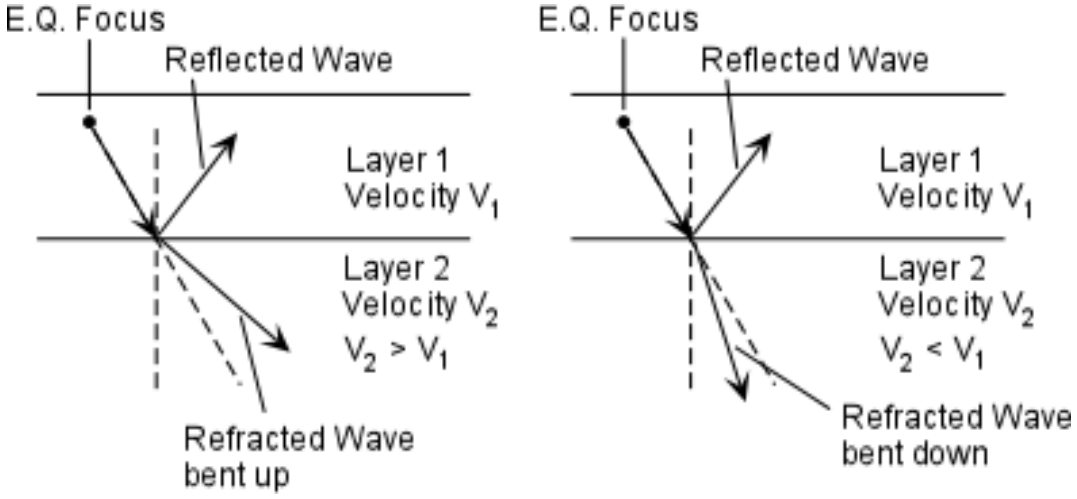

- If the seismic wave velocity decreases when passing into the rock below the interface, the waves will be refracted down relative to their original path.

If the seismic wave velocities gradually increase with depth in the Earth, the waves will continually be refracted along curved paths that curve back toward the Earth's surface.

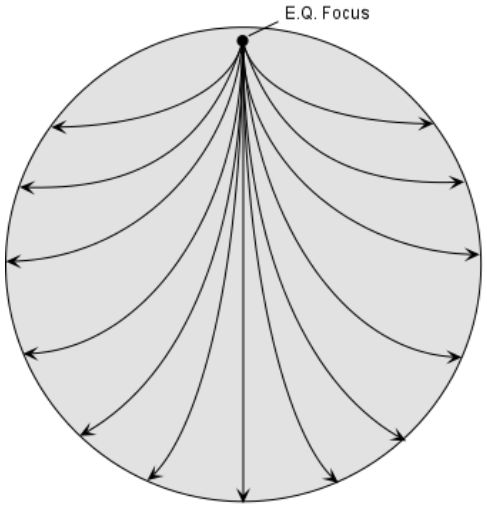

If wave velocity continuously increases downward
all waves will travel along curved paths refracting back
toward the surface

One of the earliest discoveries of seismology was a discontinuity at a depth of 2900 km where the velocity of P-waves suddenly decreases. This boundary is the boundary between the mantle and the core and was discovered because of a zone on the opposite side of the Earth from an earthquake focus receives no direct P-waves because the P-waves are refracted inward as a result of the sudden decrease in velocity at the boundary. This zone is called a P-wave shadow zone.

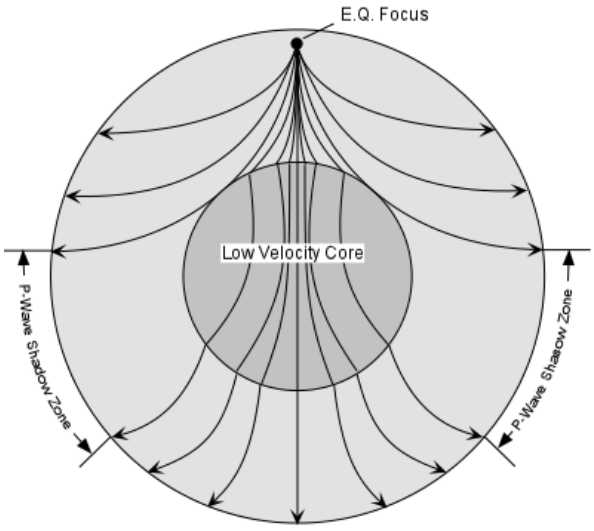

This discovery was followed by the discovery of an S-wave shadow zone. The S-wave shadow zone occurs because no S-waves reach the area on the opposite side of the Earth from the focus. Since no direct S-waves arrive in this zone, it implies that no S-waves pass through the core. This further implies the velocity of S-wave in the core is 0. In liquids $\mu = 0$, so S-wave velocity is also equal to 0. From this it is deduced that the core, or at least part of the core is in the liquid state, since no S-waves are transmitted through liquids.

Thus, the S-wave shadow zone is best explained by a liquid outer core.

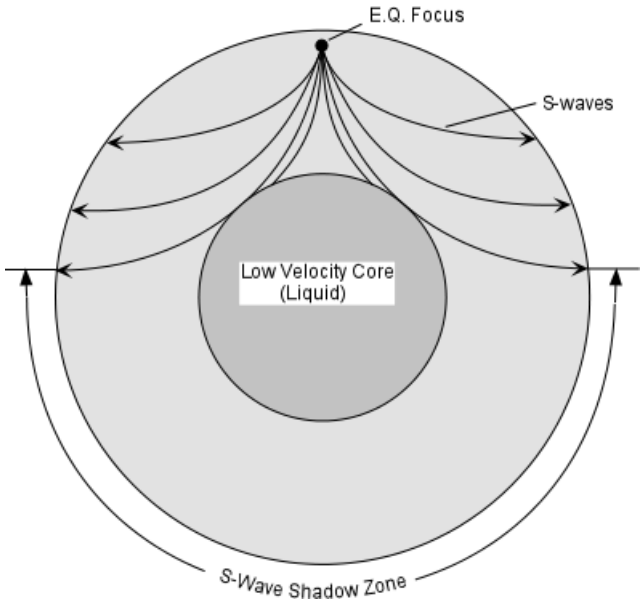

Seismic Wave Velocities in the Earth

Over the years seismologists have collected data on how seismic wave velocities vary with depth in the Earth. Distinct boundaries, called discontinuities are observed when there is sudden change in physical properties or chemical composition of the Earth. From these discontinuities, we can deduce something about the nature of the various layers in the Earth. As we discussed way back at the beginning of the course, we can look at the Earth in terms of layers of differing chemical composition, and layers of differing physical properties.

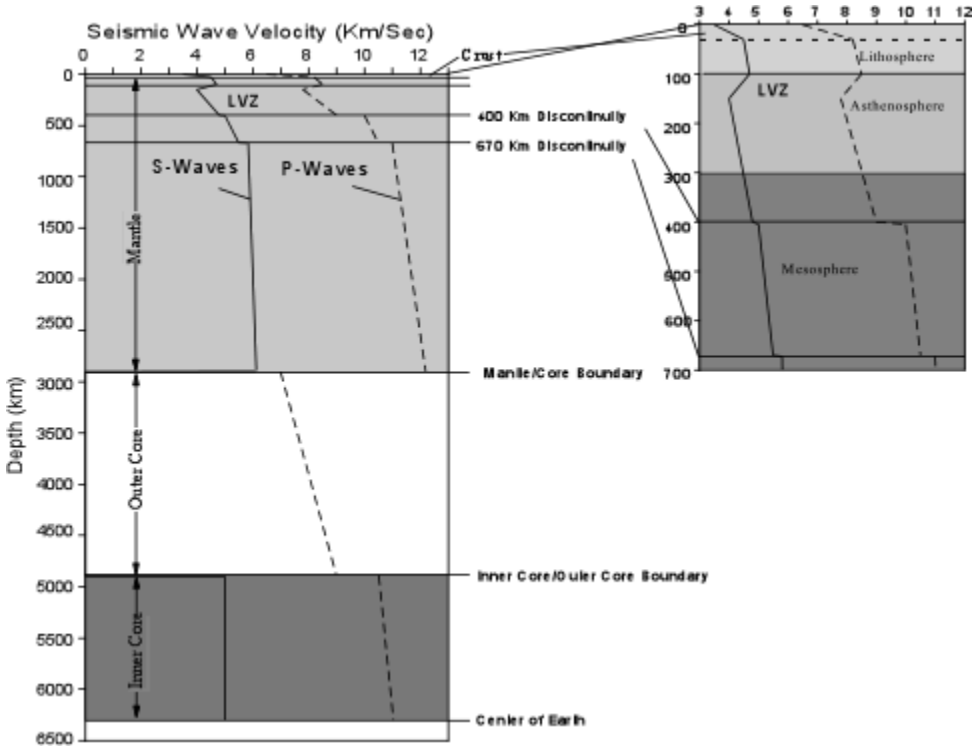

- ***Layers of Differing Composition*** - The Crust - Mohorovicic discovered boundary the boundary between crust and mantle, thus it is named the ***Mohorovicic Discontinuity*** or ***Moho***, for short. The composition of the crust can be determined from seismic waves by comparing seismic wave velocities measured on rocks in the

laboratory with seismic wave velocities observed in the crust. Then from travel times of waves on many earthquakes and from many seismic stations, the thickness and composition of the crust can be inferred.

- In the ocean basins crust is about 8 to 10 km thick, and has a composition that is basaltic.
- Continental crust varies between 20 and 60 km thick. The thickest continental crust occurs beneath mountain ranges and the thinnest beneath lowlands. The composition of continental crust varies from granitic near the top to gabbroic near the Moho.
- The Mantle - Seismic wave velocities increase abruptly at the Moho. In the mantle wave velocities are consistent with a rock composition of peridotite which consists of olivine, pyroxene, and garnet.
- The Core - At a depth of 2900 Km P-wave velocities suddenly decrease and S-wave velocities go to zero. This is the top of the outer core. As discussed above, the outer core must be liquid since S-wave velocities are 0. At a depth of about 4800 km the sudden increase in P-wave velocities indicate a solid inner core. The core appears to have a composition consistent with mostly Iron with small amounts of Nickel.

Layers of Different Physical Properties

- At a depth of about 100 km there is a sudden decrease in both P and S-wave velocities. This boundary marks the base of the lithosphere and the top of the asthenosphere. The lithosphere is composed of both crust and part of the upper mantle. It is a brittle layer that makes up the plates in plate tectonics, and appears to float and move around on top of the more ductile asthenosphere.

- At the top of the asthenosphere is a zone where both P- and S-wave velocities are low. This zone is called the ***Low-Velocity Zone*** (LVZ). It is thought that the low velocities of seismic waves in this zone are caused by temperatures approaching the partial melting temperature of the mantle, causing the mantle in this zone to behave in a very ductile manner.

- At a depth of 400 km there is an abrupt increase in the velocities of seismic waves, thus this boundary is known as the ***400 - Km Discontinuity***. Experiments on mantle rocks indicate that this represents a temperature and pressure where there is a polymorphic phase transition, involving a change in the crystal structure of Olivine, one of the most abundant minerals in the mantle.

- Another abrupt increase in seismic wave velocities occurs at a depth of 670 km. It is uncertain whether this discontinuity, known as the ***670 Km Discontinuity***, is the result of a polymorphic phase transition involving other mantle minerals or a compositional change in the mantle, or both.

Reference

http://www.geo.mtu.edu/UPSeis/waves.html

http://www.acs.psu.edu/drussell/Demos/waves/wavemotion.html

Part 2:

Geophysical Data Processing

By:

Dr. Ahmed Mohammed Abdel Gawad

Special course: Geophysical data processing course outlie

Course contents:

1- Introduction to geophysical data processing.
2- Digitization of geophysical data
3- Spectral Analysis
4- Digital filtering
5- Frequency filtering
6- Deconvolution
7- Processing of potential field data
8- Geophysical modeling

Textbooks:

– Kearey P., Brooks M., and Hill I. (2002): An Introduction to Geophysical Exploration, 3rd Edition. Wiley-Blackwell publishing, 288p.
– Yilmaz O. (2001): Seismic Data Analysis. Society of Exploration Geophysicists, 2065p.
– Sheriff, R., & Geldart, L. (1995). Exploration Seismology (2nd ed.). Cambridge: Cambridge University Press. doi:10.1017/CBO9781139168359
– Harsh K. Gupta (2011), Encyclopedia of Solid Earth Geophysics, Springer, DOI 10.1007/978-90-481-8702-7

Introduction

The definition of the geophysical data processing includes three items:

- Geophysics,
- Data,
- Processing.

What is geophysics?

Geophysics is the application of physics to **explore the inner earth components** by studying the contrasts in the physical properties of the rock layers within the earth. These properties include; the electric resistivity, the magnetic properties of the rocks, the densities, the rock strengths… etc. These contrasts cause an **anomaly** of the measured property. The anomaly is the variation of a specific property from its normal values. This anomaly is the target of most of the geophysical surveys. In Exploration Geophysics, geophysical data are used to analyze potential petroleum reservoirs and mineral deposits, locate groundwater, find archaeological relics, determine the thickness of glaciers and soils, and assess sites for environmental remediation. According to the measured physical property of the rock, the exploration geophysics are divided into several methods, such as the gravity, magnetic, seismic, electric, electromagnetic…etc.

Geophysical methods:

- **Gravity method:**

  The gravity method measures differences in the earth's gravitational field at specific locations caused by the contrasts between the densities of the different rocks (Figure 1, 2 and 3). The purpose of gravity surveys is to aid in the detection and delineation of subsurface geological features. Gravity meters (Figure 1) measure the differences in gravitational attraction between points of measurement. Nongeological effects are removed from the measured values to produce ***gravity anomalies*** that are caused by rocks having anomalous density in comparison with the density of the surrounding rocks (Figure 2). The results of a gravity survey can be represented as a 2D profile (Figure 2) and a contour map of the resulted gravity values (Figure 3) where the locations of the anomalous features can be detected.

Figure 1: The measurement of the gravity data by a gravity meter during a survey.

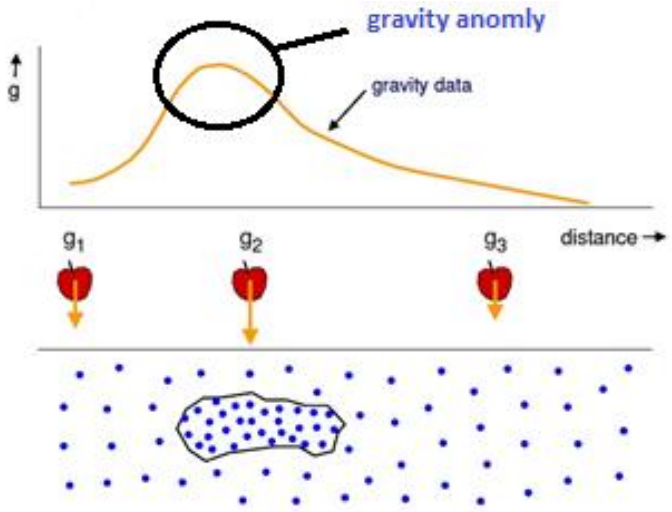

Figure 2: A measured gravity profile and the peak of the represented curve indicate the gravity anomaly which is caused by the buried body which have a higher density than the surroundings.

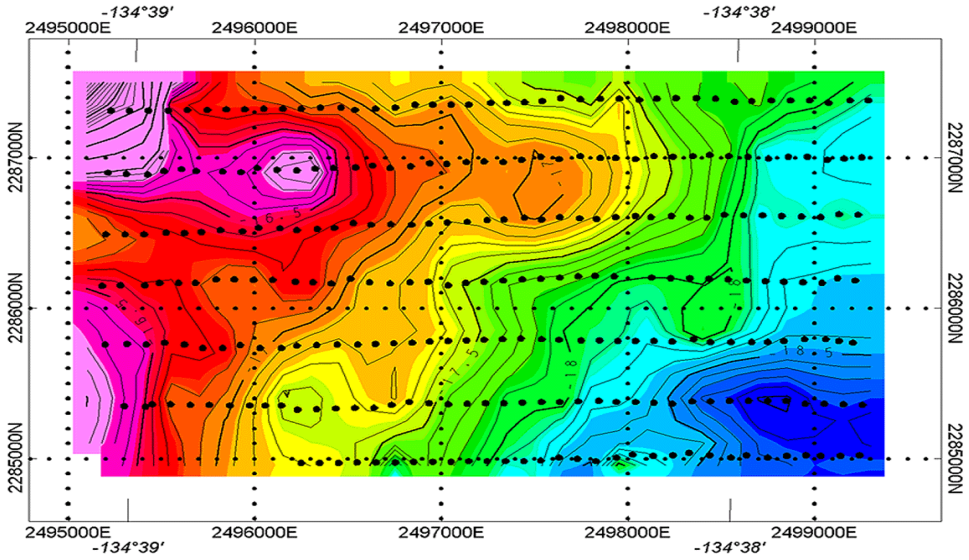

Figure 3: A contour map resulted from a gravity survey.

- **Magnetic method:**

The aim of a magnetic survey is to investigate subsurface geology on the basis of the anomalies in the earth's magnetic field resulting from the magnetic properties of the underlying rocks. In general, the magnetic content (susceptibility) of rocks is extremely variable depending on the type of rock and the environment it is in.

The magnetic properties of naturally occurring materials such as magnetic ore bodies and basic igneous rocks allows them to be identified and mapped by magnetic surveys. Strong local magnetic fields or anomalies are also produced by buried steel objects. Magnetometer surveys (Figure 4 and 5) find underground storage tanks, drums, piles and reinforced concrete foundations by detecting the magnetic anomalies they produce.

Figure 4: A magnetic survey where a magnetometer is used to detect the magnetic anomalies caused by buried steel objects.

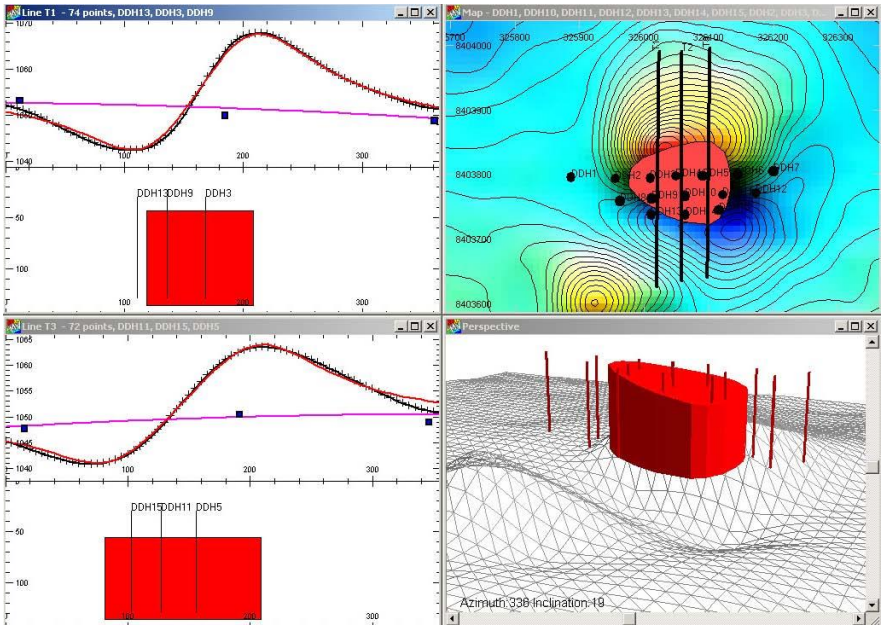

Figure 5: The results of a magnetic survey represented as a curve where the buried body is detected and interpreted.

- **Seismic method:**

The basic principle of all seismic methods is the controlled generation of elastic waves by a seismic source in order to obtain an image of the subsurface (Figure 6 and 7). Seismic waves are pulses of strain energy that propagate in solids and fluids. In a seismic survey elastic waves are generated by different energy sources (e.g., explosives, vibrator, weight-drop, sledgehammer). The seismic response is simultaneously recorded by a number of receivers (geophones, seismometers). These are positioned along straight profile lines (2D seismics) or over an area in 3-D seismic surveying and connected to a seismograph. The signals of individual geophones or groups of geophones are recorded by a seismograph, processed and displayed in seismic sections to image the subsurface structure.

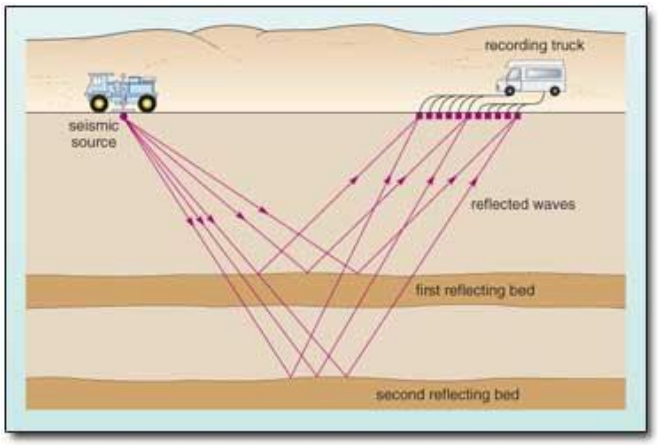

Figure 6: A plan of a seismic survey where the seismic waves are generated and pass through the ground and reflected back to the surface.

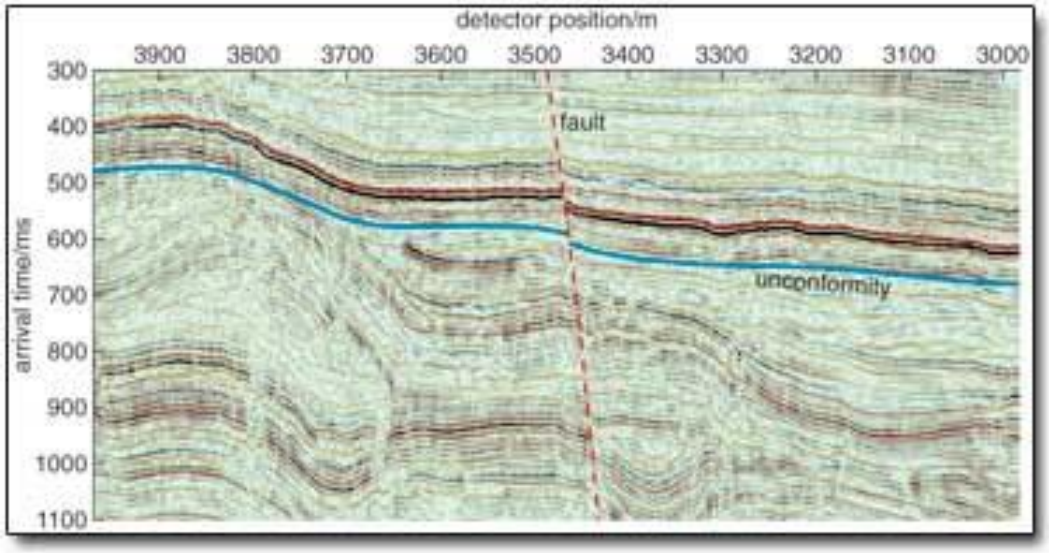

Figure 7: A seismic section resulted from a seismic survey where the geologic features are detected and interpreted.

- **Electric resistivity method:**

  This method utilize differences in electric potential to identify subsurface material. Surface electrical resistivity surveying is based on the principle that the distribution of electrical potential in the ground around a current-carrying electrode depends on the electrical resistivities and distribution of the surrounding soils and rocks (Figure 8). The usual practice in the field is to apply an electrical direct current (DC) between two electrodes implanted in the ground and to measure the difference of potential between two additional electrodes that do not carry current. All analysis and interpretation are done on the basis of direct currents. The distribution of potential can be related theoretically to ground. The resistivity sections (Figure 9) are correlated with ground interfaces such as soil and fill layers or soil-bedrock interfaces, to provide engineers with detailed information on subsurface ground conditions.

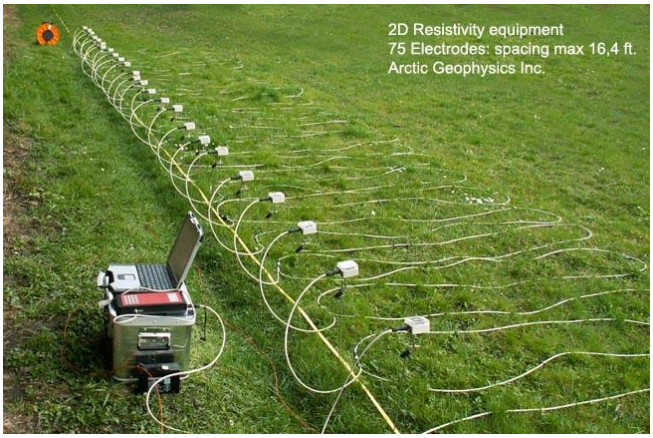

Figure 8: the resistivity survey where electric current is passed from the electrodes into the ground and the potential deference is measured at other electrodes.

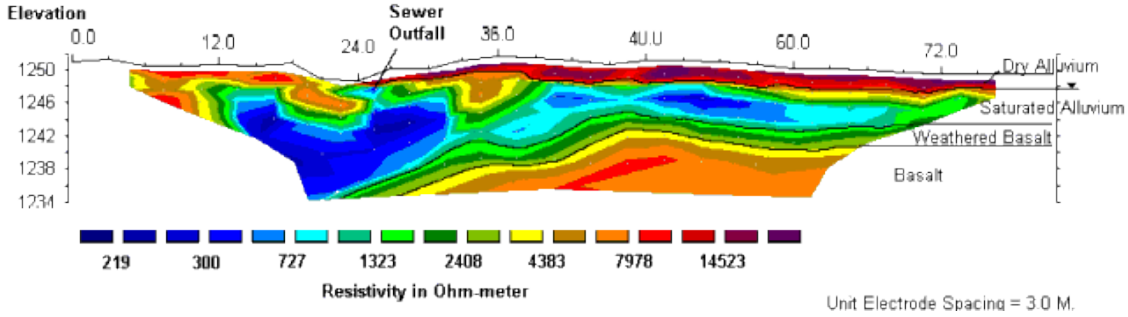

Figure 9: The resistivity section resulted by the electric resistivity survey.

What is data??

Data is a collection of facts, such as numbers, words, measurements, observations or even just descriptions of things. Data can be qualitative or quantitative.

- **Qualitative data** is descriptive information (it *describes* something)
- **Quantitative data** is numerical information (numbers)

In general, there are two types of data:

- Analogue data: are the tangible data, such as words on papers, audio tapes, printable images… etc.
- Digital data: the data when converted into the computers where the data are in the form of codes and program languages.

Geophysical data:

Recording of the geophysical data in the field is called **data acquisition.** During the acquisition, the geophysical data can be measured along **profiles** or on **grids.** Measuring the geophysical data along the profiles is performed when the measurement points (also called **stations**) are aligned along a straight line (Figure 10). In this case the data can be represented as curves where the measured value is varied with distance (Figure 10). In the grid survey, the measurement of the data is carried out along parallel profiles and perpendicular profiles (Figure 11). In some methods such as the gravity and magnetic methods, the intersection points of the parallel and perpendicular profiles represent the measuring stations. In this case, the measured data can be represented as contour maps where the data are plotted on the grid intersection points then contoured (Figure 11).

Geophysical data can be recorded in both analogue and digital form. Analogue geophysical data that are recorded into notes on papers and magnetic tapes or prints, such as the field sheets by which the electric data are recorded (Figure 12).

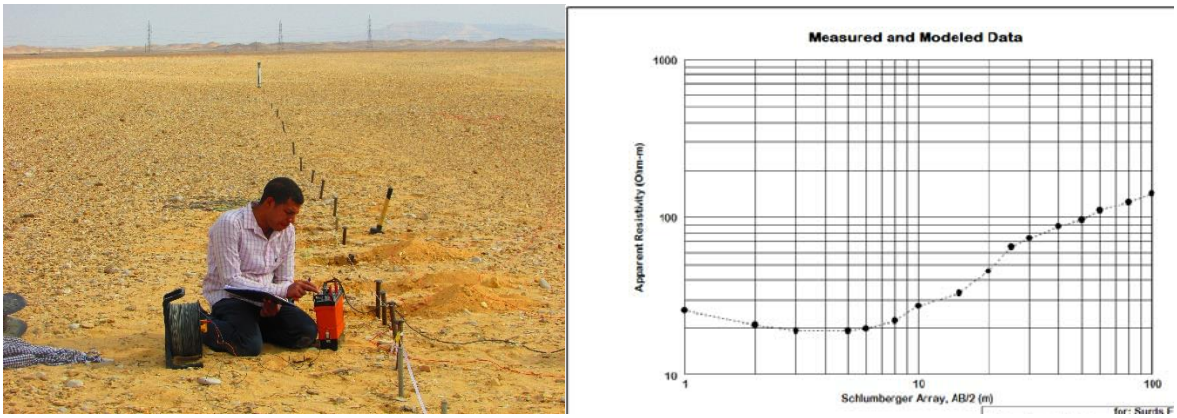

Figure 10: The acquisition of the electric resistivity data in the field along a straight profile. The acquired data are represented as a curve where the measured resistivity values are varied with the distance.

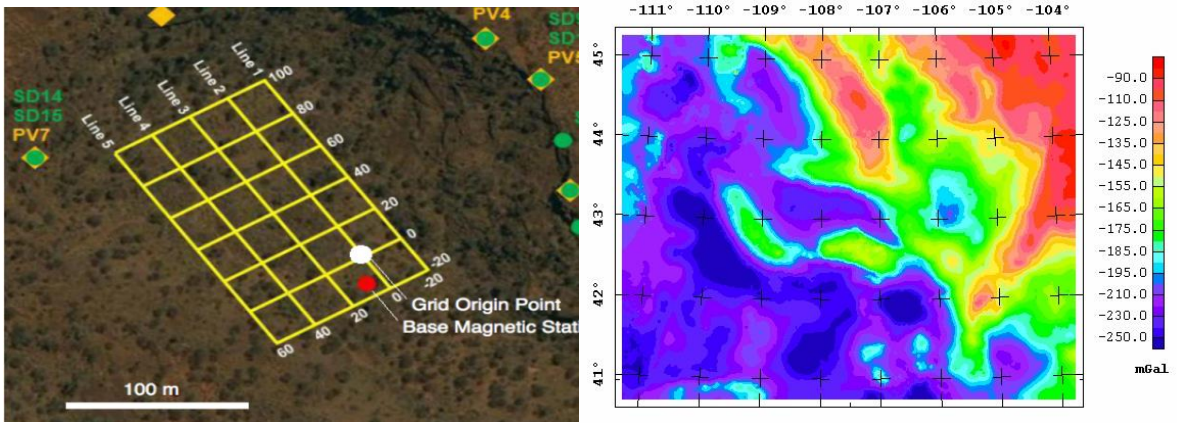

Figure 11:The acquiring of the magnetic data on a grid, where the measured data can be plotted on the map and contoured.

Figure 12: Recording the electric resistivity data on the field sheet.

The digital data that are recorded directly using computers, such as GPR and seismic data (Figure 13).

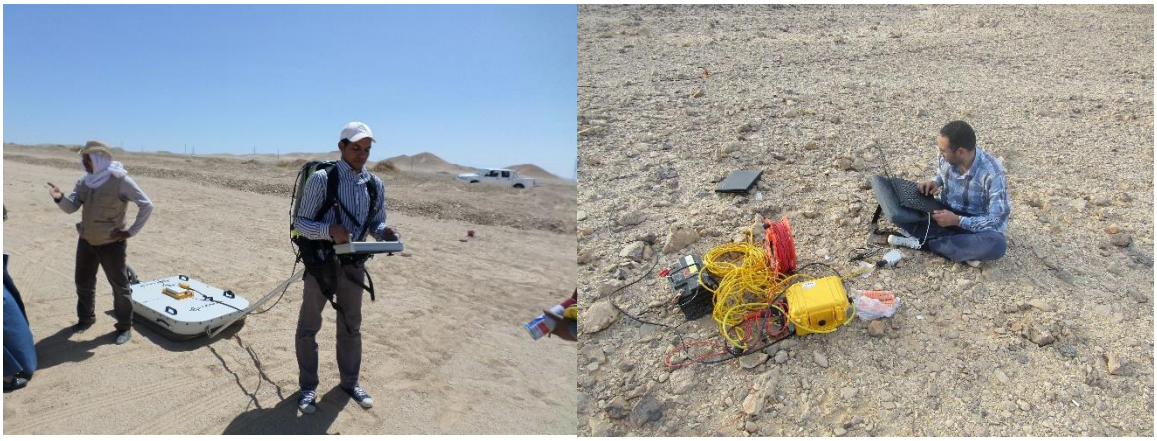

Figure 13: Recording the geophysical data digitally in the GPR and seismic methods.

Whether the data is analogue or digital, they have two forms during the acquisition. The measured geophysical data can be discrete or continuous. **Discrete** geophysical data are the data measured in discrete points (stations) and recorded as separate values. An example of these data is the data of the measured electric resistivity method that are recorded along points on each distance (Figure 14). The **continuous** geophysical data (also called signal) are those data which are recorded as continuous signal or connected points, such as the seismic data which are recorded as a continuous signal in a certain time span (Figure 15). Such data also have a waveform shape and thus can be also called **waveforms.**

(A)

Job I.D: Water N11° 22.157, E006° 19.134
Location: Federal Polytechnic along Bye-pass
L. G. A: Birnin Kebbi **Elevation: 556**
State: Kebbi **Date**: 11/06/2015
Instrument: Terrameter **Survey No:** VES 1

ELECTRODE SPACING IN METERS		RESISTIVITY READINGS IN OHMS	CALCULATED APPARENT RESISTIVITY IN OHMS M.	GEOMETRIC FACTOR	REMARKS
AB/2	MN/2				
1	0.5	154.7	371.28	2.4	
1.5	0.5	86.9	521.4	6.0	
2	0.5	62.2	746.4	12.0	
3	0.5	37.5	1012.5	27.0	
5	0.5	20.4	1591.2	78	
5	1	40.4	1535.2	38.0	
7	1	25.3	1897.5	75	
10	1	13.07	2038.9	156.0	
10	3	46.7	2241.6	48.0	
15	3	18.17	2053.2	113.0	
20	3	8.82	1808.1	205.0	
25	3	4.63	1495.5	323	
30	3	2.50	1167.5	467	
30	10	5.90	743.4	126	
35	10	4.65	823.05	177	
40	10	2.31	545.2	236	
50	10	3.35	1262.95	377	
60	10	2.54	1397.0	550	
70	10	7.83	5903.82	754	
80	10	3.08	3049.2	990	
90	10	3.48	4374.36	1257	
100	10	3.52	5473.6	1555	

(B)

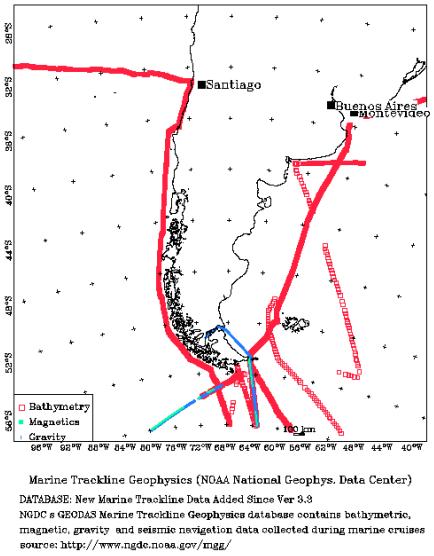

Figure 14: Example of discrete geophysical data, including: (A) the measured electrical resistivity data which are measured in points at different distances, and (B) the gravity data which are measured in points at fixed distances along a grid.

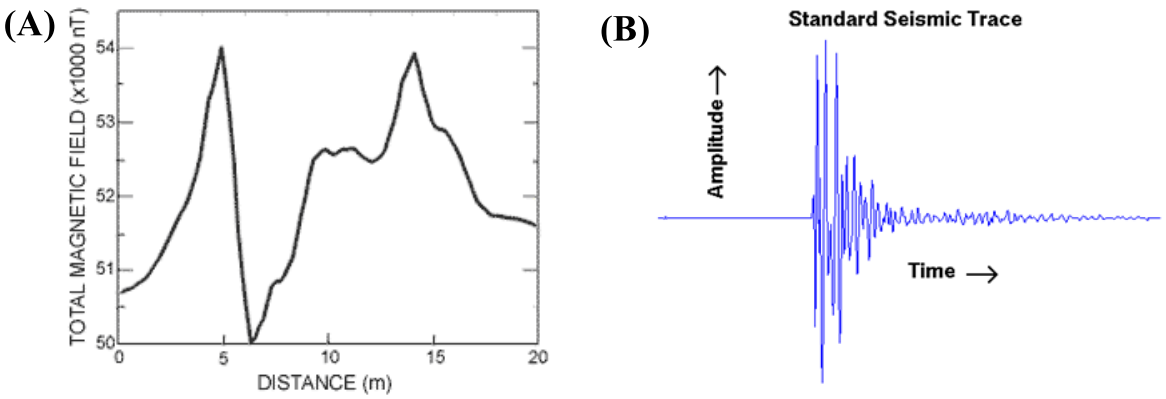

Figure 15: Example of continuous digital data including: (A) magnetic data represented as a curve composed of connected values plotted against distance, and (B) seismic signal that is recorded as a continuous signal in a specific time period.

Geophysical data domains:

The geophysical data domain is the dimension by which the geophysical data are measured in respect to. The dimensions by which the data are measured include the space dimension (x,y,z) and the time dimension (x,t). We refer to the data that measured in the space dimensions as being made in the **space domain** (such as the gravity and magnetic data), while those are measured both space and time as being recorded in the **time domain** (such as the seismic data). The data measured in the space domain are recorded at several points at fixed distances along a profile or grid (Figure 16 A and 17 A). For each of these points, the measured value will have three coordinates; the x coordinate (may represent the longitude), the y coordinate (may represent the latitude), and z which represent the measured physical property. The data measured in the time domain are recorded in a specific time period for each point at fixed distances (Figure 16 B and 17 B).

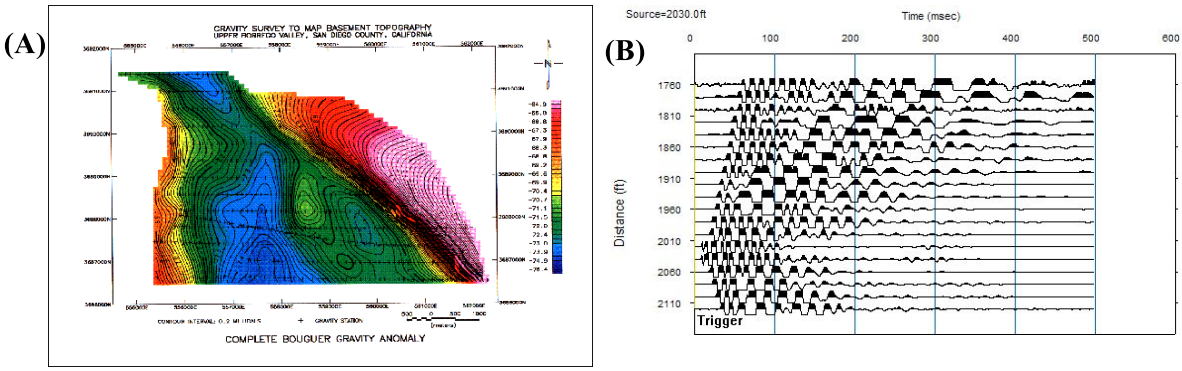

Figure 16: (A) an example of the geophysical data in the space domain where the gravity data are contoured in respect to longitude (x), latitude (y) and measured gravity (z). (B) An example of the geophysical data in the time domain where the seismic data are recorded at each distance (x) in a specific time period (t).

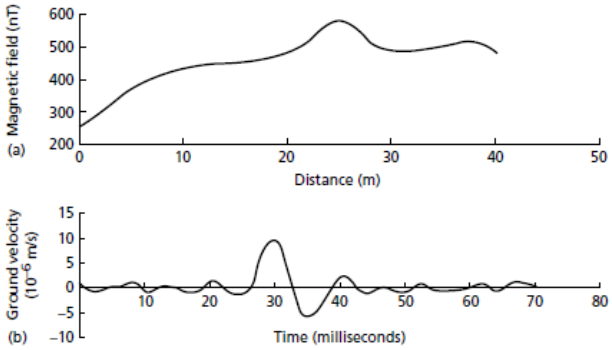

Figure 17: (a) A graph showing a typical magnetic field strength variation which may be measured along a profile. (b) A graph of a typical seismogram, showing variation of particle velocities in the ground as a function of time during the passage of a seismic wave.

What is data processing??

Data processing is the series of operations that are carried out on data, especially by computers, in order to present, interpret, or obtain information.

Signal processing in Geophysics typically involves sampling continuous signals in time or space in order to:

- Removing noise i, e, enhancement of the geophysical data,
- understand the source of the signal,
- understand the media through which the signal passes.

Noise in geophysics can be defined as the unwanted signals that interfere with the real geophysical data. Such noise has many sources and can distort the geophysical data. The geophysicist's task is to separate the 'signal' from the 'noise' and interpret the signal in terms of ground structure. So, processing methods are primarily applied to the measured data in order to remove this noise and thus enhancing the data, making them in a form that can be easily interpreted (Figure 18).

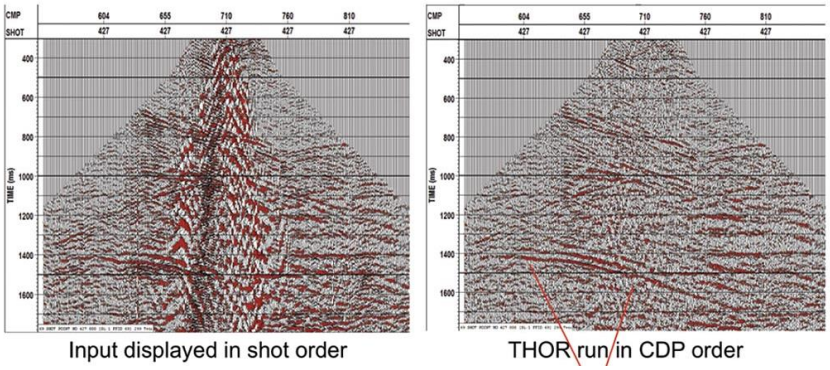

Figure 18: An example of removing the noise from seismic data.

Digitization of geophysical data

The geophysical analogue data can be converted into digital data when transported to the computers manually (Figure 19) or automatically. This process is called **analogue-to-digital conversion.** Modern devices can record the data as analogue data then convert the data automatically to digital form with a unit called **A/D convertor** (Analogue-to-Digital convertor).

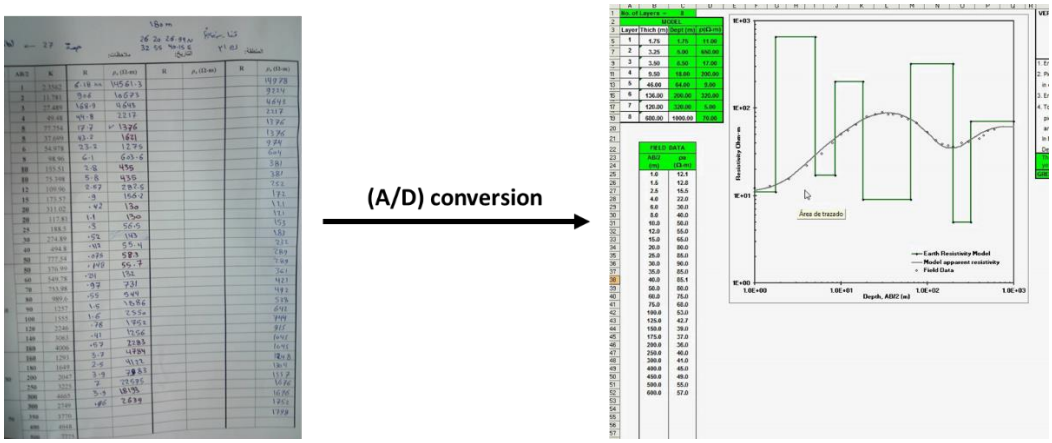

Figure 19: An example of converting measured electric data into digital data.

Also, when the data recorded in analogue form, they can be converted to the digital form through a process called **digitization** or **sampling**. Waveforms of geophysical interest are generally continuous (analogue) functions of time or distance. To apply the power of digital computers to the task of analysis, the data need to be expressed in digital form, whatever the form in which they were originally recorded. Computers require discrete values for computation so geophysical data must be *digitized* for analysis. Gravity and magnetic measurements are inherently discrete because the instruments are moved from point to point where time is required to make a reading. Seismic and electromagnetic sensors electronically measure time domain signals continuously. Ideally, digitizing is performed at equal time or space intervals. Digitization can be applied to the data in both curve or map forms.

A continuous, smooth function of time or distance can be expressed digitally by sampling the function at a fixed interval and recording the instantaneous value of the function at each sampling point. Thus, the analogue function of time f(t) shown in Figure 20 (a) can be represented as the digital function g(t) shown in Figure 20 (b) in which the continuous function has been replaced by a series of discrete values at fixed, equal, intervals of time. This process is inherent in many geophysical surveys, where readings are taken of the value

of some parameter (e.g. magnetic field strength) at points along survey lines. The extent to which the digital values faithfully represent the original waveform will depend on the accuracy of the amplitude measurement and the intervals between measured samples. Stated more formally, these two parameters of a digitizing system are the sampling precision (dynamic range) and the sampling frequency. **In other words, when digitizing a signal, we have; amplitude sampling and time/distance sampling.**

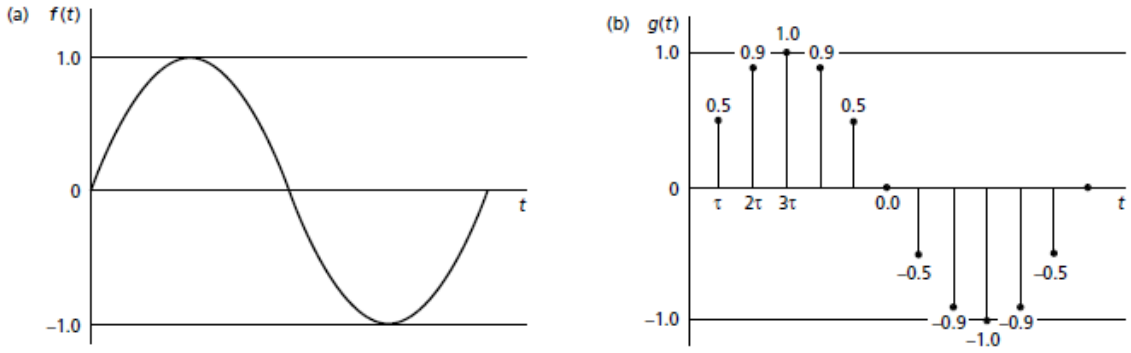

Figure 20: (a) Analogue representation of a sinusoidal function. (b) Digital representation of the same function.

1. Signal Amplitude Sampling:

What is amplitude??

The distance from the x-axis to any part of the waveform. It can be positive or negative.

Amplitude sampling is often not within our control since commercial equipment will have an *A-to-D converter* that operates with a fixed, finite number of *bits*. The amplitude values are recorded as binary numbers where each digit is a 0 or 1. Each binary digit is called a bit; the binary number represented by a sequence of bits is called a *word*. **A word is used to represent the amplitude of the signal at a particular time or space.**

Geophysical recording systems are often rated by the number of bits used in A-to-D conversion. New, modern systems typically have 16-24 bits. Another common way of describing the performance of digital equipment is to use the ratio of the full recording range to the step size. This ratio of the largest possible recorded signal to the smallest one is called the dynamic range and is expressed in decibels or dB.

2. Time (Space) Sampling:

In digital recording, the signal amplitudes are sampled at discrete (fixed), equally spaced times or distances. The distance between every time or distance sample is called **sample**

interval (Δt or Δx). The number of sampling points in unit time or unit distance is called **sampling frequency.**

Thus, if a waveform is sampled every two milliseconds (sampling interval), the sampling frequency is 500 samples per second (or 500 Hz). The sampling interval must be chosen to avoid or minimize aliasing. Aliasing is the distortion of the signal. If the sampling interval is too small, you will record much more data than necessary resulting in excessive storage requirements and redundant data. If the sampling interval is too large, it's much worse. In fact, the recorded data may be totally worthless since the entire spectral (frequency) content of the signal can be distorted.

To do so, the maximum frequency (fmax) of a signal should be known first. In this case, the proper sample interval should be chosen as follows:

$$Fmax>1/2\ \mathbf{\Delta t\ (or\ 1/2\ \Delta x)}$$

Frequency of half the sampling frequency is known as the *Nyquist frequency* (f_N) and the *Nyquist interval* is the frequency range from zero up to fN:

$$fN=1/2\ \Delta t$$

In other words, Nyquist frequency is the highest frequency observed in digital data. Nyquist has to be higher than all of the frequencies in the observed signal to allow perfect reconstruction of the signal from the samples.

Spectral Analysis

What is spectral analysis?

Analysis of the frequency content of geophysical data is called *spectral analysis.*

Geophysical data collected in the space domain have ***spatial frequencies*** which are expressed in cycles/distance, e.g., cycles/km or cycles/m. While geophysical data acquired in the time domain have ***temporal frequency*** expressed in cycles/second.

One can usually visualize frequency components in geophysical data while still in the space or time domains. For example, we can easily identify three very different frequency components in the magnetic data shown in Figure 1. One is at approximately 1 cycle/4 m, one is at 1 cycle/2 m, and one is at 1 cycle/1 m. There are many more frequency components in this magnetic signal, but they are not as easy to identify with the eye.

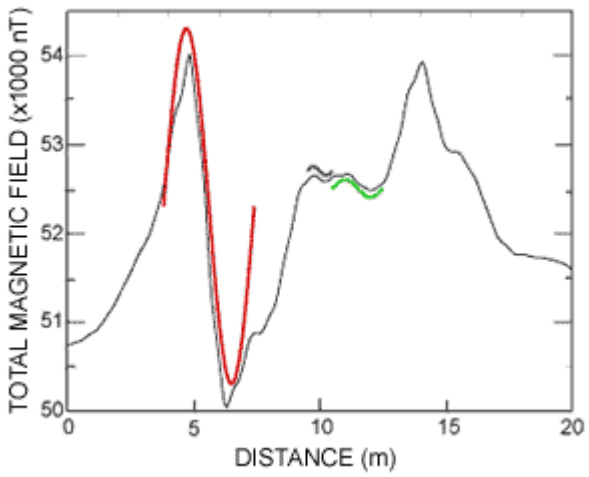

Figure 1: Visualizing spatial frequency components in space domain magnetic data.

Fourier analysis describes how to obtain all of the spectral components. Fourier analysis works because geophysical signals (with very few exceptions) can be made up exclusively of trigonometric functions (sines and cosines). For some signals, the number of frequency components is only a few, for others it literally takes an infinite number of frequency contributions to construct the complex waveform. To understand Fourier analysis, we should first know what the frequency domain is.

Frequency domain:

The **frequency domain** refers to the analysis of signals with respect to frequency, rather than time or distance. A time or distance-domain graph shows how a signal changes over time or

distance, whereas a frequency-domain graph shows how much of the signal lies within each given frequency band over a range of frequencies.

For each domain (*t*,*x*,*y*,*z*) we have a corresponding frequency (ω, k_x, k_y, k_z). The *k*'s are spatial frequencies, $\omega$is the temporal frequency.

A given signal can be converted between the time/distance and frequency domains with a pair of mathematical operators called transforms. An example is the Fourier transform, which converts a time or distance function into a sum or integral of sine or cosine waves of different frequencies, each of which represents a frequency component. The '**spectrum**' of frequency components is the frequency-domain representation of the signal. For any geophysical signal, it can be expressed in the frequency domain by the **amplitude and phase** of its constituent sine or cosine waves as a function of frequency. So, there will be two spectra for a signal; **amplitude spectra** which is the plot of signal amplitude as a function of frequency and **phase spectra** which is a plot of the signal phase as a function of frequency. They can be combined into a complex spectrum known as **frequency spectrum.**

Phase is the position of a point in time (an instant) on a waveform cycle. It is expressed in radians (π, 2π, 3π…._) or degrees as shown in Figure 2.

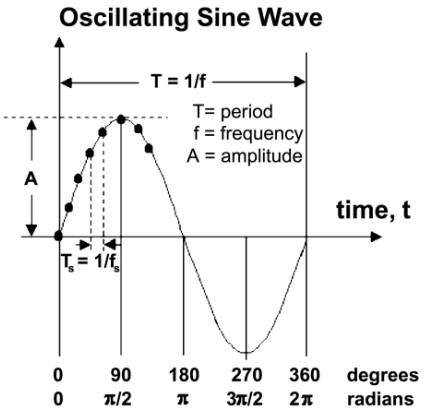

Figure 2: A graph shows one cycle constitutes 360º of phase.

Why we do spectral analysis?

Viewing geophysical data in the frequency domain can more clearly reveal the sought after features in the measurements. For example, gravity and magnetic data with higher spatial frequency content are sensing smaller and/or shallower subsurface variations while low frequencies originate from deeper layers compared to high frequency data. Solving the geophysical problems in the time or distance domains is done with the differential equations

which are hard to be performed. While converting the data into the frequency domain makes use of the algebraic equations which are easier to be performed.

Fourier Analysis:

Fourier analysis is based on that most geophysical signals can be expressed as a decomposition of the signal into sine and cosine functions of different frequencies (also referred to as *harmonics*). These sine and cosine functions expressed as a *Fourier series* are used to represent a periodic function of time. For example, the complex waveform of Figure 3 is built up from the addition of the two individual sine wave components.

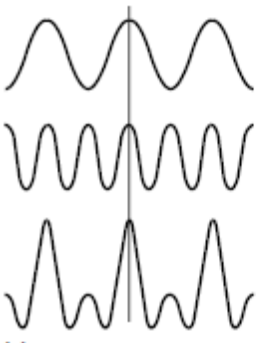

Figure 3: Complex waveforms resulting from the summation of two sine wave components of frequency f and 2f. The two sine wave components are of equal amplitude and in phase

Sine and cosine waves are signal waveforms which are identical to each other. The main difference between the two is that cosine wave leads the sine wave by an amount of 90 degrees (1/4 cycles) in Figure 4.

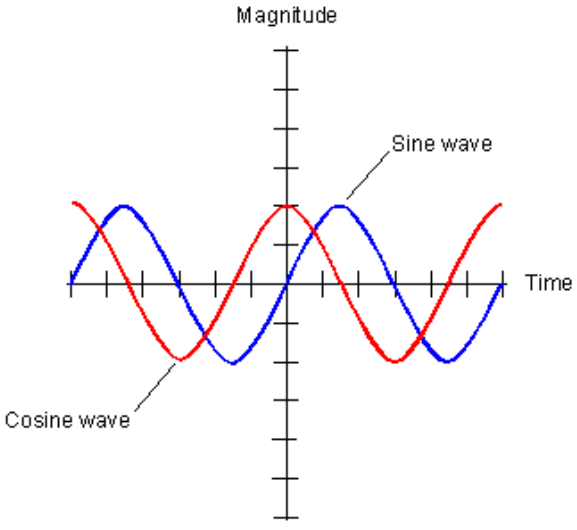

Figure 4: plot of sine and cosine waves

To express any waveform in terms of its constituent sine wave components, it is necessary to define not only the frequency of each component but also its **amplitude and phase**.

The main process by which Fourier analysis is performed is called **Fourier Transformation.**

Simply, a time or space domain data (t, x, y, z) can be converted into frequency domain (ω, Kx, Ky, Kz) using Fourier transform, and the resulted frequencies can be then converted back into the space and time domain using **inverse Fourier transform**. This can be expressed as:

$$f(t) \leftrightarrow F(\omega)$$

$$f(x) \leftrightarrow F(K)$$

Mathematically, for the continuous signal f(t) can be expressed as the Fourier integral:

$F(\omega) = \int_{-\infty}^{\infty} f(t)\, e^{-i2\pi\omega t}\, dt$ Fourier transform of f(t)

$f(t) = \int_{-\infty}^{\infty} F(\omega)\, e^{i2\pi\omega t}\, d\omega$ Inverse Fourier transform

The *inverse Fourier transform* recovers f(t) back from F(ω). These equations are at the heart of spectral analysis and they are so tightly connected that they are usually called the ***Fourier transform pair*.** F(ω) and f(t) are referred to as the frequency domain and time domain representations of the signal, respectively and are also called Fourier pair.

The transform kernel exp(i2πωt) can be expressed as:

$$e^{i2\pi\omega t} = \cos 2\pi\omega t + i \sin 2\pi\omega t$$

this equation shows that the Fourier transform pair have sine and cosine terms. It is clear that the Fourier transform is really the expression of a infinite, continuous "summation" of sine and cosine functions. In fact, the Fourier transform can be expressed using separate sine and cosine transforms. So, Fourier analysis expressed by the Fourier transform is simply **the decomposition of a signal into its composite frequency (sine and cosine) components.** Therefore, for a given signal, there will be **sine transform** and **a cosine transform**.

Filtering

1- What is filtering?

Filtering describes the process when *input* signal being modified or transformed into a new *output* signal. Filtering modifies a waveform by discriminating between its constituent wave components to alter their relative amplitudes or phase relations, or both. Filtering is used in geophysical data processing to remove unwanted signals (**noise**). Noise is defined on the data records based on its characteristic frequency components. So, filtering is used to remove the frequencies of the noise and leave the frequencies of the data sources. It is also used to emphasize a certain frequency.

Filtering can be applied in the space/time domain and the frequency domain. When it is applied in the space or time domain, it is called **digital filtering**. It is used for in case of small data sets and also might be used during data acquisition in the presence of a noise source with a known frequency. This process is called **acquisition filtering**.

When the filtering processes are applied in the frequency domain, it is called **frequency filtering**. It is applied to the data after transforming them through Fourier transformation into their frequency components. Frequency filtering is usually used in case of large datasets. This is because, in this case, the time domain operations become more complicated and will require longer time.

2- Digital filtering

In the beginning, a filter is a tool that is designed based on the data itself. It might be frequencies or just digital values that interact mathematically with the data. This interaction between the data and the filter alters or modifies the original data and produces an output data that is free of unwanted signals. In case of digital filtering, the mathematical processes that describes the filtering operations are:

A) Convolution
B) Deconvolution
C) Cross-correlation

These operations quantitatively describe how a waveform is affected by a filter.

A- Convolution:

Convolution is a mathematical operation defining the change of shape of a waveform resulting from its passage through a filter. Thus, for example, a seismic pulse generated by an explosion is altered in shape by filtering effects, both in the ground and in the recording system, so that the seismogram (the filtered output) differs significantly from the initial seismic pulse (the input). In this case, an input signal s(t) is convolved with the filter, then producing an output signal y(t) [figure 1]. The output signal that is produced by filtering through the convolution process is called **filter effect or filter response.**

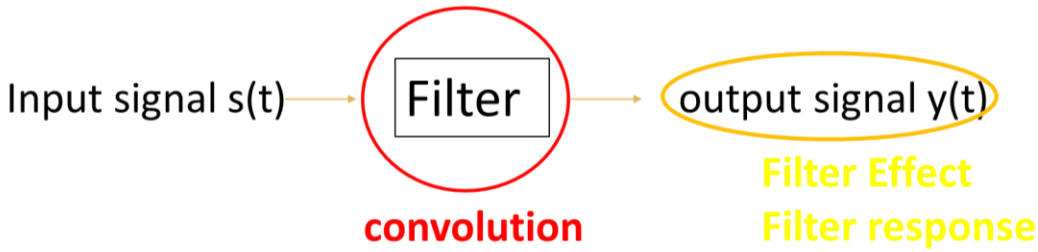

Figure 1: Illustration of digital filtering operation

When the input signal is in the form of a spike function (spike function is a single data point in time with a define amplitude value.. in other words; it is a single digital data sample), the output of the filtering operation on this signal will be in the form of a single waveform (or pulse) [figure 2]. In this case, the filter response is called the **impulse response**. Impulse response is defined as the output of the filter when the input is a spike function. This will have a great importance later in the deconvolution process.

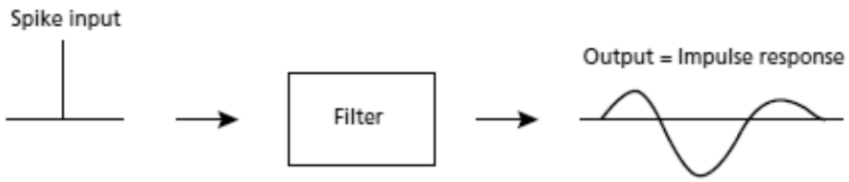

Figure 2: The impulse response of a filter.

The effect of a filter is described mathematically by a convolution operation such that, if the input signal g(t) to the filter is convolved with the impulse response f(t) of the filter, known as the **convolution operator**, the filtered output y(t) is obtained:

$s(t)*f(t)=y(t)$

where the asterisk denotes the convolution operation.

Figure 3(a) shows a spike function input to a filter and its impulse response in figure 3(b) that represents the output for a spike input. Figure 3(c) shows an input comprising two separate spike functions and the filtered output (Figure 3(d)) is now the superposition of the two impulse response functions offset in time by the separation of the input spikes and scaled according to the individual spike amplitudes. Since any transient wave can be represented as a series of spike functions (Fig. 3(e)), the general form of a filtered output (Fig. 3(f)) can be regarded as the summation of a set of impulse responses related to a succession of spikes simulating the overall shape of the input wave.

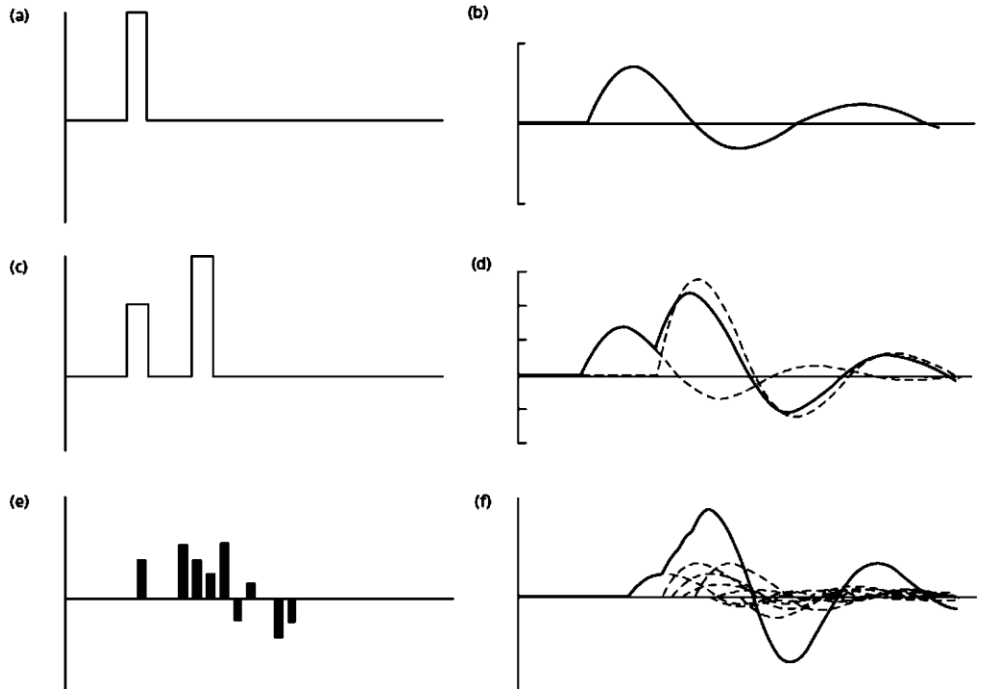

Figure 3: Examples of filtering. (a) A spike input. (b) Filtered output equivalent to impulse response of filter. (c) An input comprising two spikes. (d) Filtered output given by summation of two impulse response functions offset in time. (e) A complex input represented by a series of contiguous spike functions. (f) Filtered output given by the summation of a set of impulse responses.

The mathematical implementation of convolution involves time inversion (or folding) of one of the functions and its progressive sliding past the other function, the individual terms in the convolved output being derived by summation of the cross-multiplication products over the overlapping parts of the two functions. In Fig 4 the individual steps in the convolution process are shown for two digital functions, a double spike function given by g(t) = 2, 0, 1 and a filter function f(t) = 4, 3, 2, 1, where the numbers refer to discrete amplitude values at the sampling points of the two functions.

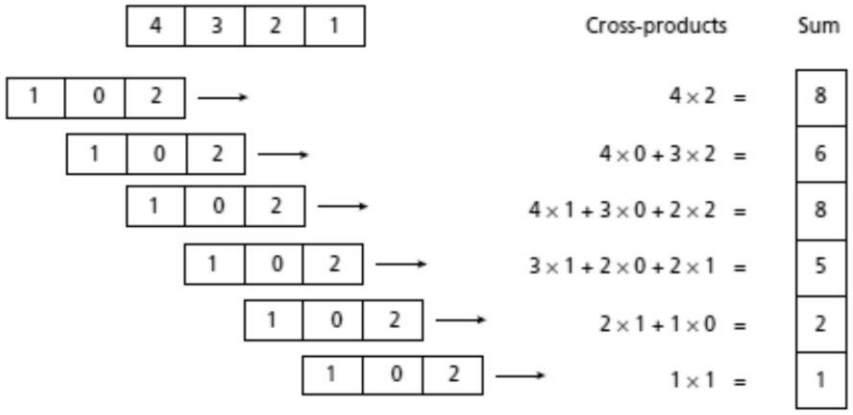

Figure 4: A method of calculating the convolution of two digital functions.

The convolution of two functions in the time domain becomes increasingly laborious as the functions become longer. Typical geophysical applications may have functions which are each from 250 to a few thousand samples long. The same mathematical result may be obtained by transforming the functions to the frequency domain, and applying the frequency filtering. The resulting output amplitude and phase spectra can then be transformed back to the time domain. Thus, digital filtering can be enacted in either the time domain or the frequency domain. With large data sets, filtering by computer is more efficiently carried out in the frequency domain since fewer mathematical operations are involved.

B- Deconvolution:

Deconvolution or inverse filtering is a process that counteracts a previous convolution (or filtering) action. Consider the convolution operation given in the equation:

g(t)*f(t)=y(t)

y(t) is the filtered output derived by passing the input waveform g(t) through a filter f(t). Knowing y(t) and f(t), the recovery of g(t) represents a deconvolution operation:

y(t)*f`(t)=g(t)

The function f`(t) represents the deconvolution operator. Deconvolution is an essential aspect of seismic data processing, being used to improve seismic records by removing the adverse filtering effects encountered by seismic waves during their passage through the ground.

C- Correlation:

Cross-correlation of two digital waveforms involves cross-multiplication of the individual waveform elements and summation of the cross-multiplication products over the common time interval of the waveforms. The cross-correlation function involves progressively sliding one waveform past the other and, for each time shift, or lag, summing the cross-multiplication products to derive the cross-correlation as a function of lag value. The cross-correlation operation is similar to convolution but does not involve folding of one of the waveforms. Example of the cross-correlation of two functions; Waveform1 (2, 1, -1, 0, 0) and Wavefrom2 (0, ,0, 2, 1, -1) is shown in Figure 5.

				2	1	-1	0	0					Output	Lag
0	0	2	1	-1									-2	-4
	0	0	2	1	-1								1	-3
		0	0	2	1	-1							6	-2
			0	0	2	1	-1						1	-1
				0	0	2	1	-1					-2	0
					0	0	2	1	-1				0	1
						0	0	2	1	-1			0	2
							0	0	2	1	-1		0	3
								0	0	2	1	-1	0	4

Figure 5: A method of calculating the cross-correlation of two digital functions.

An important application of cross-correlation is in the detection of weak signals embedded in noise. If a waveform contains a known signal concealed in noise at unknown time, cross-correlation of the waveform with the signal function will produce a cross-correlation function centred on the time value at which the signal function and its concealed equivalent in the waveform are in phase (Fig. 2.14).

A special case of correlation is that in which a waveform is cross-correlated with itself, is called **autocorrelation**.

2-Frequency filtering:

Signal and noise:

Waveform data is a combination of signal and noise. The signal is that part of the waveform that relates to the geological structures under investigation. The noise is all other components of the waveform.

The relative amounts of signal and noise in a measurement are quantified by the signal-to-noise ratio (SNR). Signal-to-noise ratio is a ratio that compares the level of a desired signal to the level of background noise. A ratio higher than 1:1 indicates more signal than noise. Lower SNR indicates noisy data that needs special processing.

There are two kinds of noises found in seismic data: random noise and coherent noise.

A. Random noise:

Random noise is noise generated by activities in the environment where seismic acquisition work is being carried out. In a land acquisition, random noise can be created by the acquisition truck, vehicles, and people working in the survey area, wind, electrical power lines, and animal movement. This noise is not repetitive or continuous and appears in a seismic record as spikes (Figure 6). In a marine acquisition, random noise can be created by ship props, drilling, other seismic boats, and wind/tidal waves.

Random noise can be reduced or removed from data by repeating the acquisition or, filtering during acquisition or processing.

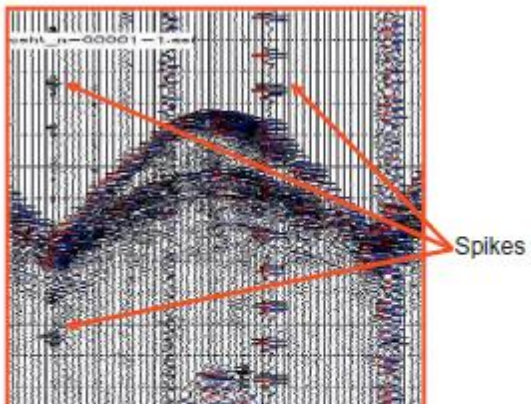

Figure 6: an example of seismic data containing random noise in the form of spikes

B. Coherent or source -generated noise:

Source-generated noise is created by the seismic source. Source-generated noises are coherent noise trains and they exist in an organized form from trace to trace (in all the data records) and yet they contain no geologic information. Source-generated noises essentially obscure the entire desired primary reflection. Source-generated noises noticed in seismic records are:

- Groundroll
- Guided waves
- Side-scattered noise
- Cable noise
- Air waves
- Power lines

1- Groundroll:

Ground roll (Rayleigh wave) is a type of coherent noise observed in seismic field record. Ground roll occurs as a set of dispersed wave trains with low velocity, low frequency, and high amplitude. Ground roll can obscure the primary reflected events and degrade overall data quality (Figure 7). Lateral inhomogeneities in the near surface layer increases the effect of the groundroll. They can be suppressed in the field by modifying the receiver arrays or later by filtering.

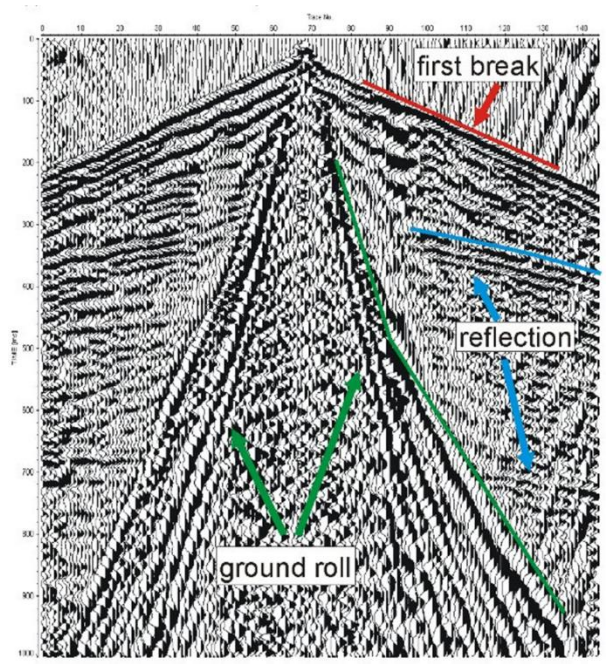

Figure 7: An example of seismic data containing groundroll noise.

2- Guided waves:

Guided waves are occurred in the shallow marine records due to the strong contrast between the water layer and the substratum. This causes the seismic waves trapped within and guided laterally through the water layer (Figure 8). They can be suppressed by CMP stacking and filtering.

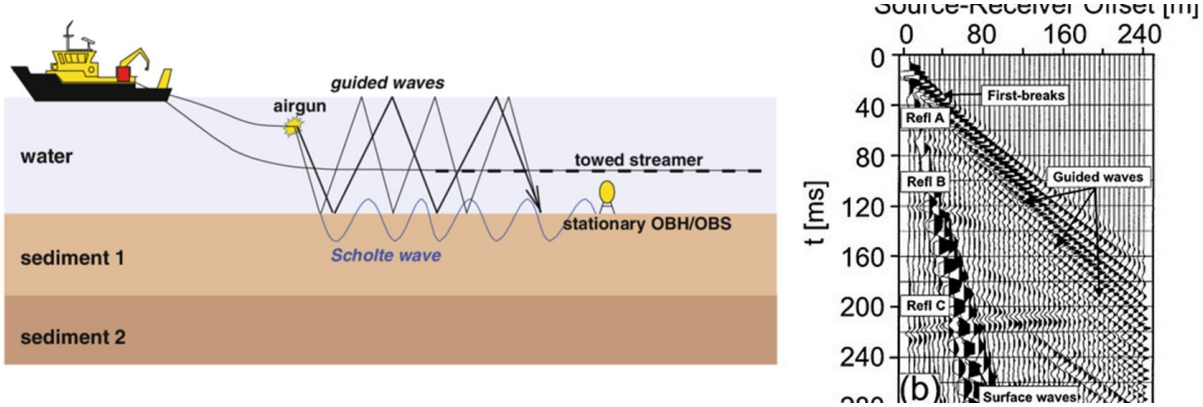

Figure 8: Illustration of the creation of the guided waves during a marine survey as well as the form of the guided wave noise in a seismic record.

3- Side-scattered noise:

They are caused by irregular water bottom surface where irregularities act as point sources that diffract the seismic waves (figure 9).

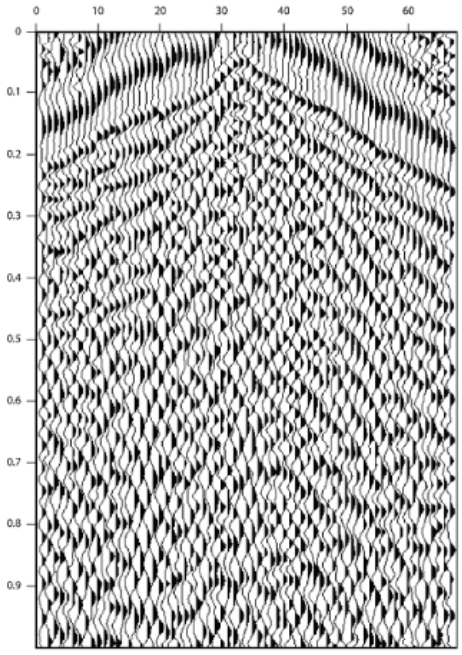

Figure 9: A seismic shot record showing contamination with strong side-scattered noise.

4- Cable noise:

They are linear and low-amplitude and low-frequency noise that appear on data as later arrivals (Figure 10).

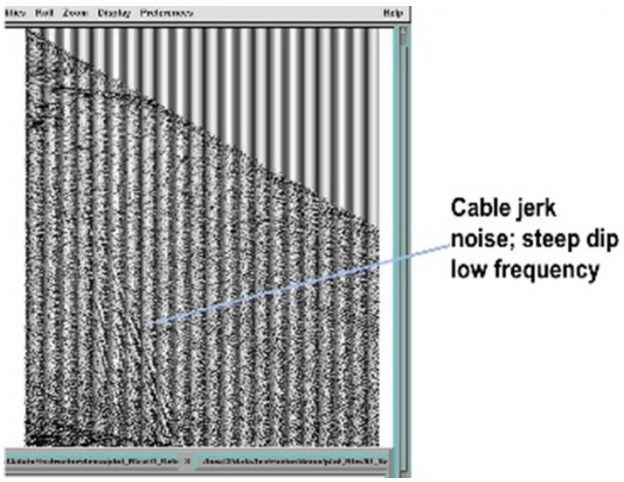

Figure 10: A seismic record containing cable noise.

5- Air waves:

They are caused by surface charges (explosives) when are used as seismic sources during a seismic survey. It has a velocity of 300 m/s and low frequency and appeared as shown in figure 11. They can be removed by notch filters.

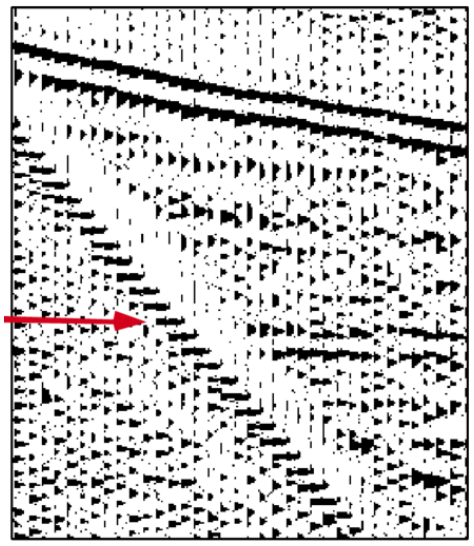

Figure 11: A seismic record containing the air waves noise, which illustrated by the red arrow.

6- Power lines noise:

Power lines cause noisy traces in the form of monofrequency wave (50-60 Hz) (Figure 12). They can be removed by notch filters during acquisition (acquisition filters).

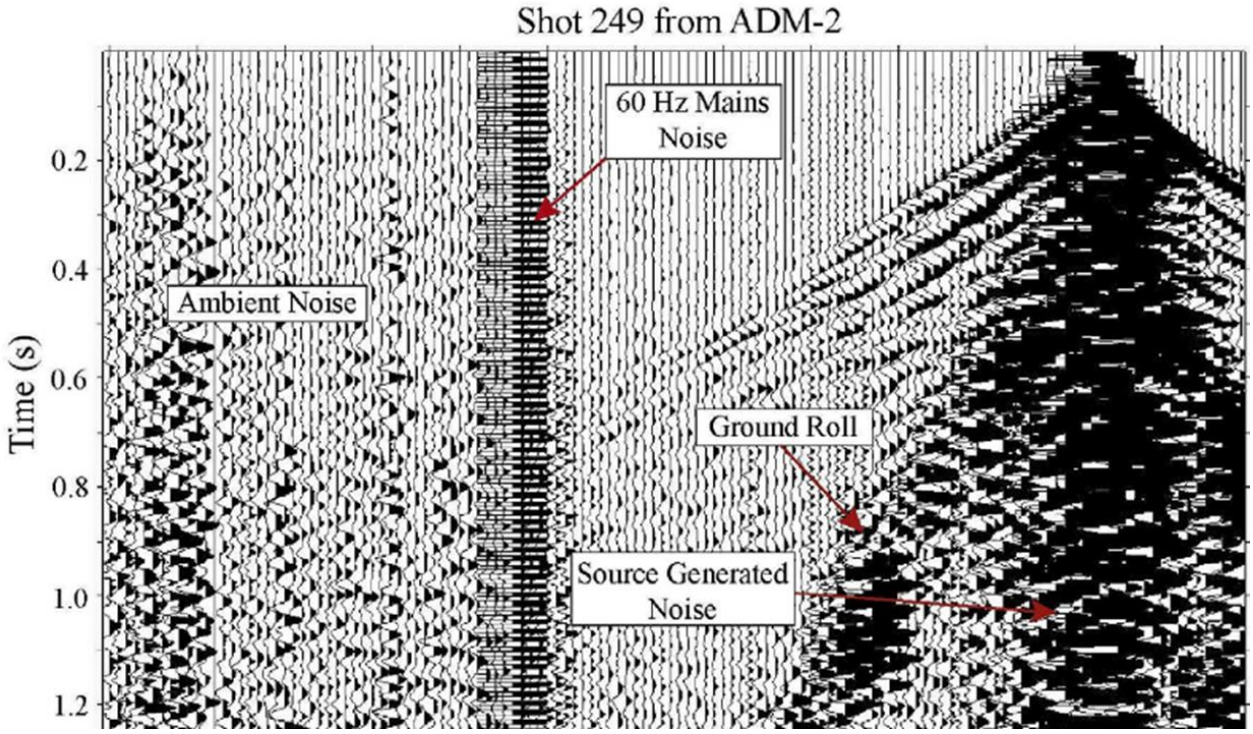

Figure 12: A shot record shows power line noise contamination.

7- Multiples:

Multiples are seismic energy that has been reflected more than once. They are occurred at the marine seismic surveys due to the great acoustic impedance (density*velocity) between the water and the seabed. Multiple reflections are produced when energy from the seismic shot travels down to the seabed, then up to the surface, reflecting multiple times and are appeared as separated reflections on the data (Figure 13).

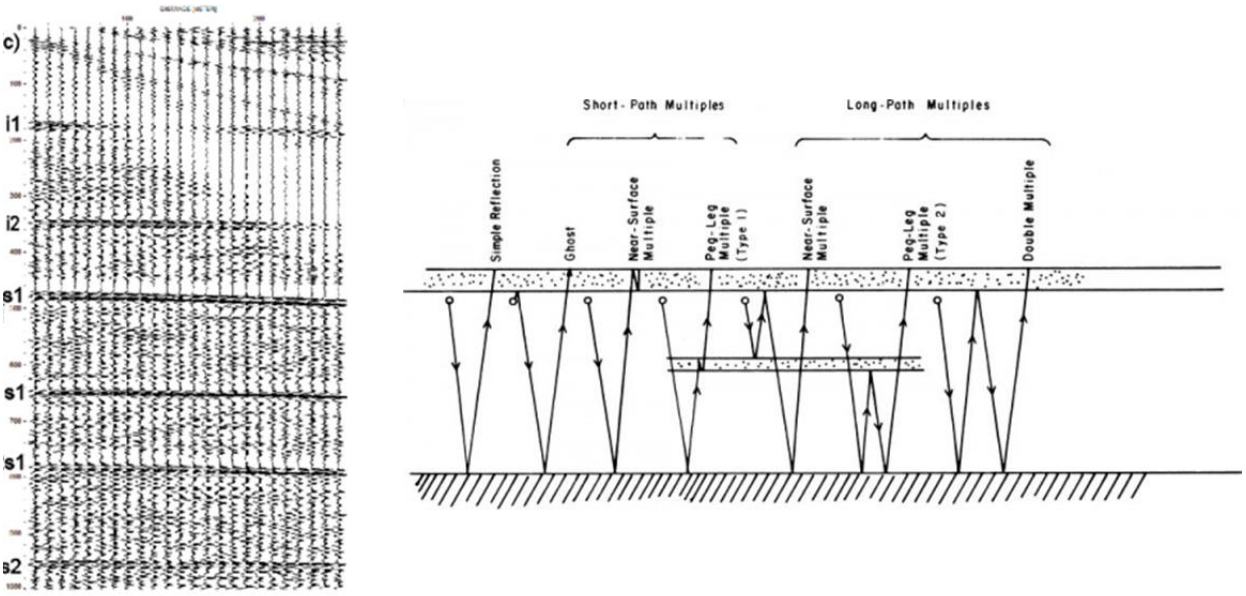

Figure 13: An illustration of the multiples on seismic record and how they are formed.

Frequency filters:

Frequency filters discriminate against selected frequency components of an input waveform. They are employed when the signal and noise components of a waveform have different frequency characteristics and can therefore be separated on this basis.

Noise may be removed by identifying the characteristic frequencies of that noise and designing a special filter to remove it. The characteristics of the noise can be detected through spectral analysis.

In the digital filtering, the filter operates by the convolution process but in frequency filtering, multiplication is the mathematical process that applied to the filter. In other words, **convolution in the time domain is equivalent to multiplication in the frequency domain**. Multiplication is simple and easy to apply for large datasets than convolution.

Types of frequency filters (Figure 14):

A- Low-pass (high-cut) filter (Fig. 14A):

This filter removes the frequencies higher than a specified cut-off frequency value and passes signals with a frequency lower than this cut-off frequency.

$$LP(f) = \begin{cases} 1 \; for \; f \leq f_c \\ 0 \; elsewhere \end{cases}$$

Where f is the required frequency and fc is the cut-off frequency. 1 means the filter should keep the amplitudes of the frequencies that achieve the condition. 0 means that the amplitudes of the frequencies that do not achieve the condition will be equal to zero, i.e they will be removed

B- High-pass filter (Fig. 14B):

This filter passes signals with a frequency higher than a certain cutoff frequency and removes signals with frequencies lower than the cutoff frequency.

$$HP(f) = \begin{cases} 1 \; for \; f \geq f_c \\ 0 \; elsewhere \end{cases}$$

C- Band-pass filter (Fig. 14C):

This filter keeps the specified frequency band between a low- and a high-frequency cut-off value (fc1 and fc2, respectively). In other words, it passes frequencies within a certain range and rejects (attenuates) frequencies outside that range.

$$BP(f) = \begin{cases} 1 \; for \; f_{c1} \leq f \leq f_{c2} \\ 0 \; elsewhere \end{cases}$$

D- Notch (band-reject) filter (Fig. 14D):

This filter removes only one specified frequency value or a very narrow frequency band typically used to filter out specific monofrequency noise components such as 50- or 60-Hz powerline interference.

$$BR(f) = \begin{cases} 0 \; for \; f_{c1} \leq f \leq f_{c2} \\ 1 \; elsewhere \end{cases}$$

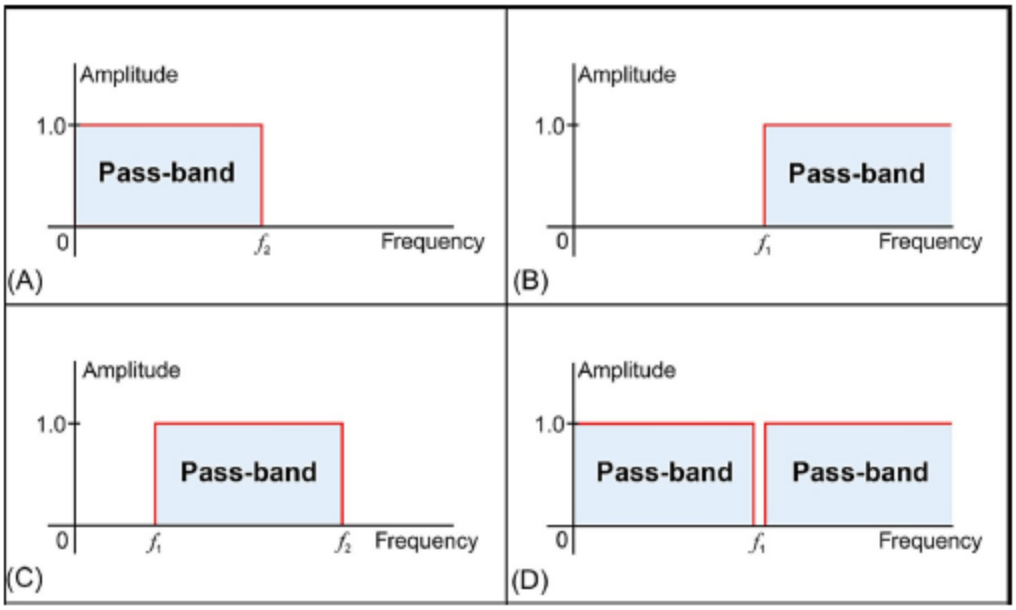

Figure 14: (A) Low-pass filter. (B) High-pass filter. (C) Band-pass filter. (D) Notch filter.

Deconvolution

Deconvolution can be defined as the process of filtering a signal to compensate for an undesired convolution. The goal of deconvolution is to recreate the signal as it existed before the convolution took place. In other words, deconvolution can be considered as convolving with an inverse filter. Deconvolution is nearly impossible to understand in the time domain, but quite straightforward in the frequency domain.

Deconvolution is used to:

- Extract the earth's reflectivity function and thus increases the resolution of the data
- Undo the effects of prior filters,
- attenuates reverberations and multiples

The earth reflectivity function $r(t)$ represents the acoustic impedance contrasts in the layered medium. The acoustic impedance is the product of seismic velocity and density of the rock (Pv). It is an internal property of the rocks and the acoustic impedance contrast increases where the rock changes into another rock, i.e at the boundary between successive rocks. This increased contrast gives a strong reflection on the measured seismic record and thus the boundary between the rocks can be detected on the record.

To understand the role of deconvolution of extracting the earth reflectivity function, we need to know that the final seismic trace (also called seismogram; it the record of the seismic data at one receiver or geophone) contains many effects as the seismic wave propagate through the inhomogeneous ground then measured on the surface. The final trace can then be regarded as a product of convolution of many effects including source effect s(t), receiver effect g(t), offset effect h(t) (offset is the distance between the source and any of the receivers), the earth impulse response e(t), and background noise n(t) – Figure 1. This can be expressed by the following equation:

$X(t) = s(t)*g(t)*h(t)*e(t)*n(t)$

So, the deconvolution tries to recover the earth impulse response from the recorded seismogram which contains all these effects, i.e the deconvolution remove all the effects leaving only the earth impulse response. This leads to compressing the basic wavelet (Fig 2) and thus increasing the

resolution. Note the differences between a seismic record before and after deconvolution in the Figure 3.

For using the source wavelet for deconvolution, there are two situations. The first situation is when the source wavelet is known. In this case, the solution of the above equation is said to be **deterministic**. The other situation is when the source wavelet is unknown and the solution in this case is said to be **statistical**.

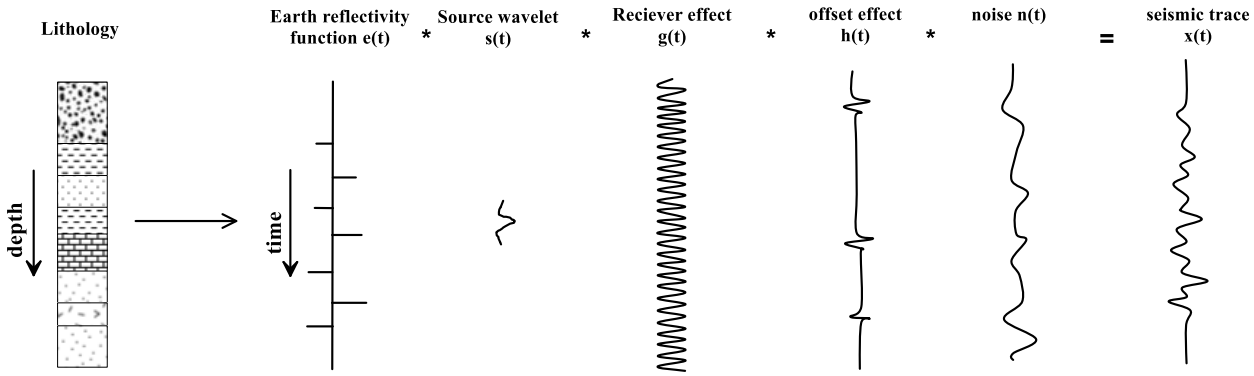

Figure 1: The components of a seismic trace.

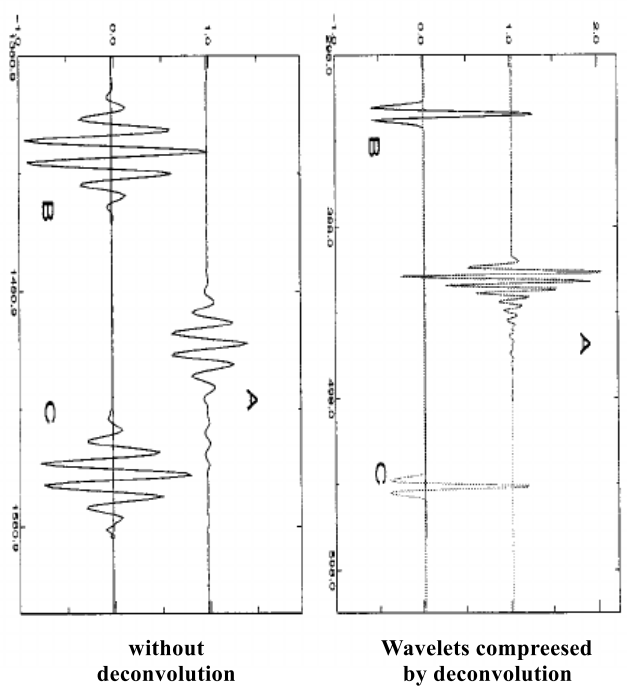

Figure 2: compressing the wavelets by the deconvolution

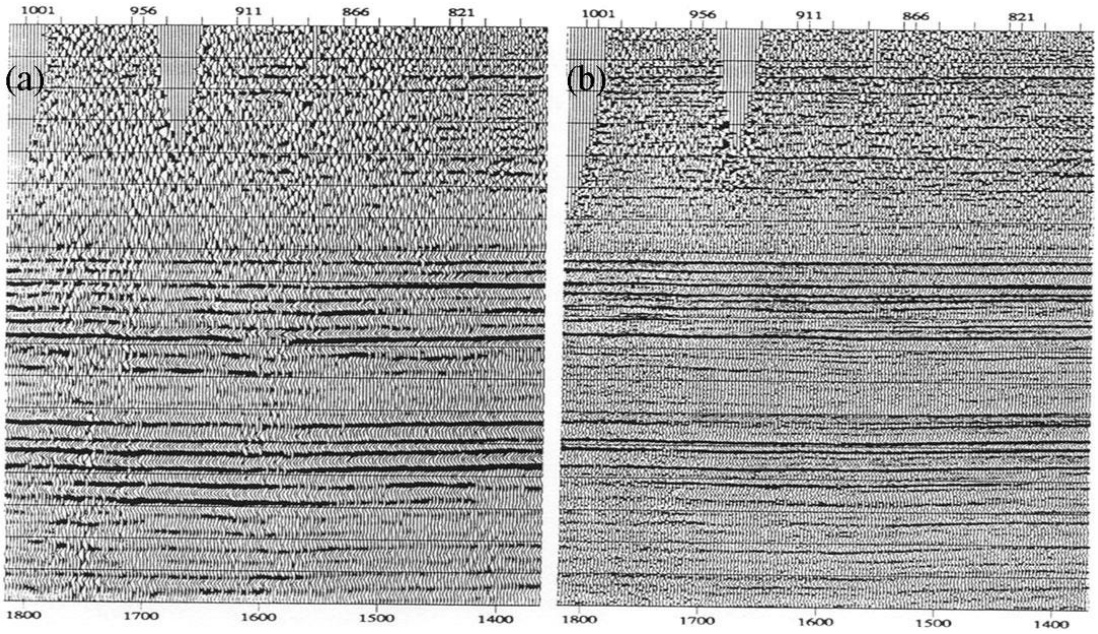

Before deconvolution **After deconvolution**

Figure 3: Seismic line without deconvolution and with deconvolution.

Types of deconvolution:

1- Spiking deconvolution:

It is the deconvolution by which the seismic wavelet is compressed and become as close as possible to a spike. Figure 4 shows the effect of spiking deconvolution on a seismic reflection record. After applying spiking deconvolution, the frequency content and resolution of the data have improved significantly. Event can be seen clearly on the seismic section. Spiking deconvolution can be achieved by inverse filtering.

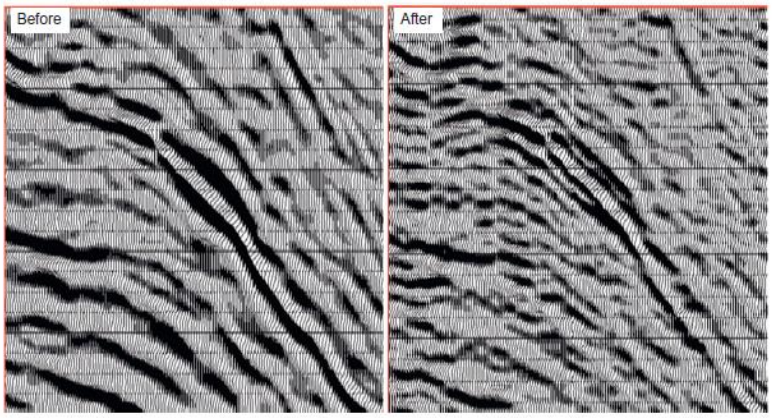

Figure 4: Seismic section before spiking deconvolution and the same data after applying spiking deconvolution.

Inverse filtering:

Inverse filtering of a method of deconvolution that converts a seismogram into a series of spikes that defines the earth impulse response (reflectivity function – figure 1), provided that the source wavelet is known (deterministic solution). The wavelets are converted into spikes as the other effected components removed. This is an application of the previously mentioned rule that the deconvolution of a wavelet is a spike (Figure 5). In other words, an inverse filter is designed so that the original source wavelet is contracted to a narrower and symmetric form (Figure 6). This can enhance the vertical resolution as the wavelets become sharper.

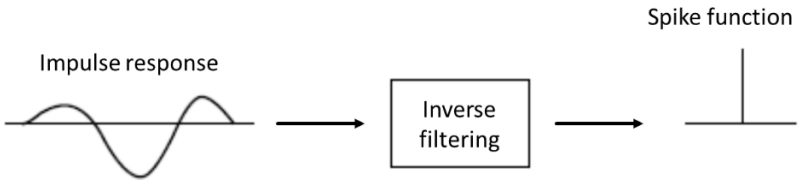

Figure 5: the deconvolution of a wavelet is a spike.

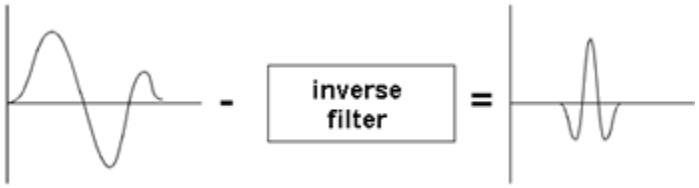

Figure 6: inverse filtering sharpens the seismic wavelet.

2- Predictive deconvolution:

In predictive deconvolution, the predictable component of the seismic trace which is the multiple reflections is eliminated, while the reflectivity series which is the unpredictable component of the seismic trace is left untouched. Figure 7 shows the effect of predictive deconvolution. Looking at the shot gather after applying predictive deconvolution, you will notice that reflection continuity has improved, and events are easier to trace. A special type of this deconvolution is deghosting.

Deghosting:

In marine work a source is detonated slightly below the water surface. The primary seismic wavelet propagates downward but there is an upward propagating wave that reflects from the water surface and then propagates downward. The latter reflection is referred to as a "ghost" (Figure 8 A). The ghost reflection also formed in land work when the source is detonated below the base of a

weathering layer. A wavelet travels upward and then reflected back at the base of the weathering layer (Figure 8 B). Both of the main wavelet and the ghost wavelet are recorded at the surface receivers forming fake reflections on the seismic record.

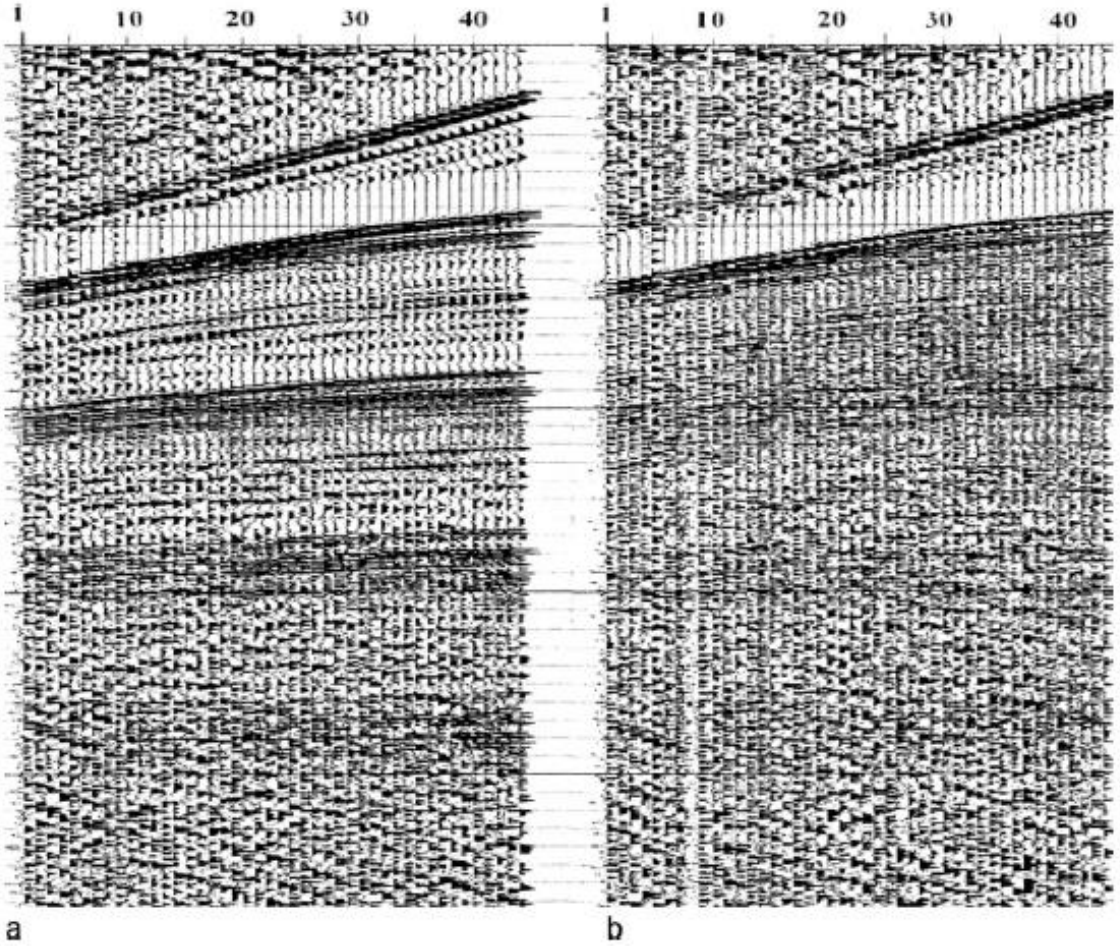

Figure 7 (a) Shot gather with short-period multiples. (b) The same shot gather after application of predictive deconvolution to eliminate the multiples

In both cases, a seismic wavelet is composed of the original wavelet plus a closely spaced reflection. This complicates the wavelet as shown in figure 9. The ghost reflections can be confirmed when doing spectral analysis for the measured seismic data. Considering the frequency response of a ghosted signal, a repetitive pattern of constructive and destructive interference enhances and deteriorates signal amplitudes, respectively, causing periodic 'ghost notches' to appear within the frequency spectrum (Figure 10). Figure 11 shows an example of seismic reflection record affected by ghost reflections before and after deghosting.

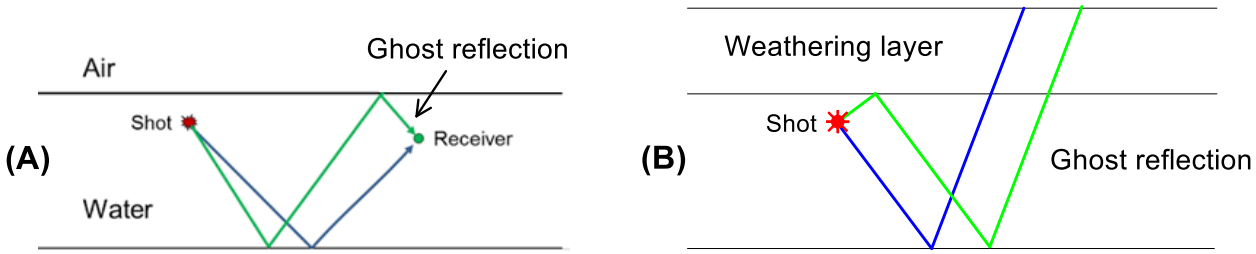

Figure 8: (A) Formation of ghost reflections in marine seismic recording. (B) Formation of ghost reflections in land seismic acquisition.

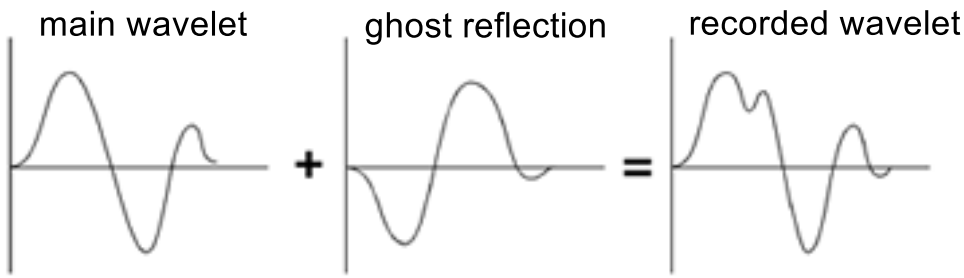

Figure 9: The effect of the ghost reflection on the measured seismic wavelet.

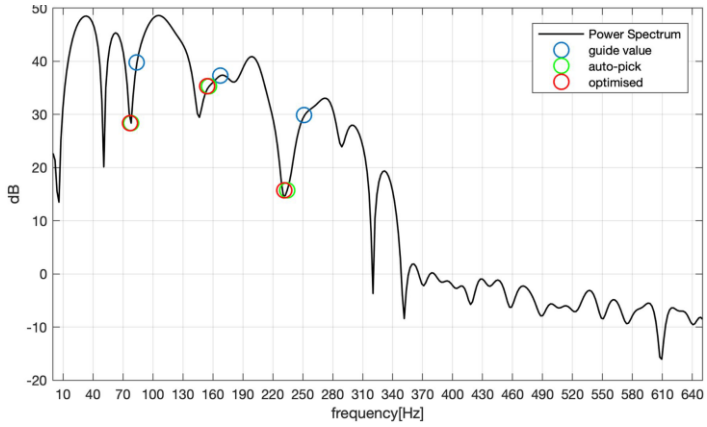

Figure 10: notches in frequency spectrum for seismic data affects by ghost reflections.

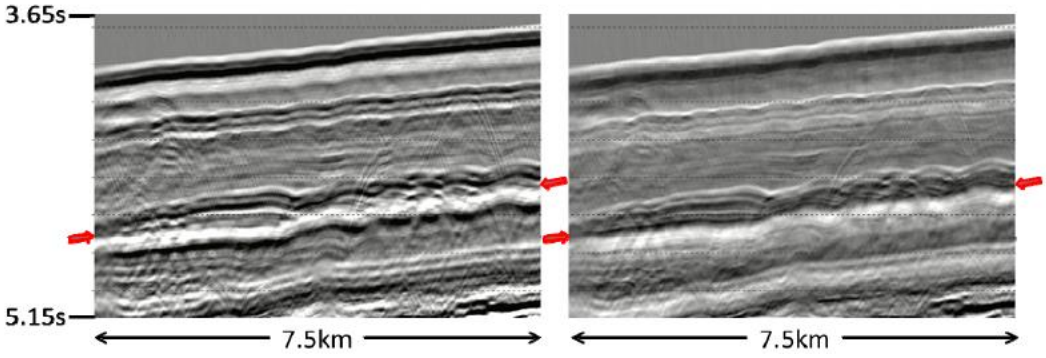

Figure 11: An example of reflection data record before and after deghosting

Post-processing: geophysical modeling

In general, post-processing of the geophysical data describes the operations applied to the data after passing through the different processing schemes. Processing of the geophysical data is used to remove the noise that contaminated the data during the acquisition and to enhance the data. After the processing, the data should be in a form that is suitable to be interpreted according to the geology.

Accordingly, a complete geophysical survey includes three main stages (figure 1):

1- The data is acquired in the field by the proper instruments (data acquisition).

2- The data is processed by different processing methods (data processing).

3- The data is converted to a form that is related to geology (interpretation).

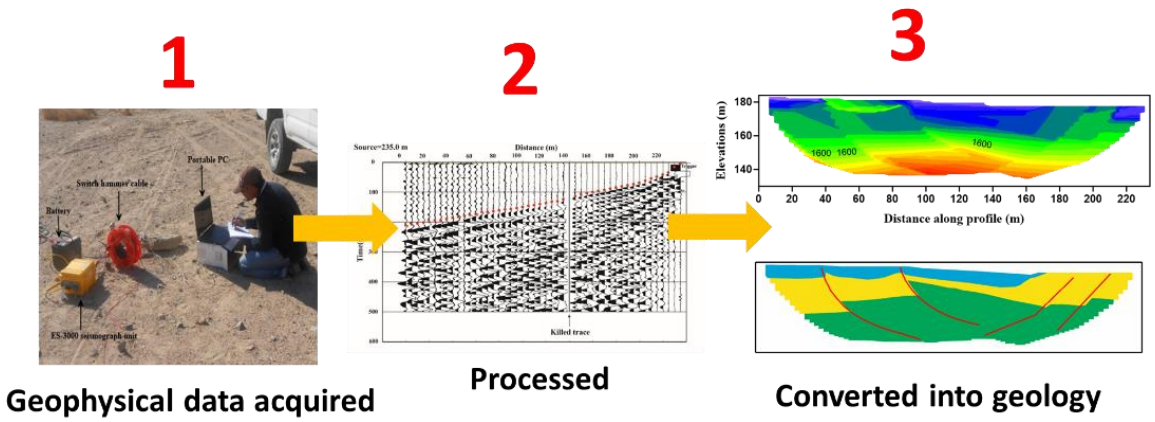

Figure 1: Stages of geophysical survey (After Abdel Gowad, 2018).

Converting the data into geology is done using some mathematical operations by which the data is converted into simplified forms represented by cross-sections or maps. These simplified forms are called **models.** A model is defined as the mathematical representation of a geologic medium that gives a simplified image of the real conditions. The process of converting the data into a model is called **modeling.**

Types of models:

A- General types of models (Figure 2):

1. Uniform model:

   It is a model where the geophysical property (such as the seismic wave velocity, resistivity, density, magnetic susceptibility…etc) is uniform everywhere. A uniform model can be in a free space (when the model is having a closed boundaries) or in a half-space when the model has an infinite depth).

2. Buried objects:

   A model where buried geological objects are simplified by simple geometrical shapes such as spheres or cylinders. For example, a subsurface cave formed in a limestone can be modelled as a sphere. A buried river or tunnels can be also modelled as cylinders.

3. Layered models

   A. Simple layered:

      When the model represents two layers only, with the second layer having an infinite depth (half-space).

   B. Multi-layered:

      When the model represents a larger number of layers.

4. Sheet or plate model:

   In these models, geologic features that have sheet or plate shapes such as dikes, joints and fault planes. It can be represented by:

   A. Sheet in free space

   B. Sheet in a half-space

   C. Sheet in a layered model

B- Types of models according to dimensions (Figure 3):

1. 1D (one-dimensional) model (Figure 3 A):

It is a model that include one spatial dimension, *x*, *y* or *z*, within the chosen coordinate system and represents the variation of the geophysical property along one dimension only in a single location point such as the variation of the seismic velocity with depth below a certain point. It represented as a cracked line below a point on the

acquisition profile. The vertical direction for the line represents the dimension of the model (such as depth).

2. 2D (Two-dimensional) model (Figure 3 B):

A model that represents the variation of the geophysical property two spatial dimensions (cross-section). The horizontal dimension is usually the distance, and the vertical dimension might be the depth or elevation.

3. 3D (three-dimensional) (Figure 3 C):

A model that represents the variation of the geophysical property in the three spatial dimensions (x,y,z).

4. 4D (Four-dimensional) (Figure 3 D):

When the property is changed through the time, such as depth to the water table, a 4D model can be estimated. It is a 3D model, but it is calculated at different times. For example, in some regions, the depth to the water table is changed with time depending on the amount of the rains. A 3D geophysical survey can be performed on these regions at a specific time interval (every 6 months). The resulted 3D models will show the change in the depth to the water table every 6 months.

An example of the types of models according to their dimension is shown in Figure 4 based on true seismic refraction data. The 1D model shows the variation of the shear wave velocity with depth below on point on the acquisition profile. The 2D model shows the lateral and vertical variation in of the P-wave velocities two dimensions; the horizontal dimension (x) which represents the distances in meters along the acquisition profile, and the vertical dimension (z) which represents the elevations. The model is a cross-section of the P-wave velocities that can be interpreted later according to geology. The 3D model shows the three-dimensional distribution of the P-wave velocities in the survey area. Figure 5 shows a real-data example showing the variation of CO2 content within a subsurface storage facility represented in 4D model where the data were measured every 2 years.

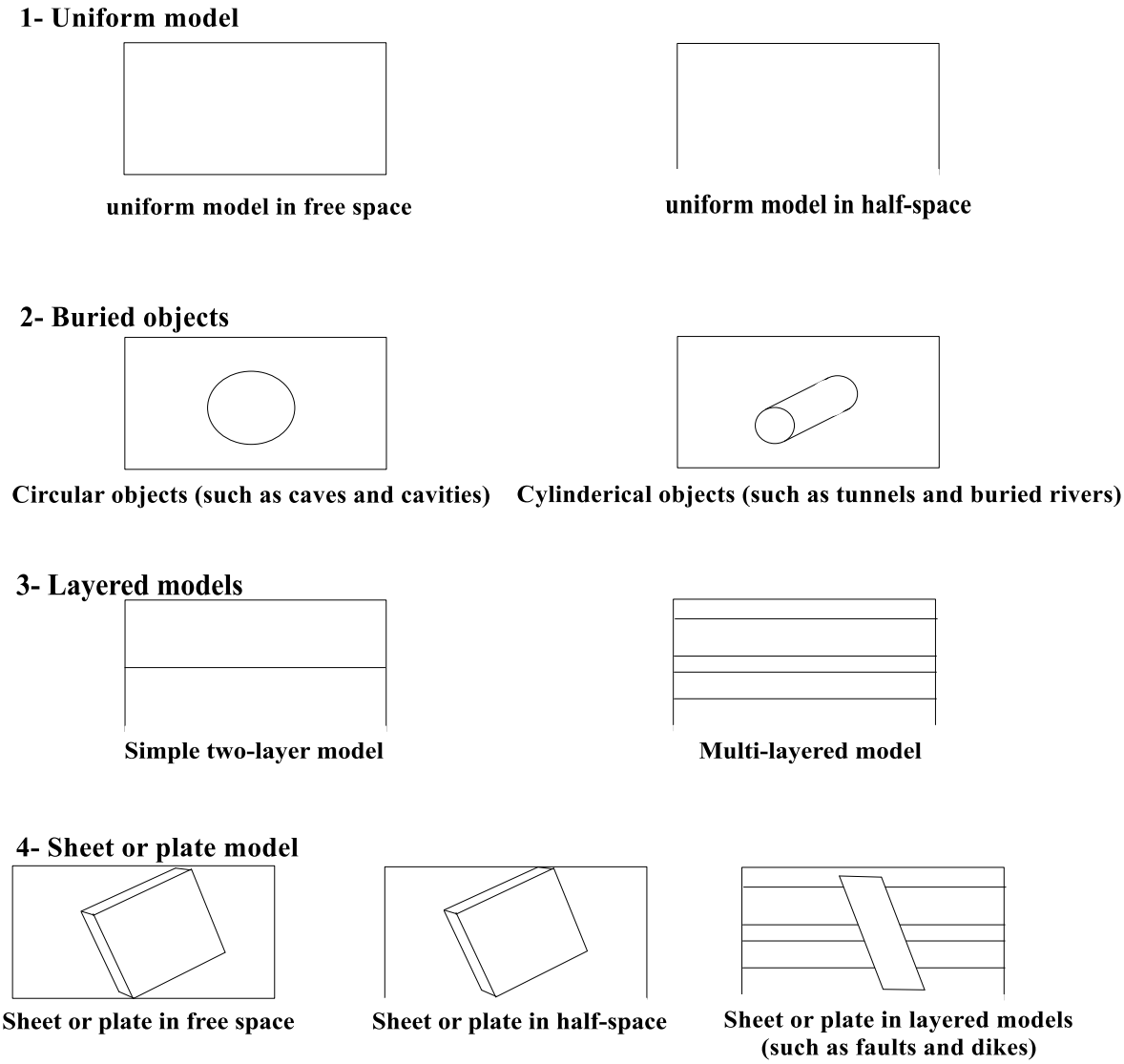

Figure 2: General types of models.

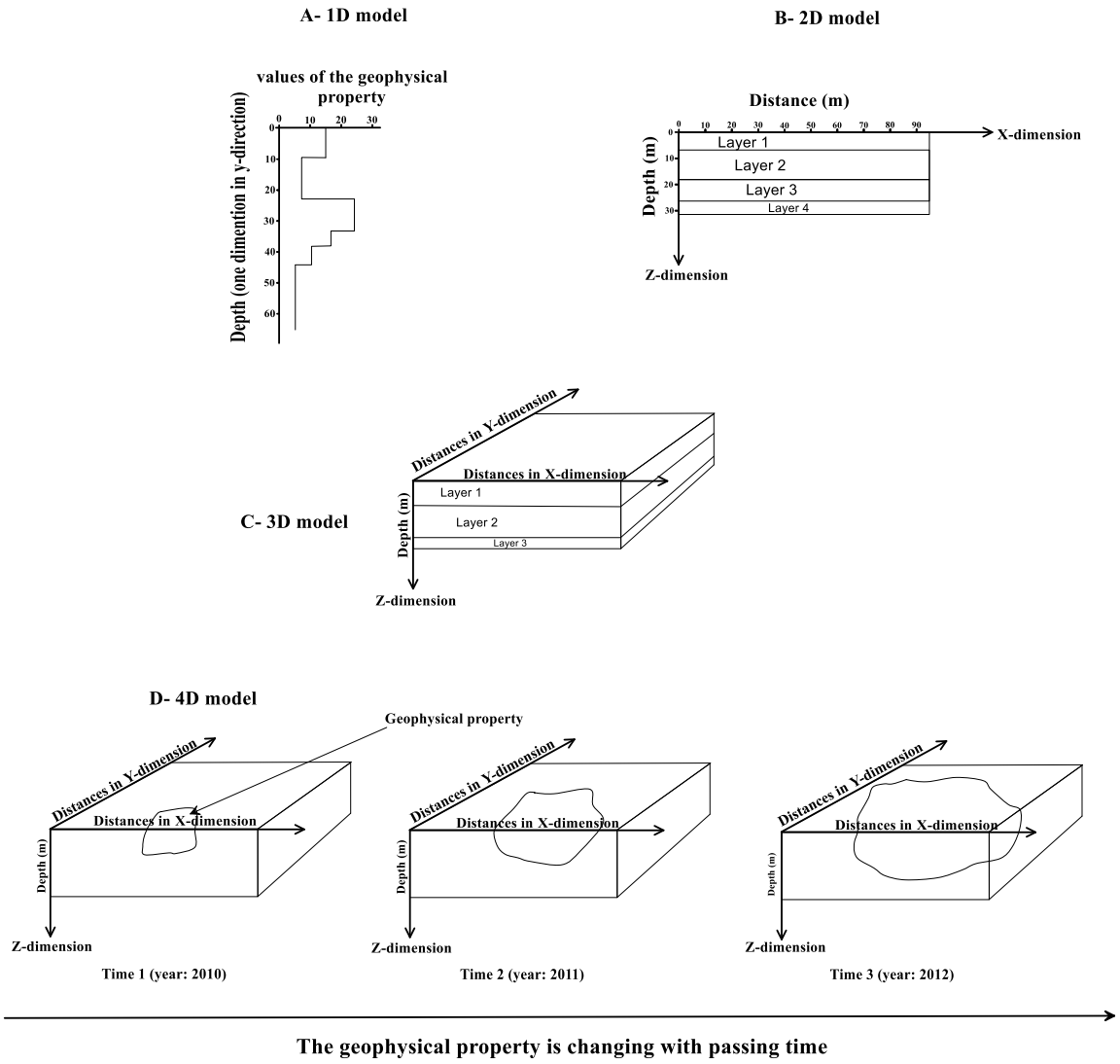

Figure 3: Types of models according to dimension.

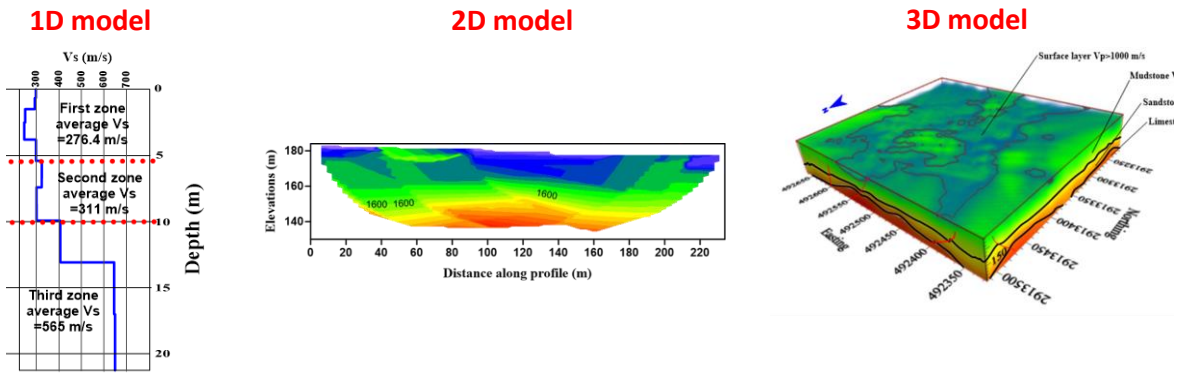

Figure 4: Example of the types of models resulted from real seismic refraction survey in Qena-Safaga KM 30 area by Abdel Gowad, 2018.

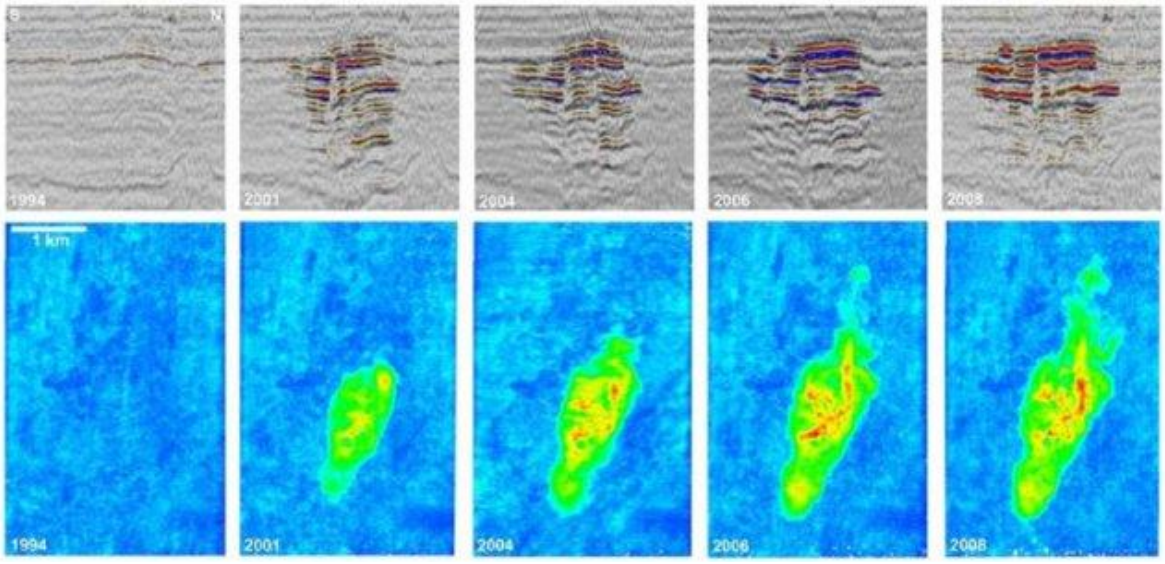

Figure 5: A real example of 4D seimic model shows the variation of CO_2 in a storage site (After Chadwick et al., 2010).

Modeling techniques:

Modeling of the geophysical data can be defined as a mathematical technique by which a model representing a geophysical property is obtained from the observed data.

Why we do modeling?

1. Explain complex data sets.
2. Explains the data with geology:

   Defines the depth, volume, geometry and physical properties of the geological features.
3. Can quality control the data:

   - Identify problematic data
   - Identify acquisition problems.

Modeling can be performed using two techniques: Forward and inverse modeling.

1- Forward modeling:

Forward modeling is based on comparing the observed data acquired in the field with calculated data of a theoretical model computed based on geological concepts. Forward modeling can be performed with the following steps:

1. Input the acquired data into the forward modeling program.

2. Create a model based on the known geology. This model is known as the **initial or primary model**. The initial model will have parameters such as number of subsurface layers, thicknesses of these layers, depths of these layers and the values of the geophysical properties of these layers. These parameters can be defined based on studying the geology of the area and using any drilled wells in the survey area. Defining the parameters of the initial model is called **parametrization process**. If these parameters are mostly known, the initial model is called **parametric model**. If the parameters are unknown, the initial model is said to be **generalized model**.

3. Calculate the initial model response. In this step, the program will calculate the data of the initial model as if the acquisition is done on this model. The created data is called **theoretical or calculated data**.

4. The program will compare the observed data (the data that is acquired in the field) with the theoretical data. This process is called **fitting of the observed data with the theoretical data**. This process is done automatically on several steps where the program calculates the difference between the observed and theoretical data in every step. The difference is represented by an error value called **RMSE (Root-mean-square-error)**. In every step, the RMSE is calculated and the initial model parameters is modified in the following step to reduce the value of the RMSE. Every step of calculation is called **iteration** and the number of iterations is defined on the program before starting the modeling. Usually, a number of 5 to 10 iterations are used in most geophysical surveys. After the iterations are finished, there are two probabilities:

    A. If the RMSE value is too small (less than 4), the observed data will be fitted with the theoretical data and modeling is finished.

    B. If the RMSE value is high (more than 4), the observed and theoretical data don't fit with each other. In this case, the parameters of the initial model are modified.

5. Steps repeated until a **best fit** is obtained between the observed and calculated data.

6. Final model output.

2- Inverse modeling (inversion):

In the inverse modeling, the final model is derived directly from the observed data by mathematical means. In this case, we don’t need an initial model or performing iterations. The final model is calculated directly from the observed data.

References

1. Öz Yilmaz (2001): Seismic data analysis. Society of Exploration Geophysicists. 2065p.
2. Enwenode Onajite, (2014): Chapter 7 - Understanding Deconvolution, in Editor(s): Enwenode Onajite: Seismic Data Analysis Techniques in Hydrocarbon Exploration, Elsevier, Pages 93-103, ISBN 9780124200234, https://doi.org/10.1016/B978-0-12-420023-4.00007-1
3. Robert E. Sheriff (2004): What is deconvolution?. Single article. 3p.
4. Yilmaz, Orhan & Baysal, Edip. (2015). An Effective Ghost Removal Method for Marine Broadband Seismic Data Processing. 10.3997/2214-4609.201413195.
5. Provenzano, G., Henstock, T.J., Bull, J.M. *et al.* Attenuation of receiver ghosts in variable-depth streamer high-resolution seismic reflection data. *Mar Geophys Res* **41,** 11 (2020). https://doi.org/10.1007/s11001-020-09407-9
6. Abdel Gowad, A. M. (2018) Seismic refraction for shallow investigations on Qena-Safaga road, Eastern Desert, Egypt. PhD Thesis, South Valley University.
7. A. Chadwick, G. Williams, N. Del'epine, V. Clochard, K. Labat, S. Sturton, Maike-L Buddensiek, M. Dillen, M. Nickel, A. L. Lima, R. Arts, F. Neele and G. Rossi (2010): Quantitative analysis of time-lapse seismic monitoring data at the Sleipner CO2 storage operation. The Leading Edge, V. 29, No.2, pp. 113–240, DOI: https://doi.org/10.1190/1.3304820

Part 3:

Introduction to Geoelectric Methods

By:

Dr. Ismail Sayed Ahmed

Chapter 8

Resistivity Methods

8.1. INTRODUCTION

All resistivity methods employ an artificial source of current, which is introduced into the ground through point electrodes or long line contacts; the latter arrangement is rarely used nowadays. The procedure is to measure potentials at other electrodes in the vicinity of the current flow. Because the current is measured as well, it is possible to determine an effective or apparent resistivity of the subsurface.

In this regard the resistivity technique is superior, at least theoretically, to all the other electrical methods, because quantitative results are obtained by using a controlled source of specific dimensions. Practically, as in other geophysical methods, the maximum potentialities of resistivity are never realized. The chief drawback is its high sensitivity to minor variations in conductivity near surface; in electronic parlance the noise level is high. An analogous situation would exist in ground magnetic surveys if one were to employ a magnetometer with sensitivity in the picotesla range.

This limitation, added to the practical difficulty involved in dragging several electrodes and long wires through rough wooded terrain, has made the electromagnetic method more popular than resistivity in mineral exploration. Nor is resistivity particularly suitable for oil prospecting. However, it is by no means obsolete, because the rapid development of the induced polarization technique, which includes resistivity data, guarantees its continued use. Furthermore the search for geothermal reservoirs normally involves resistivity surveying and it is also employed routinely in groundwater exploration, which is of increasing worldwide importance, and in civil engineering.

8.2. ELEMENTARY THEORY

8.2.1. Potentials in Homogeneous Media

Consider a continuous current flowing in an isotropic homogeneous medium. (This analysis will also apply to ac if the frequency is low enough that displacement currents are insignificant.) If $\delta\mathbf{A}$ is an element of surface and $\mathbf{J}$ the current density in amperes per square meters, then the current passing through $\delta\mathbf{A}$ is $\mathbf{J} \cdot \delta\mathbf{A}$. The current density $\mathbf{J}$ and the electric field $\mathbf{E}$ are related through Ohm's law:

$$\mathbf{J} = \sigma\mathbf{E} \tag{8.1}$$

where $\mathbf{E}$ is in volts per meter and σ is the conductivity of the medium in siemens per meter (S/m).

The electric field is the gradient of a scalar potential,

$$\mathbf{E} = -\nabla V \tag{8.2}$$

Thus we have

$$J = -\sigma\nabla V \tag{8.3}$$

From Equation (6.7), $\nabla \cdot \mathbf{J} = 0$, so

$$\nabla \cdot (\sigma\nabla V) = 0 \tag{8.4}$$

Using Equation (A.21), we have

$$\nabla\sigma \cdot \nabla V + \sigma\nabla^2 V = 0 \tag{8.5}$$

If σ is constant throughout, the first term vanishes and we have Laplace's equation, that is, the potential is harmonic:

$$\nabla^2 V = 0 \tag{8.6}$$

There are two boundary conditions that must hold at any contact between two regions of different conductivity. In Section 6.2.4 we gave boundary conditions for interfaces where σ and μ change abruptly. The first and third of these may be written in the form

$$E_{x_1} = E_{x_2} \quad \text{and} \quad \sigma_1 E_{z_1} = \sigma_2 E_{z_2} \tag{8.7a}$$

where the x and z axes are tangential and normal, respectively, to the interface, E_{x_1} being the tangen-

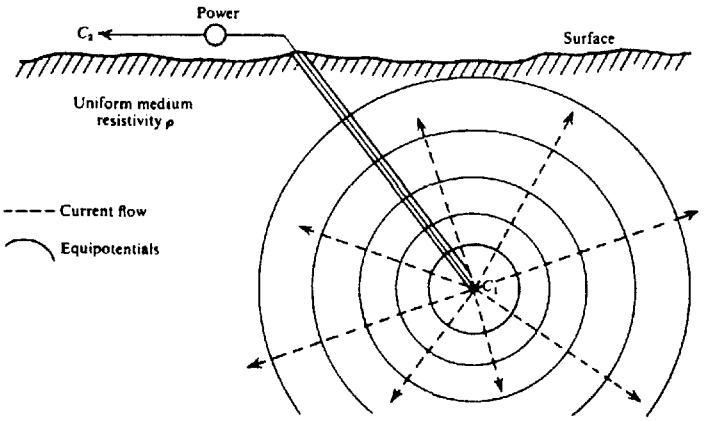

Figure 8.1. Buried point source of current in homogeneous ground.

tial component in medium 1, and so forth. In addition,

$$V_1 = V_2 \tag{8.7b}$$

8.2.2. Single Current Electrode at Depth

There are several field configurations used in resistivity that we will consider in turn. In the first of these we have an electrode of small dimensions buried in a homogeneous isotropic medium. This corresponds to the *mise-à-la-masse* method (see §8.5.4d) where the single electrode is down a drill hole or otherwise under the ground. The current circuit is completed through another electrode, usually at surface, but in any case far enough away that its influence is negligible.

From the symmetry of the system, the potential will be a function of r only, where r is the distance from the first electrode. Under these conditions Laplace's equation, in spherical coordinates, simplifies to

$$\nabla^2 V = d^2V/dr^2 + (2/r)\, dV/dr = 0 \tag{8.8}$$

Multiplying by r^2 and integrating, we get

$$\frac{dV}{dr} = \frac{A}{r^2} \tag{8.9}$$

integrating again, we have

$$V = -A/r + B \tag{8.10}$$

where A and B are constants. Because $V = 0$ when $r \to \infty$, we get $B = 0$. In addition, the current flows radially outward in all directions from the point electrode. Thus the total current crossing a spherical surface is given by

$$I = 4\pi r^2 J = -4\pi r^2 \sigma \frac{dV}{dr} = -4\pi\sigma A$$

from Equations (8.3) and (8.9), so that

$$A = -\frac{I\rho}{4\pi}$$

hence,

$$V = \left(\frac{I\rho}{4\pi}\right)\frac{1}{r} \quad \text{or} \quad \rho = \frac{4\pi r V}{I} \tag{8.11}$$

The equipotentials, which are everywhere orthogonal to the current flow lines, will be spherical surfaces given by r = constant. These are illustrated in Figure 8.1.

8.2.3. Single Current Electrode at Surface

If the point electrode delivering I amperes is located at the surface of the homogeneous isotropic medium and if the air above has zero conductivity, then we have the single probe or three-point system used in surface resistivity layouts. Again the return current electrode is at a great distance.

Because of the symmetry, Laplace's equation in spherical coordinates is applicable, the solution being given again by Equation (8.10) with $B = 0$. The boundary condition at the surface requires that $E_z = \partial V/\partial z = 0$ at $z = 0$ (because $\sigma_{air} = 0$). This is already fulfilled because $\partial V/\partial z = \partial(-A/r)/\partial z = -d/dr(A/r)(\partial r/\partial z) = Az/r^3 = 0$ at $z = 0$.

In addition all the current now flows through a hemispherical surface in the lower medium, or

$$A = -\frac{I\rho}{2\pi}$$

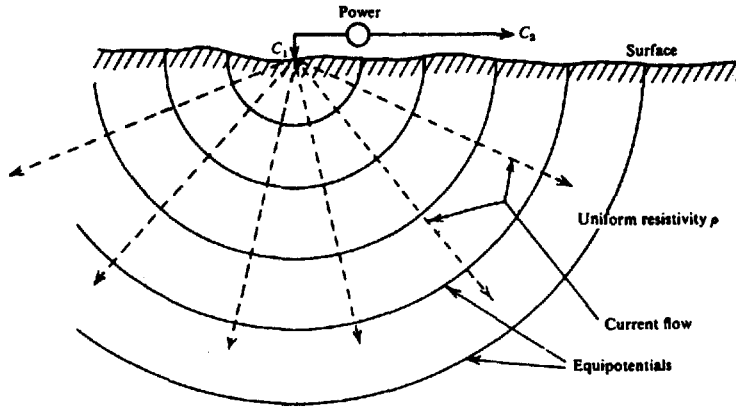

Figure 8.2. Point source of current at the surface of a homogeneous medium.

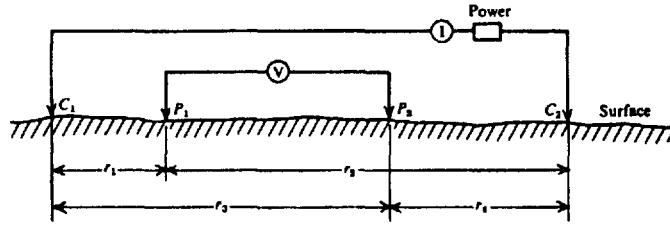

Figure 8.3. Two current and two potential electrodes on the surface of homogeneous isotropic ground of resistivity ρ.

so that in this case

$$V = \left(\frac{I\rho}{2\pi}\right)\frac{1}{r} \quad \text{or} \quad \rho = \frac{2\pi r V}{I} \tag{8.12}$$

Here the equipotentials are hemispherical surfaces below ground as shown in Figure 8.2.

8.2.4. Two Current Electrodes at Surface

When the distance between the two current electrodes is finite (Fig. 8.3), the potential at any nearby surface point will be affected by both current electrodes. As before, the potential due to C_1 at P_1 is

$$V_1 = -\frac{A_1}{r_1} \quad \text{where} \quad A_1 = -\frac{I\rho}{2\pi}$$

Because the currents at the two electrodes are equal and opposite in direction, the potential due to C_2 at P_1 is

$$V_2 = -\frac{A_2}{r_2} \quad \text{where} \quad A_2 = \frac{I\rho}{2\pi} = -A_1$$

Thus, we have

$$V_1 + V_2 = \frac{I\rho}{2\pi}\left(\frac{1}{r_1} - \frac{1}{r_2}\right)$$

Finally, by introducing a second potential electrode at P_2 we can measure the difference in potential between P_1 and P_2, which will be

$$\Delta V = \frac{I\rho}{2\pi}\left\{\left(\frac{1}{r_1} - \frac{1}{r_2}\right) - \left(\frac{1}{r_3} - \frac{1}{r_4}\right)\right\} \tag{8.13}$$

Such an arrangement corresponds to the four-electrode spreads normally used in resistivity field work. In this configuration the current-flow lines and equipotentials are distorted by the proximity of the second current electrode C_2. The equipotentials and orthogonal current lines obtained by plotting the relations

$$\frac{1}{R_1} - \frac{1}{R_2} = \text{constant}$$

$$R_1^2 + R_2^2 - 2R_1R_2\cos\theta = 4L^2$$

are shown in Figure 8.4. The distortion from spherical equipotentials is most evident in the regions between the current electrodes.

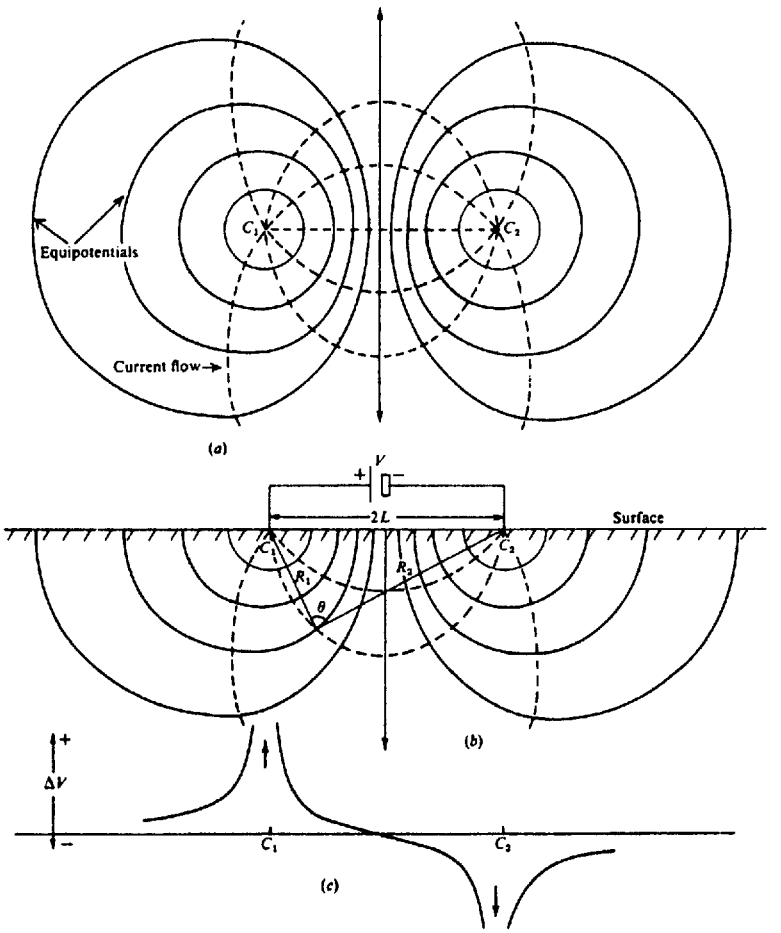

Figure 8.4. Equipotentials and current flow lines for two point sources of current on surface of homogeneous ground. (After Dobrin, 1960.) (a) Plan view. (b) Vertical section. (c) Potential variation at the surface along a straight line through the point sources.

8.2.5. Current Distribution

Figures 8.1, 8.2, and 8.4 illustrate, in a general way, the flow of current in homogeneous ground. Although they show that increasing the electrode spacing increases the penetration, the quantitative distribution in depth is not indicated. Consider the current flow in a homogeneous medium between two point electrodes C_1 and C_2 in Figure 8.5. The horizontal current density at point P is

$$\begin{aligned} J_x &= (-1/\rho)\,\partial V/\partial x \\ &= (-I/2\pi)\,\partial/\partial x(1/r_1 - 1/r_2) \\ &= (I/2\pi)\{x/r_1^3 - (x-L)/r_2^3\} \end{aligned}$$

and if this point is on the vertical plane midway between C_1 and C_2, we have $r_1 = r_2 = r$ and

$$J_x = \frac{I}{2\pi}\frac{L}{(z^2 + L^2/4)^{3/2}} \qquad (8.14)$$

Figure 8.6 shows the variation in current density with depth across this plane when the electrode separation is maintained constant. If, on the other hand, the electrode spacing is varied, it is found that J_x is a maximum when $L = \sqrt{2}z$.

We can calculate the fraction of current flowing through a strip of this vertical plane, between depths z_1 and z_2. Because $r^2 = \{(L/2)^2 + y^2 + z^2\}$, the

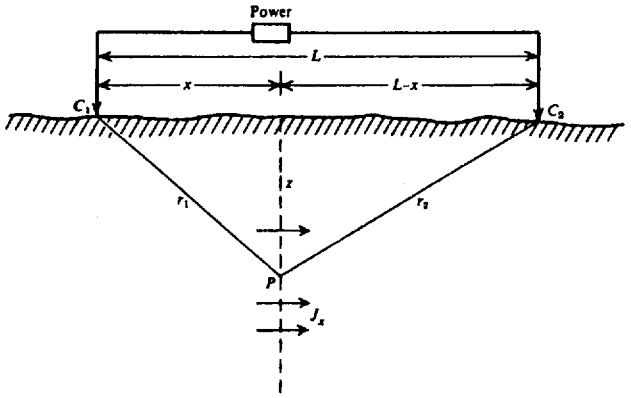

Figure 8.5. Determining the current density in uniform ground below two surface electrodes.

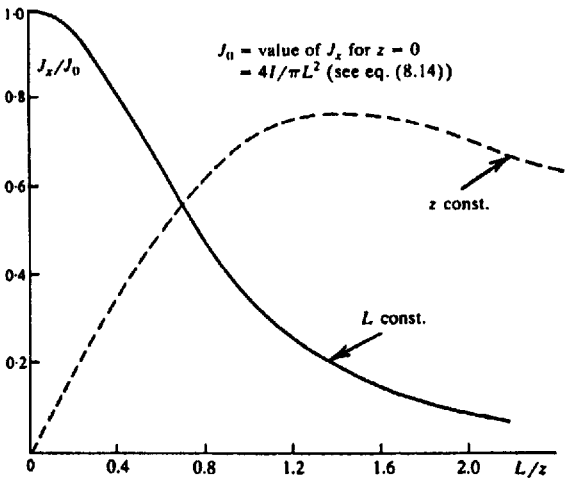

Figure 8.6. Current density versus depth (solid line) and electrode spacing (dashed line).

current through an element $dy\,dz$ of the strip is

$$\delta I_x = J_x\,dy\,dz = \frac{I}{2\pi}\frac{L}{\left\{(L/2)^2 + y^2 + z^2\right\}^{3/2}}\,dy\,dz$$

the fraction of total current through a long strip $(z_2 - z_1)$ wide will be

$$\frac{I_x}{I} = \frac{L}{2\pi}\int_{z_1}^{z_2} dz \int_{-\infty}^{\infty} \frac{dy}{\left\{(L/2)^2 + y^2 + z^2\right\}^{3/2}}$$

$$= \frac{2}{\pi}\left(\tan^{-1}\frac{2z_2}{L} - \tan^{-1}\frac{2z_1}{L}\right) \qquad (8.15a)$$

This fraction has a broad maximum when $L = 2(z_1 z_2)^{1/2}$. Taking a numerical example, if $z_1 = 180$ m, $z_2 = 300$ m, the electrode spacing should be 420 m to get the maximum horizontal current density in the slab. The concentration, however, is not very significant.

Otherwise, if $z_2 \to \infty$, Equation (8.15a) becomes

$$\frac{I_x}{I} = 1 - \frac{2}{\pi}\tan^{-1}\frac{2z_1}{L} \qquad (8.15b)$$

Figure 8.7 shows the electrode spacing necessary to force a given fraction of the current into the ground below a depth z_1. From this plot we see that, when $L = 2z_1$, half the current flows in the top layer, half below it.

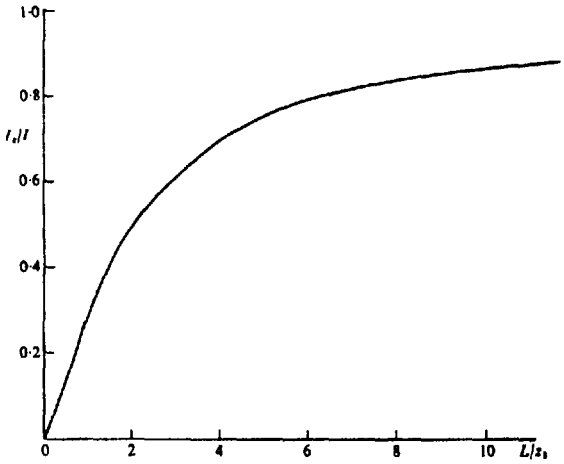

Figure 8.7. Fraction of current flowing below depth z_1 for an electrode spacing L.

Because the variations in potential, measured at surface, are proportional to the current flow below, it is desirable to get as much current into the ground as possible. For good penetration we must use large enough spacing that sufficient current reaches the target depth; if the latter is 100 m, about one-third of the current will pass below this depth when the spacing is also 100 m. Compared to magnetotellurics, for instance, this places an inherent limitation on the resistivity method. However the controlled power source provides certain advantages.

8.3. EFFECT OF INHOMOGENEOUS GROUND

8.3.1. Introduction

So far we have considered current flow and potential in and over homogeneous ground, a situation which is extremely rare in the field and which would be of no practical significance anyway. What we want to detect is the presence of anomalous conductivity in various forms, such as lumped (three-dimensional) bodies, dikes, faults, and vertical or horizontal contacts between beds. The resistivity method is most suitable for outlining horizontal beds and vertical contacts, less useful on bodies of irregular shape.

8.3.2. Distortion of Current Flow at a Plane Interface

Consider two homogeneous media of resistivities ρ_1 and ρ_2 separated by a plane boundary as in Figure 8.8. Suppose that a current of density J_1 is flowing in medium (1) in such a direction as to meet the boundary at an angle θ_1 to the normal. To determine the

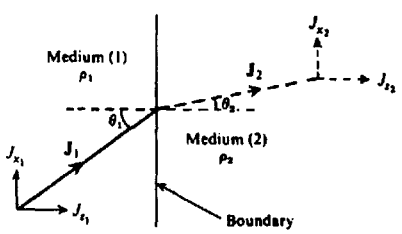

Figure 8.8. Distortion of current flow at a plane boundary when $\rho_1 < \rho_2$.

direction of this current in medium (2) we recall the conditions given in Equation (8.7); using Ohm's law to express these results in terms of the current density, we obtain

$$J_{x_1}\rho_1 = J_{x_2}\rho_2 \quad \text{and} \quad J_{z_1} = J_{z_2}$$

Dividing these expressions, we have

$$\rho_1(J_{x_1}/J_{z_1}) = \rho_2(J_{x_2}/J_{z_2}) \quad \text{or} \quad \rho_1 \tan\theta_1 = \rho_2 \tan\theta_2$$

so that

$$\tan\theta_2/\tan\theta_1 = \rho_1/\rho_2 \qquad (8.16)$$

Thus the current lines are bent in crossing the boundary. If $\rho_1 < \rho_2$, they will be bent toward the normal and vice versa.

8.3.3. Distortion of Potential at a Plane Interface

Clearly if the current flow is distorted in passing from a medium of one resistivity into another, the equipotentials also will be distorted. It is possible to

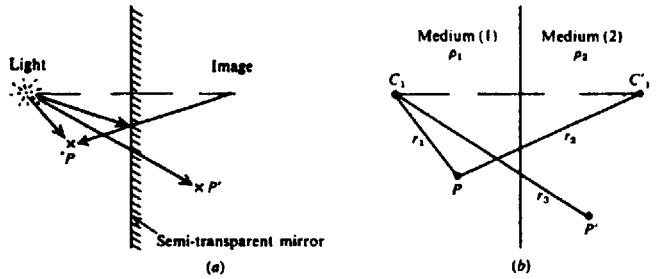

Figure 8.9. Analogy between optical and electrical images. (a) Optical image. (b) Electrical image.

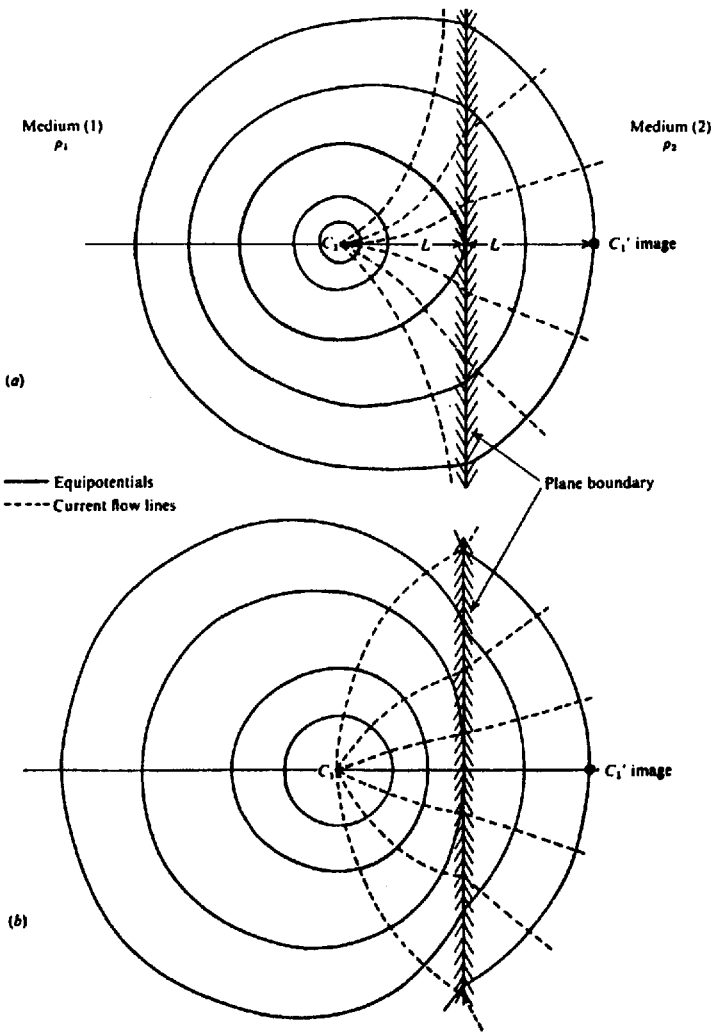

Figure 8.10. Distortion of equipotentials and current flow lines at a boundary between two media of different resistivities. (a) $\rho_2/\rho_1 = 3$, $k = 0.5$. (b) $\rho_2/\rho_1 = 1/3$, $k = -0.5$.

determine the potential field mathematically by solving Laplace's equation for the appropriate boundary conditions or by integrating it directly. Both methods require considerable mathematics. A much simpler approach employs electrical images, in analogy with geometrical optics. The use of images is valid in solving only a limited number of potential problems, including the plane boundary and the sphere (see Bewley, 1963, Ch. 5).

The analogy between the electrical situation and optics is based on the fact that current density, like light ray intensity, decreases with the inverse square of distance from a point source in a medium of resistivity ρ_1, separated from an adjacent medium ρ_2 by a plane boundary.

In optics the analogous case would be a point source of light in one medium separated from another by a semitransparent mirror, having reflection and transmission coefficients k and $1 - k$. Then the light intensity at a point in the first medium is partly due to the point source and partly to its image in the second medium, the latter effect diminished by reflection from the mirror. On the other hand, the intensity at a point in the second medium is due only to the source in the first, diminished by transmission through the mirror (Fig. 8.9a).

If we replace the point source of light by a point source of current and the light intensity at a point by potential, the problem is now in the electrical domain. From Figure 8.9b we see that the potential at P in the first medium is

$$V = \frac{I\rho_1}{4\pi}\left(\frac{1}{r_1} + \frac{k}{r_2}\right) \qquad (8.17)$$

and in the second medium at P' it is

$$V' = \frac{I\rho_2}{4\pi}\left(\frac{1-k}{r_3}\right) \qquad (8.18)$$

Applying the boundary condition of Equation (8.7b), these potentials must be equal at the interface, when $r_1 = r_2 = r_3$. Thus we have

$$\frac{\rho_1}{\rho_2} = \frac{1-k}{1+k} \quad \text{or} \quad k = \frac{\rho_2 - \rho_1}{\rho_2 + \rho_1} \qquad (8.19)$$

In this expression k is a *reflection coefficient* whose value lies between ± 1, depending on the relative resistivities in the two media.

Figure 8.10 shows the traces of equipotential surfaces plotted from the relations in Equations (8.17) and (8.18) for $k = \pm \frac{1}{2}$. A few current flow lines are also drawn. This situation corresponds to the practical case of resistivity logging with respect to a plane boundary underground or the measurement of surface potentials across a vertical contact.

8.3.4. Surface Potential Due to Horizontal Beds

If the current source and potential point are located on surface, above a horizontal boundary separating two media, the upper resistivity ρ_1, the lower ρ_2, the analysis is more complicated. Because of the ground surface there are now three media, separated by two interfaces. As a result there is an infinite set of images above and below the current electrode, as illustrated in Figure 8.11. The original image C_1', at depth $2z$ below surface, is reflected in the surface boundary to give an image C_1'' a distance $2z$ above C_1. This second image, reflected in the lower boundary, produces a third C_1''' at a depth $4z$, and so on.

The effect of each successive image on the potential at P is reduced by the reflection coefficient between the boundaries. For the current source and its first image below ground, the potential, is, as in Equation (8.17),

$$V' = \frac{I\rho_1}{2\pi}\left(\frac{1}{r} + \frac{k}{r_1}\right)$$

The effect of the second image at C_1'', $2z$ above ground, is

$$V'' = \frac{I\rho_1}{2\pi}\left(\frac{k \times k_a}{r_1}\right)$$

where k_a is the reflection coefficient at the surface boundary. Because ρ_a is essentially infinite this coefficient is unity, and from Equation (8.19),

$$V' + V'' = \frac{I\rho_1}{2\pi}\left(\frac{1}{r} + \frac{2k}{r_1}\right)$$

The potential due to the third image C_1''', $4z$ below ground, will be further reduced, as will that of its image $4z$ above ground, hence

$$V''' + V^{IV} = \frac{I\rho_1}{2\pi}\left(\frac{k \times k}{r_2} + \frac{k \times k \times k_a}{r_2}\right) = \frac{I\rho_1}{2\pi}\left(\frac{2k^2}{r_2}\right)$$

The resultant total potential at P can thus be expressed as an infinite series of the form

$$V = \frac{I\rho_1}{2\pi}\left\{\frac{1}{r} + \frac{2k}{r_1} + \frac{2k^2}{r_2} + \cdots + \frac{2k^m}{r_m} + \ldots\right\} \qquad (8.20)$$

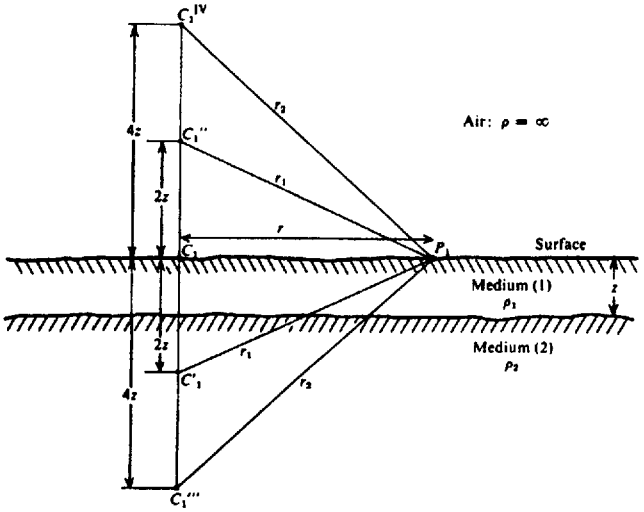

Figure 8.11. Images resulting from two horizontal beds.

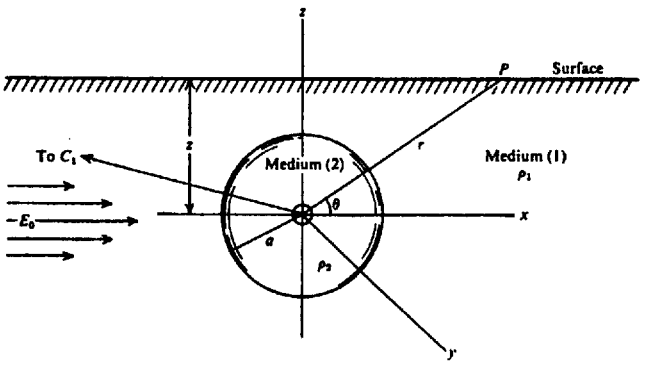

Figure 8.12. Buried conducting sphere in uniform field.

where

$$r_1 = \left\{r^2 + (2z)^2\right\}^{1/2}$$

$$r_2 = \left\{r^2 + (4z)^2\right\}^{1/2}$$

$$r_m = \left\{r^2 + (2mz)^2\right\}^{1/2}$$

This series can be written in the compact form

$$V = \frac{I\rho_1}{2\pi}\left[\frac{1}{r} + 2\sum_{m=1}^{\infty}\frac{k^m}{\left\{r^2 + (2mz)^2\right\}^{1/2}}\right]$$

$$= \frac{I\rho_1}{2\pi r}\left[1 + 2\sum_{m=1}^{\infty}\frac{k^m}{\left\{1 + (2mz/r)^2\right\}^{1/2}}\right] \quad (8.21)$$

This series is convergent, because $|k| < 1$, whereas the denominator increases indefinitely. The number of terms necessary to get a reasonable answer depends mainly on the value of k and partly on the ratio z/r. For a fixed value of r, the potential differs from that measured over uniform ground. The latter is given by the first term in the bracket of Equation (8.21) and is called the *normal potential*. The portion expressed by the infinite series is the *disturbing potential*. When k is positive and approximately unity, the total potential at P may be increased by a factor of 2 or more.

8.3.5. Potential Due to Buried Sphere

A three-dimensional body for which the external potential may be developed is the sphere. Figure 8.12 illustrates this case, in which we use spherical coordi-

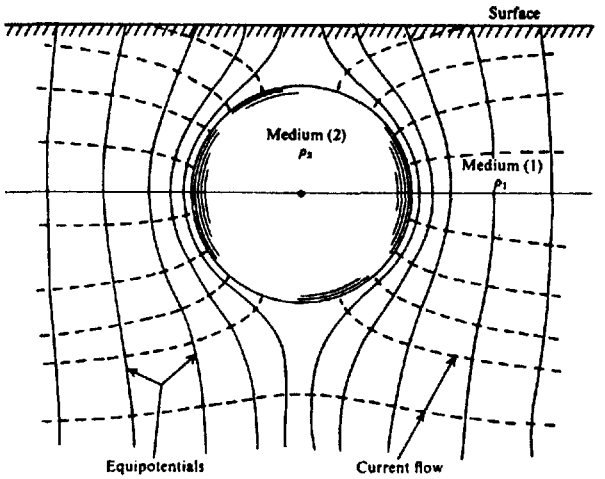

Figure 8.13. Equipotentials and current flow lines for buried conductive sphere.

nates with the sphere center as origin and the polar axis parallel to the x axis. The problem is to find solutions of Laplace's equation for particular boundary conditions; for simplicity we assume the sphere to be in a uniform field E_0 parallel to the x axis. This is equivalent to having the current electrode at considerable distance from the sphere.

Using spherical coordinates and applying the boundary conditions of Equation (8.7), we can solve Laplace's equation in the form of a series of Legendre polynomials (§2.7.4), satisfying potential relations inside and outside the sphere. For $r > a$, we get

$$V_1 = -E_0 r\cos\theta\left\{1 - \frac{(\rho_1 - \rho_2)}{(\rho_1 + 2\rho_2)}\left(\frac{a}{r}\right)^3\right\} \quad (8.22)$$

If the potential is measured at the ground surface, the sphere will have an image that will double the second term. In addition, if we consider the field to be generated by a current source C_1 at a distance R from the origin, we can write

$$V_1 = -\frac{I\rho_1}{2\pi R^2}\left\{1 - 2\frac{(\rho_1 - \rho_2)}{(\rho_1 + 2\rho_2)}\left(\frac{a}{r}\right)^3\right\} r\cos\theta \quad (8.23)$$

As in Equation (8.21) we have two terms, the first being the normal potential, the second the disturbing potential caused by the sphere. Equipotential and current flow lines are illustrated in the section shown in Figure 8.13.

Note that we have made two assumptions here that are not necessarily valid, first that the external or normal field is uniform and second that there is no interaction between the sphere and its image. Both are strictly true only when the sphere is a great distance from both the current source and surface, in which case the anomaly could not be detected anyway. However, if the distance between the sphere's center and the surface is not less than 1.3 times the radius, the approximation is reasonably good.

8.3.6. Effect of Anisotropic Ground

Most rock masses are anything but homogeneous and isotropic in the electrical sense because they are full of fractures. In particular, shales, slates, and frequently limestones and schists have a definite anisotropic character, especially with respect to the bedding planes.

As an example of this type of anisotropy, consider a point source at the surface of a semiinfinite medium in which the resistivity is uniform in the horizontal direction and has the value ρ_h; in the vertical direction it is also constant and has a different magnitude ρ_v, ρ_v almost invariably being larger than ρ_h (§5.2.2c).

Proceeding as in Section 8.2.3 with modifications to allow for the difference between horizontal and vertical directions, we find the equipotential surfaces to be ellipsoidal and symmetrical about the z axis. Mathematically this may be expressed by

$$V = -I\rho_h\lambda/2\pi\left(x^2 + y^2 + \lambda^2 z^2\right)^{1/2} \quad (8.24)$$

where $\lambda = (\rho_v/\rho_h)^{1/2}$ is the *coefficient of anisotropy*. This relation is similar to Equation (8.12) with

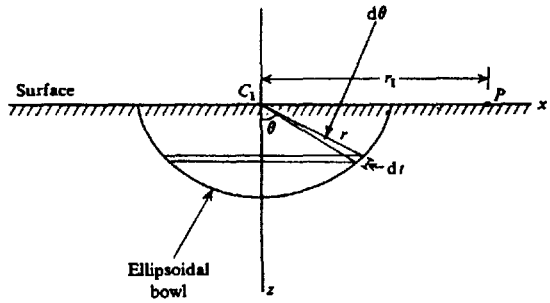

Figure 8.14. Point current source at the surface of anisotropic ground having resistivities ρ_h and ρ_v in the horizontal and vertical directions, respectively.

$\lambda/(x^2 + y^2 + \lambda^2 z^2)^{1/2}$ replacing r to represent the departure from spherical symmetry.

The potential at a surface point P, a distance r_1 from the current electrode C_1, will be

$$V_p = \frac{-I\rho_h\lambda}{2\pi r_1} = \frac{-I(\rho_h\rho_v)^{1/2}}{2\pi r_1} \qquad (8.25)$$

that is, the potential is equivalent to that for an isotropic medium of resistivity $(\rho_h\rho_v)^{1/2}$. Thus it is not possible to detect this type of anisotropy from field measurements.

From Equation (8.25) and Figure 8.14 it is obvious that the resistivity measured over horizontal beds is larger than the actual horizontal resistivity in the beds, but smaller than the vertical resistivity. On the other hand, if the beds have a steep dip and the measurement is made with a spread perpendicular to strike, the apparent resistivity will be smaller than the true resistivity normal to the bedding, just the opposite to the result over horizontal layers; this is known as the "paradox of anisotropy" (Bhattacharyya and Sen, 1981). If the array is parallel to the strike of the dipping beds, the apparent resistivity may be too large, depending on the current–electrode separation.

8.3.7. Effect of Topography

As mentioned earlier, resistivity measurements are strongly influenced by local variations in surface conductivity, caused by weathering and moisture content. Rugged topography will have a similar effect, because the current flow is concentrated or focused in valleys and dispersed or diverged beneath a hill. The equipotential surfaces are distorted as a result, producing false anomalies due to the topography alone. This effect may distort or mask a real anomaly.

Fox et al. (1980) made an analytical study of resistivity and IP response, obtained with a dipole-dipole array (§8.5.3d) over common 2-D terrain features; slopes, ridges, valleys. This approach was extended to three dimensions by Holcombe and Jiracek (1984). In the former report, the finite-element numerical method was used for modeling, because it offers more flexibility for matching irregular boundaries. Potentials are assigned to each interior mesh, based on its boundary geometry and electrical properties, and recomputed by successive sweeps through the whole section until the residuals become insignificantly small. They found that at the surface of homogeneous ground, resistivity is anomalously low on hills and ridges, high in valleys and 3-D depressions. Figure 8.15a illustrates the finite-element mesh representing a 2-D ridge, whereas Figure 8.15b shows the distortion of a uniform field produced by the ridge.

The terrain effect increases with surface relief, being insignificant for slopes of less than 10°. Furthermore the resistivity array complicates the effect. A double-dipole system straddling a hill produces current focusing and a resistivity high, whereas a valley results in a low resistivity, just the opposite to the results of Fox et al. described above.

The response is also sensitive to the direction of the measuring array; for 2-D structures the anomaly is smaller if the spread is parallel, rather than normal, to strike. Analysis of the type described above allows us to reduce the field data to a flat earth by removing or at least minimizing the terrain anomaly.

8.4. EQUIPMENT FOR RESISTIVITY FIELD WORK

8.4.1. Power Sources

The necessary components for making resistivity measurements include a power source, meters for measuring current and voltage (which may be combined in one meter to read resistance), electrodes, cable, and reels. The power may be either dc or low frequency ac, preferably less than 60 Hz.

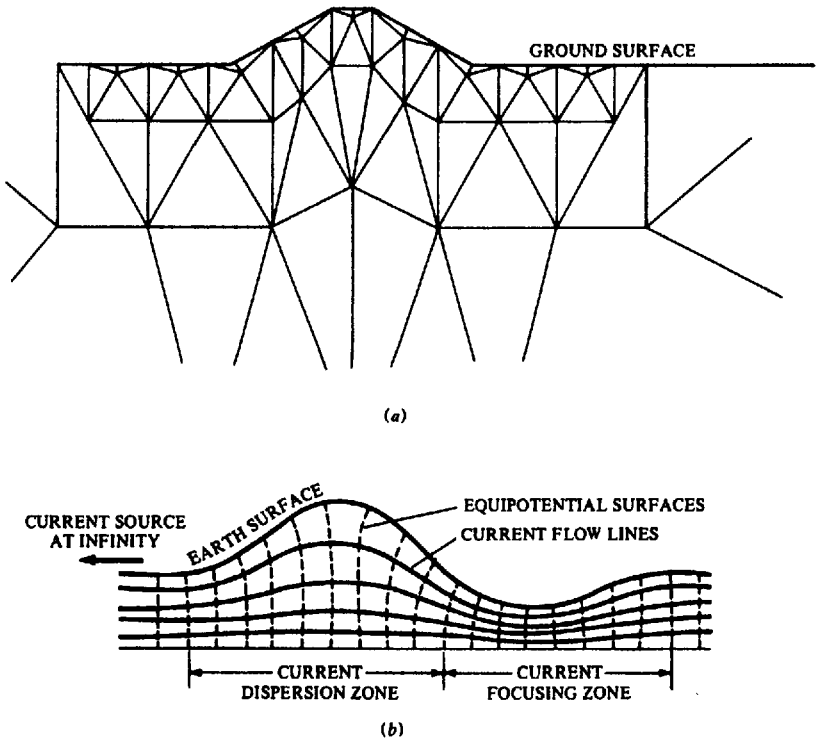

Figure 8.15. Effect of a 2-D ridge on a uniform field. (After Fox et al. 1980.) (a) Finite-element mesh used to calculate terrain effect of ridge. (b) Distortion of uniform field by ridge.

The power source is usually a motor generator of several hundred watts or a few kilowatts as in IP surveys. Equipment of this type, because of its bulk and weight, is only semiportable; it would not be moved each time the electrodes were shifted. When dc is used, one or more storage batteries or occasionally a set of B cells connected in series may be employed, although such sources are limited to small-scale work, such as overburden or engineering surveys.

To avoid the effects of electrolytic polarization caused by unidirectional current, the dc polarity should be reversed periodically, either by hand with a reversing switch, or by a mechanical commutator, relay system, or vibrator. The rate of commutation may range from three or four times a minute to 100 times per second.

Alternating current is also employed in place of commutated (effectively square-wave) dc. A low-frequency sine-wave transistor oscillator with transformer output of a few watts makes a convenient portable source. Larger power can be obtained from a motor-driven alternator.

Each of these devices obviously has advantages and limitations. The dc source permits measurement of true dc resistivity – which is desirable – but it also measures spontaneous potentials. This requires that porous pots be used as potential electrodes; the SP effect must be noted before the source is turned on, and then subtracted, either directly or by means of a compensating voltage, from the potential measured when current is flowing.

The use of ac or rapidly interrupted dc eliminates the SP effect. In addition, narrow-band amplifiers tuned to the source frequency can be employed to increase the signal-to-noise ratio. However, the resistivity measured will generally be lower than the true dc value. More serious, inductive coupling between long current and adjacent potential leads, as well as leakage currents, particularly on wet ground, may give erratic readings. All these effects increase with the frequency (§9.4.4c).

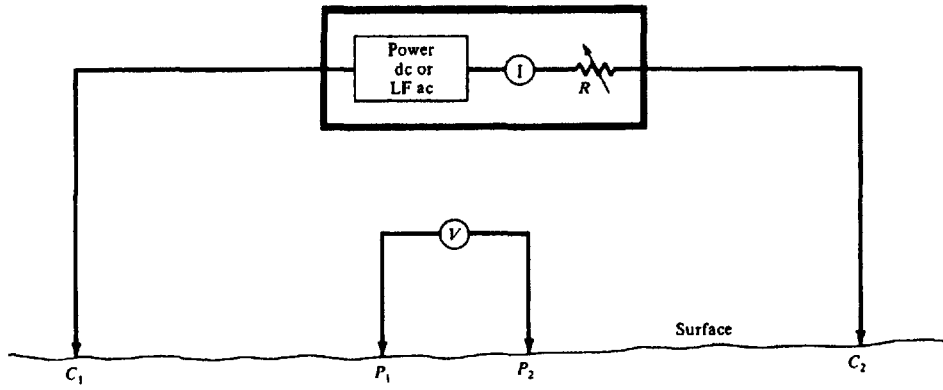

Figure 8.16. Schematic of equipment for measuring resistivity.

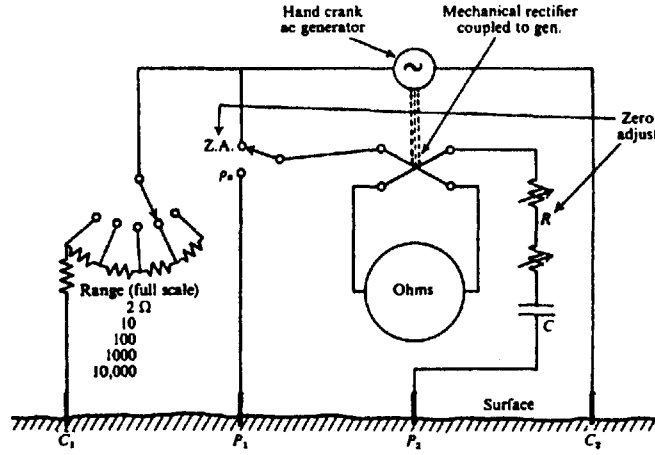

Figure 8.17. Portable equipment for measuring resistivity (schematic).

8.4.2. Meters

With dc or long-period commutated dc sources, the current is measured with a dc milliammeter, whose range should be from about 5 to 500 mA, depending on the electrode spread, type of ground, and power used. Potential is normally measured with a dc voltmeter of high input impedance (1 MΩ or greater) and range 10 mV to perhaps 20 V. When ac sources are used, ac meters are of course necessary.

A typical resistivity set with voltage and current meters is illustrated schematically in Figure 8.16. In some resistivity equipment the current is maintained constant with a regulator, which eliminates the current measurement.

An instrument that measures the ratio of potential to current (that is, resistance) – usually associated with the trade name *Megger* – has been frequently employed for resistivity work. Originally developed for testing cable insulation, this device was easily modified to measure ground resistance. Power is developed by hand cranking a dc generator or magneto; the output is ~ 100 V and a dc current coil is connected in series with one side. The output then is commutated on the generator shaft and applied to the current electrodes, the rate of reversal, being regulated by a governor. The potential electrodes are connected to a second commutator, synchronized with the other, which rectifies the ac potential and applies it to the potential coil. The latter is mounted with the current coil in such a way as to make the needle deflection proportional to V/I. This instrument is shown schematically in Figure 8.17.

Several other all-in-one resistivity instruments are also available, employing a vibrator powered by dry cells or low-frequency transistor oscillator. Such devices, like the Megger, necessarily have low power output. Furthermore, with some electrode spreads,

the combination of power source and both meters in one box may be a definite disadvantage. However, such instruments are compact and completely portable.

8.4.3. Electrodes and Wire

With ac power sources, all the electrodes may be steel, aluminum, or brass; stainless steel is probably best for combined strength and resistance to corrosion. Metal electrodes should be at least $\frac{1}{2}$ m long so they can be driven into the ground several centimeters for good electrical contact. In very dry surfaces this contact may be improved by watering the electrodes. If dc power is used the potential electrodes should be porous pots as in SP work.

Connecting wires, which must be insulated and as light as possible, are wound on portable reels. Plastic insulation is more durable than rubber against abrasion and moisture; however, some plastics deteriorate in cold weather and animals seem to find them very tasty in any season.

8.5. ELECTRODE LAYOUTS AND FIELD PROCEDURE

8.5.1. General

An enormous number of electrode spreads have been used in resistivity at various times; not more than a half dozen have survived to any extent. In principle it is not necessary to use a collinear array. Practically, however, the electrodes are almost always in line; otherwise interpretation of results becomes difficult and the field work is complicated.

One drawback in resistivity work is the practical difficulty of moving stakes with great lengths of wire attached, a slow and expensive task in relation to magnetics, EM, and some other electrical survey methods. Thus it is an advantage to use electrode spreads that may require only one or two electrodes to be moved, and these at close spacing where possible.

8.5.2. Apparent Resistivity

Before discussing the various electrode spreads, it is necessary to consider what is actually measured by an array of current and potential electrodes. We can rearrange the terms in Equation (8.13) to obtain

$$\rho = \frac{2\pi\Delta V}{I}\frac{1}{\{(1/r_1 - 1/r_2) - (1/r_3 - 1/r_4)\}} = \left(\frac{2\pi\Delta V}{I}\right)p \qquad (8.26)$$

where the parameter p has to do with the electrode geometry. By measuring ΔV and I and knowing the electrode configuration, we obtain a resistivity ρ. Over homogeneous isotropic ground this resistivity will be constant for any current and electrode arrangement.

If the ground is inhomogeneous, however, and the electrode spacing is varied, or the spacing remains fixed while the whole array is moved, then the ratio will, in general, change. This results in a different value of ρ for each measurement. The magnitude is intimately related to the arrangement of electrodes. This measured quantity is known as the *apparent resistivity*, ρ_a. Although it is diagnostic, to some extent, of the actual resistivity of a zone in the vicinity of the electrode array, the apparent resistivity is definitely not an average value and only in the case of homogeneous grounds is it equal to the actual resistivity.

Another term that is frequently found in the literature is the so-called *surface resistivity*. This is the value of ρ_a obtained with small electrode spacing. Obviously it is equal to the true surface resistivity only when the ground is uniform over a volume roughly of the dimensions of the electrode separation.

8.5.3. Electrode Arrays (Spreads)

(a) Wenner array. The most commonly used point-electrode systems are illustrated in Figure 8.18. The first two examples, the *Wenner and Schlumberger arrays*, were formerly most popular; since the development of the pseudodepth section (§9.5.1) in IP work, the double-dipole configuration has become equally so.

In the Wenner spread (Fig. 8.18a) the electrodes are uniformly spaced in a line. Setting $r_1 = r_4 = a$ and $r_2 = r_3 = 2a$, in Equation (8.26), the apparent resistivity becomes

$$\rho_a = 2\pi a\,\Delta V/I \qquad (8.27)$$

In spite of the simple geometry, this arrangement is often quite inconvenient for field work, and has some disadvantages from a theoretical point of view as well. For depth exploration using the Wenner spread, the electrodes are expanded about a fixed center, increasing the spacing a in steps. For lateral exploration or mapping, the spacing remains constant and all four electrodes are moved along the line, then along another line, and so on. In mapping, the apparent resistivity for each array position is plotted against the center of the spread.

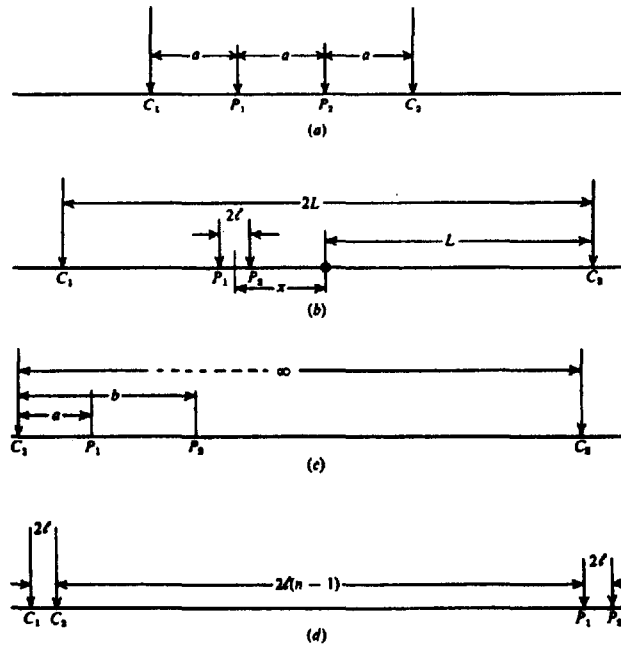

Figure 8.18. Electrode arrays in common use. (a) Wenner. (b) Schlumberger. (c) Pole-dipole. (d) Double-dipole.

(b) Schlumberger (gradient) array. For the Schlumberger array the current electrodes are spaced much further apart than the potential electrodes. From Figures 8.3 and 8.18b, we find that

$$r_1 = (L - x) - \ell$$
$$r_2 = (L + x) + \ell$$
$$r_3 = (L - x) + \ell$$

and

$$r_4 = (L + x) - \ell$$

Substituting these values in Equation (8.26), we get

$$\rho_a = \frac{2\pi\Delta V}{I}\left[\left\{\frac{1}{(L-x)-\ell} - \frac{1}{(L+x)+\ell}\right\} - \left\{\frac{1}{(L-x)+\ell} - \frac{1}{(L+x)-\ell}\right\}\right]^{-1} \quad (8.28)$$

If the smallest current-potential electrode distance is always considerably greater than the distance between the two potential electrodes (by a factor of 10 or more), then $(L - x) \gg 3\ell$ and we have to the first approximation

$$\rho_a \approx \frac{\pi}{2\ell}\frac{(L^2 - x^2)^2}{(L^2 + x^2)}\left(\frac{\Delta V}{I}\right) \quad (8.29a)$$

This array is often used symmetrically, that is, $x = 0$, in which case

$$\rho_a \approx \frac{\pi L^2}{2\ell}\left(\frac{\Delta V}{I}\right) \quad (8.29b)$$

Alternate symbols for the Schlumberger array are frequently found in the literature; for example, A, B, M, and N are used for C_1, C_2, P_1, and P_2, respectively; in this case $L = \frac{1}{2}AB$, $\ell = \frac{1}{2}MN$.

In vertical sounding (§8.5.4b) the potential electrodes remain fixed while the current-electrode spacing is expanded symmetrically about the center of the spread. For large values of L it may be necessary to increase ℓ also in order to maintain a measurable potential. Equation (8.29a) applies in this case. This procedure is more convenient than the Wenner expanding spread because only two electrodes need move. In addition, the effect of shallow resistivity variations is constant with fixed potential electrodes. Figures 8.42 and 8.44 illustrate vertical sounding results.

Lateral profiling (§8.5.4c) may be done in two ways. With a very large fixed separation of the current electrodes (300 m or more), the potential pair is moved between them, also with fixed spacing, subject to the limitation $(L - x) \gg 3\ell$ [Eq. (8.29a)]. Apparent resistivity is plotted against the midpoint of the potential electrodes.

The other layout is similar to the Wenner in that the electrode spacing remains fixed ($L \gg \ell$) and the whole array is moved along the line in suitable steps. This arrangement is less convenient than the first because it requires that all four electrodes be moved for each station.

In lateral profiling with the Schlumberger array (and with the pole-dipole array; see next section) it is permissible to measure potential somewhat off the line between fixed current electrodes, that is, to map the surface in two dimensions (because C_1 and C_2 are far apart, the current density is roughly uniform over a considerable lateral extent).

(c) Pole-dipole (three-point) array. One of the current electrodes is fixed at a great distance from the other three, all of which can have various spacings. The values in Equation (8.26) are now

$$r_1 = a$$
$$r_3 = b$$
$$r_2 = r_4 = \infty$$

so that

$$\rho_a = \frac{2\pi ab}{b-a}\left(\frac{\Delta V}{I}\right) \qquad (8.30a)$$

When $b = 2a$ this becomes

$$\rho_a = 4\pi a\left(\frac{\Delta V}{I}\right) \qquad (8.30b)$$

or double the ratio in the Wenner array [Eq. (8.27)]. When the potential spacing is very small compared to the distance of either potential electrode from C_1 (C_2 still at ∞), we write $r_1 = a - \delta a/2$, $r_3 = a + \delta a/2$, and the apparent resistivity becomes

$$\rho_a \approx \frac{2\pi a^2}{I}\left(\frac{\partial V}{\partial a}\right) \qquad (8.30c)$$

This arrangement is equivalent to a *half-Schlumberger array*. Equation (8.30c) is similar to Equation (8.34) with $a = L$, $\partial a = \Delta r$, that is, both electrode configurations measure potential gradient.

Because the electrode C_2 is remote, it is not necessary to have it in line with the other three. This permits lateral exploration on radial lines from a fixed position of C_1, by moving one or both potential electrodes, a particularly convenient method for resistivity mapping in the vicinity of a conductor of limited extent. This electrode arrangement is effectively the same as the *lateral spread* used in well logging, described in Section 11.2.3. It is also similar to the *mise-à-la-masse* method (§8.5.4d) in which the electrode C_1 is in contact with the conducting zone.

A further variation on the pole-dipole array is obtained by moving one of the potential electrodes, say P_2, to a distant point, which is also remote from C_2. In this case, $r_3 = b = \infty$ as well, and Equation (8.30a) is the same as Equation (8.27) for the Wenner spread, hence this array is known as the *half-Wenner array*. Although it is only necessary to move one potential electrode, the long connecting wire to the other is a disadvantage.

In field work the location of an electrode at infinity requires that it have very little influence on the rest of the array. For instance, when using a Wenner spread, the remote electrode or electrodes must be at least 10 times the spacing to reduce the effect to 10% or less. With the Schlumberger system, because the potential electrodes are close together, the far current electrode need only be about three times as far away as the one nearby to get the same result.

However, because the subsurface resistivity may vary laterally, these spacing estimates can be much too low and may have to be increased by a factor of 10 or more, depending on the resistivity contrast.

(d) Double-dipole (dipole-dipole) system. The potential electrodes are closely spaced and remote from the current electrodes, which are also close together. In this case, from Figure 8.18d and Equation (8.26) we get

$$r_1 = r_4 = 2n\ell$$
$$r_2 = 2\ell(n-1)$$
$$r_3 = 2\ell(n+1) \quad \text{where } n \gg 1$$

Then, dropping the minus,

$$\rho_a = 2\pi(n-1)n(n+1)\ell\Delta V/I \qquad (8.31)$$

When n is 5 or less, this is the spread commonly used in IP work (§9.4.3). Inductive coupling between potential and current cables is reduced with this arrangement.

When the dipoles are widely separated, $n \gg 1$ and we have

$$\rho_a = 2\pi n^3\ell\Delta V/I \qquad (8.32)$$

this is the approximation usually applied in resistivity surveys. The dipoles may also be placed broadside, bisected by the traverse line. In this case,

$$r_1 = r_4 = 2n\ell$$

$$r_2 = r_3 = 2\left\{(n\ell)^2 + \ell^2\right\}^{1/2} \approx 2n\ell\left(1 + 1/2n^2\right)$$

and

$$\rho_a \approx 4\pi n^3\ell\Delta V/I \qquad (8.33)$$

In all the above electrode layouts the potential and current electrodes may be interchanged. By the principle of reciprocity, the apparent resistivity should be the same in either case. The switching of current and potential electrodes could be desirable, for instance, in using high voltages with large spreads in Schlumberger and, possibly, Wenner layouts.

8.5.4. Resistivity Field Procedures

(a) Introduction. Regardless of the specific electrode spread employed, there are really only two basic procedures in resistivity work. The particular procedure to be used depends on whether one is interested in resistivity variations with depth or with lateral extent. The first is called *vertical*, *electric*, or *vertical-electric* (*VES*) sounding, the second *lateral profiling* or *mapping*.

(b) Vertical sounding. Because the fraction of total current that flows at depth varies with the current-electrode separation, as described in §8.2.5, the field procedure is to use a fixed center with an expanding spread. Although the pole-dipole array is not suited to this technique, any of the other three configurations may be used, the Schlumberger having the advantages mentioned in Section 8.5.3b. The presence of horizontal or gently dipping beds of different resistivities is best detected by the expanding spread. Hence the method is useful in determining depth of overburden, depth, structure, and resistivity of flat-lying sedimentary beds and possibly of the basement also if it is not too deep.

It is frequently necessary to carry out this expansion procedure at several locations in an area, even when the main interest may be in lateral exploration, to establish proper electrode spacings for the lateral search.

(c) Lateral profiling. This method is particularly useful in mineral exploration, where the detection of isolated bodies of anomalous resistivity is required. Any of the electrode arrangements described in Section 8.5.3 may be used, the selection depending mainly on the field situation. In Wenner, Schlumberger, and pole-dipole surveys the apparent resistivity is plotted at the midpoint of the potential electrodes, except where one of these is effectively at infinity, as in the modified three-probe system, when the station is reckoned at the near potential electrode. For the double-dipole, the station is at the array midpoint.

When the potential electrodes are closely spaced with respect to the current spread, as in the Schlumberger and possibly the three-point system, the measurement is effectively of potential gradient at the midpoint. This can be seen from Equation (8.29b) where, putting $2\ell = \Delta r$, we can write

$$\rho_a = \frac{\pi L^2}{I}\left(\frac{\Delta V}{\Delta r}\right) \tag{8.34}$$

If the current electrodes are close together and remote from the potential pair, the measurement is essentially that of the curvature of the field or the second derivative. For the double-dipole spread in Figure 8.18d, the potential gradient at the midpoint of P_1P_2 due to C_1 only is $\Delta V_1/\Delta r$, where Δr is the spacing of the potential electrodes. Similarly the potential gradient due to C_2 only is $\Delta V_2/\Delta r$. Then the measured potential gradient becomes, in the limit as $\Delta r \to 0$,

$$\frac{\Delta V}{\Delta r} = \frac{\Delta V_1 - \Delta V_2}{\Delta r} \to \left(\frac{\partial V}{\partial r}\right)_{C_1} - \left(\frac{\partial V}{\partial r}\right)_{C_2} = \Delta r\left(\frac{\partial^2 V}{\partial r^2}\right)$$

or,

$$\Delta V = (\Delta r)^2 \frac{\partial^2 V}{\partial r^2} \tag{8.35}$$

Also, with $r_1 = r_4 = r$, $r_2 = r - \Delta r$, and $r_3 = r + \Delta r$, we obtain from Equation (8.13),

$$\Delta V = \frac{I\rho_a}{2\pi}\left(\frac{1}{r} - \frac{1}{r-\Delta r} - \frac{1}{r+\Delta r} + \frac{1}{r}\right) \approx -\frac{I\rho_a}{\pi}\frac{(\Delta r)^2}{r^3}$$

using the second approximation (Eq. (A.44)). This gives

$$\rho_a \approx -\frac{\pi r^3}{(\Delta r)^2}\left(\frac{\Delta V}{I}\right) \approx -\frac{\pi r^3}{I}\left(\frac{\partial^2 V}{\partial r^2}\right) \tag{8.36}$$

Lateral exploration by resistivity measurements is best suited to detection of steeply dipping contacts and dikes of contrasting resistivity, that is, 2-D anomalies, and to a lesser extent for location of anomalous 3-D conductors such as could be roughly simulated by the sphere.

(d) Mise-à-la-masse. This is a variation on the three-point electrode system, used where some part of the conductive zone is already located and exposed, either as outcrop or in a drill hole. The near current electrode is embedded in the zone itself, the other being a large distance away on surface. The

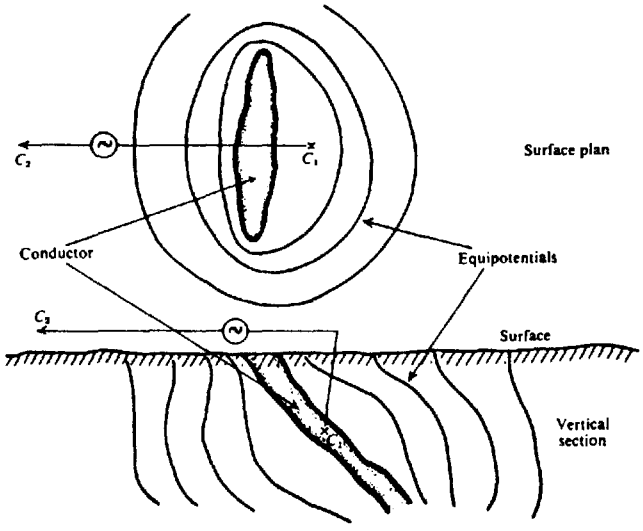

Figure 8.19. Distortion of the equipotentials around the near current electrode by a dipping conductor when using the mise-à-la-masse method.

potential electrodes are moved about, either on surface or in drill holes. The extent, dip, strike, and continuity of the zone will be better indicated by introducing the current directly into it than by the usual mapping techniques.

The effect of a dipping mineralized zone on the equipotentials is shown in Figure 8.19. Because the second current electrode is at infinity, it is possible to map the potentials in all directions around the zone without shifting the current stakes.

8.6. INTERPRETATION

8.6.1. Introduction

The mathematical analysis for quantitative interpretation of resistivity results is most highly developed for the vertical sounding technique, reasonably so for lateral profiling over large-scale contacts of steep dip, and least useful for the detection of 3-D anomalies. As in other geophysical methods where quantitative interpretation is possible, the assessment of results should progress from rough preliminary estimates made in the field toward more sophisticated methods of interpretation, eventually based on the complete survey. Such a procedure keeps the field work up-to-date, controls the day-by-day program, and indicates where more intensive work is warranted, both in the field survey and its interpretation. Van Nostrand and Cook (1966) give a very extensive bibliography of resistivity interpretation techniques.

8.6.2. Resistivity Modeling

The use of models, although not as common in resistivity as in EM, can be a useful aid in interpretation. Resistivity modeling is generally done in a water tank, the resistivity of the liquid being varied by the addition of salts such as NaCl or acids such as H_2SO_4. Sand may be used instead of liquid, provided reproducible contacts between the model electrodes and the surface can be made.

Various conducting or insulating sheets, cylinders, and blocks are immersed in the tank to simulate the field situation. The electrode spread is moved about laterally in a convenient jig mount on the surface of the tank; alternatively, in a liquid medium, the model anomaly may be moved past the electrode spread.

Scaling is not a problem in resistivity model work (§7.7.1b). The usual relation in resistivity is $\Delta V/I \propto \rho/l$, where l is scaled linearly. Rather than vary the resistivity ρ, it is simpler to change ΔV or I. However, somewhat higher frequencies could conveniently be used in the model than in the field without introducing errors.

8.6.3. Vertical sounding; Two Horizontal Beds

(a) Basic formula. The method of images developed in Section 8.3.4 is useful in dealing with soundings on two horizontal layers, as well as profiling

over elementary 2-D structures. Its application to the former also provides some simple illustrations of limiting cases of the bed parameters.

Equation (8.21) relates the potential of a single electrode to the resistivity of the upper layer in terms of the electrode spacing, the depth to the interface, and the resistivity contrast between the two beds. We want this expression in the form of an apparent resistivity, which would be measured by a four-electrode system. Using the symbols of Figure 8.3 and Equation (8.13), Equations (8.19), (8.21), and (8.26) enable us to write, for the measured potential difference between P_1 and P_2,

$$\Delta V = V_1 - V_2 = \frac{I\rho_1}{2\pi}\left[\left(\frac{1}{r_1} - \frac{1}{r_2}\right) - \left(\frac{1}{r_3} - \frac{1}{r_4}\right) + 2\sum_{m=1}^{\infty} k^m \left\{ \frac{1}{\left(r_1^2 + 4m^2z^2\right)^{1/2}} - \frac{1}{\left(r_2^2 + 4m^2z^2\right)^{1/2}} - \frac{1}{\left(r_3^2 + 4m^2z^2\right)^{1/2}} + \frac{1}{\left(r_4^2 + 4m^2z^2\right)^{1/2}} \right\}\right] \quad (8.37)$$

(b) Wenner spread. Because $r_1 = r_4 = a$, $r_2 = r_3 = 2a$ (Fig. 8.18a), Equation (8.37) is simplified to give

$$\Delta V = \frac{I\rho_1}{2\pi a}\left[1 + \sum_{m=1}^{\infty} \frac{4k^m}{\left\{1 + (2mz/a)^2\right\}^{1/2}} - \sum_{m=1}^{\infty} \frac{4k^m}{\left\{4 + (2mz/a)^2\right\}^{1/2}}\right] = \frac{I\rho_1}{2\pi a}(1 + 4D_w)$$

where

$$D_w = \sum_{m=1}^{\infty} k^m \left[\frac{1}{\left\{1 + (2mz/a)^2\right\}^{1/2}} - \frac{1}{\left\{4 + (2mz/a)^2\right\}^{1/2}}\right]$$

From Equation (8.26) we have

$$\rho_a = 2\pi\Delta V p/I = 2\pi\Delta V/I(1/a - 1/2a - 1/2a + 1/a) = 2\pi a\,\Delta V/I$$

so that the apparent resistivity is

$$\rho_a = \rho_1\left[1 + \sum_{m=1}^{\infty} \frac{4k^m}{\left\{1 + (2mz/a)^2\right\}^{1/2}} - \sum_{m=1}^{\infty} \frac{4k^m}{\left\{4 + (2mz/a)^2\right\}^{1/2}}\right] = \rho_1(1 + 4D_w) \quad (8.38)$$

(c) Schlumberger spread. When $x = 0$, $r_1 = r_4 = L - \ell$, $r_2 = r_3 = L + \ell$ (Fig. 8.18b), and the potential is

$$\Delta V = \frac{I\rho_1}{2\pi}\left[\left(\frac{2}{L-\ell} - \frac{2}{L+\ell}\right) + 4\sum_{m=1}^{\infty} k^m \times \left\{ \frac{1}{(L-\ell)\left\{1 + (2mz)^2/(L-\ell)^2\right\}^{1/2}} - \frac{1}{(L+\ell)\left\{1 + (2mz)^2/(L+\ell)^2\right\}^{1/2}} \right\}\right]$$

$$= \frac{I\rho_1 2\ell}{\pi(L^2 - \ell^2)}\left[1 + \left(\frac{L+\ell}{\ell}\right) \times \sum_{m=1}^{\infty} \frac{k^m}{\left\{1 + (2mz)^2/(L-\ell)^2\right\}^{1/2}} - \left(\frac{L-\ell}{\ell}\right)\sum_{m=1}^{\infty} \frac{k^m}{\left\{1 + (2mz)^2/(L+\ell)^2\right\}^{1/2}}\right]$$

When $L \gg \ell$, the terms inside the square brackets can be simplified; the potential difference then becomes

$$\Delta V \approx \frac{I\rho_1 2\ell}{\pi L^2}\left[1 + 2\sum_{m=1}^{\infty} \frac{k^m}{\left\{1 + (2mz/L)^2\right\}^{1/2}}\right] \approx \frac{I\rho_1 2\ell}{\pi L^2}(1 + 2D_s')$$

where

$$D_s' = \sum_{m=1}^{\infty} \frac{k^m}{\left\{1 + (2mz/L)^2\right\}^{3/2}}$$

The exact expression for apparent resistivity is

$$\rho_a = \rho_1\left[1 + \left(\frac{L+\ell}{\ell}\right) \times \sum_{m=1}^{\infty} \frac{k^m}{\left\{1 + (2mz)^2/(L-\ell)^2\right\}^{1/2}} - \left(\frac{L-\ell}{\ell}\right) \times \sum_{m=1}^{\infty} \frac{k^m}{\left\{1 + (2mz)^2/(L+\ell)^2\right\}^{1/2}}\right] = \rho_1(1 + D_s) \tag{8.39a}$$

where

$$D_s = \left(\frac{L+\ell}{\ell}\right) \sum_{m=1}^{\infty} \frac{k^m}{\left\{1 + (2mz)^2/(L-\ell)^2\right\}^{1/2}} - \left(\frac{L-\ell}{\ell}\right) \sum_{m=1}^{\infty} \frac{k^m}{\left\{1 + (2mz)^2/(L+\ell)^2\right\}^{1/2}}$$

Approximately, we have

$$\rho_a \approx \rho_1\left[1 + 2\sum_{m=1}^{\infty} \frac{k^m}{\left\{1 + (2mz/L)^2\right\}^{3/2}}\right] = \rho_1(1 + 2D_s'). \tag{8.39b}$$

This result can also be obtained by differentiating Equation (8.21) with respect to r, multiplying the result by 2 (because there are two current electrodes), and applying Equation (8.34) to get ρ_a.

(d) Double-dipole spread. Because $r_1 = r_4 = 2n\ell$, $r_2 = 2(n-1)\ell$, $r_3 = 2(n+1)\ell$ (Fig. 8.18d), the exact expression for the potential is

$$\Delta V = -\frac{I\rho_1}{2\pi(n-1)n(n+1)\ell} \times \left[1 + n(n+1) \times \sum_{m=1}^{\infty} \frac{k^m}{\left[1 + (2mz)^2/\{2(n-1)\ell\}^2\right]^{1/2}} + n(n-1) \times \sum_{m=1}^{\infty} \frac{k^m}{\left[1 + (2mz)^2/\{2(n+1)\ell\}^2\right]^{1/2}} - 2(n-1)(n+1) \times \sum_{m=1}^{\infty} \frac{k^m}{\left\{1 + (2mz/2n\ell)^2\right\}^{1/2}}\right]$$

The apparent resistivity is given by

$$\rho_a = \rho_1(1 + D_d) \tag{8.40a}$$

where $(1 + D_d)$ is the expression inside the large square brackets above.

If we make $n \gg 1$, the preceding result is simplified and we can make use of Equation (8.21). Differentiating twice,

$$\frac{\partial^2 V}{\partial r^2} = \frac{I\rho_1}{\pi r^3}\left[1 - \sum_{m=1}^{\infty} \frac{k^m}{\left\{1 + (2mz/r)^2\right\}^{3/2}} + 3\sum_{m=1}^{\infty} \frac{k^m}{\left\{1 + (2mz/r)^2\right\}^{5/2}}\right]$$

and using Equation (8.36),

$$\rho_a = \rho_1\left[1 - \sum_{m=1}^{\infty} \frac{k^m}{\left\{1 + (2mz/r)^2\right\}^{3/2}} + 3\sum_{m=1}^{\infty} \frac{k^m}{\left\{1 + (2mz/r)^2\right\}^{5/2}}\right] = \rho_1(1 + D_d') \tag{8.40b}$$

(e) Discussion of theoretical results. Quantitatively we can see how the apparent resistivity varies from Equation (8.38) through (8.40) for the different electrode spreads. When the electrode spacing is very small, that is, $r \ll z$, the series terms in all cases tend to zero, so that we measure the resistivity in the upper formation. This is the surface resistivity defined in Section 8.5.2.

Because the reflection coefficient is less than unity, when the $C - P$ electrode spacing is very large compared to z, the depth of the bed, the series expansions in all of the equations becomes the same (because the denominators ≈ 1 or 2):

$$\rho_a \approx \rho_1\left(1 + 2\sum_{m=1}^{\infty} k^m\right) \tag{8.41}$$

Because $k^2 < 1$, the summation term is an infinite geometric progression with the value

$$\sum_{m=1}^{\infty} k^m = 1/(1-k) - 1$$

Substituting $k = (\rho_2 - \rho_1)/(\rho_2 + \rho_1)$, we get $\rho_a = \rho_2$. Thus at very large spacing, the apparent resistivity is practically equal to the resistivity in the lower formation.

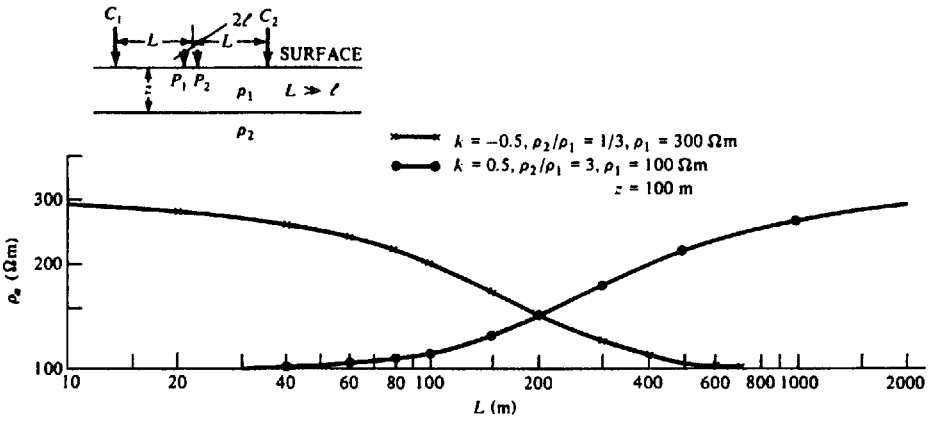

Figure 8.20. Plots of ρ_a versus L over two horizontal beds for a Schlumberger expanding spread. Curves were calculated from Equation (8.39b).

When the lower bed is an insulator, $\rho_2 = \infty$ and $k = 1$. Then the apparent resistivity increases indefinitely with electrode spacing, as is obvious from Equation (8.41). Because all the current will flow in the upper bed, it is possible to determine the value of ρ_a when $\rho_2 = \infty$ by calculating the electric field at the midpoint of the current electrodes. Because their separation is much larger than the thickness of the upper bed, it is reasonable to assume a uniform current density from top to bottom. Then the current from either electrode is found by integrating over a cylindrical equipotential surface of radius r and height z. Thus,

$$I = \int_0^{2\pi}\int_0^z Jr\,d\theta\,dz = 2\pi rzJ$$

From Equation (8.1) we have in this case (noting that the current is doubled because there are two current electrodes)

$$E = 2\rho_1 J = \rho_1 I/\pi rz$$

For the Wenner array, we get an apparent resistivity [Eq. (8.27)]

$$\rho_a = \frac{2\pi a\,\Delta V}{I} = \frac{2\pi a}{I}\int_a^{2a} E\,dr = \left(\frac{2a\rho_1}{z}\right)\ln 2$$
$$= 1.39\left(\frac{a\rho_1}{z}\right) \qquad (8.42a)$$

For the Schlumberger layout, using Equation (8.34) with $L = r$, we get

$$\rho_a = \frac{\pi L^2}{I}\frac{\partial V}{\partial r} = \frac{L\rho_1}{z} \qquad (8.42b)$$

and for the double-dipole system, Equation (8.36) gives

$$\rho_a = -\left(\frac{\pi r^3}{I}\right)\frac{\partial^2 V}{\partial r^2} = \frac{r\rho_1}{2z} \qquad (8.42c)$$

where r is the distance between centers of the current and potential dipoles.

In all three spreads we have

$$\rho_a/\rho_1 = c(\text{electrode spacing/depth to interface}) \qquad (8.42d)$$

where the constant c varies with the type of spread. Thus if we plot ρ_a/ρ_1 versus a/z, L/z, or r/z under these conditions, the curve is a straight line.

On the other hand, if the lower bed is a very good conductor, $\rho_2 \approx 0$ and $k \approx -1$. In this case $\rho_a \approx \rho_2 \approx 0$ for large spacing.

(f) Crude interpretation. Before applying the more complicated methods of interpretation it is useful to consider a few rough ideas. Figure 8.20 shows a pair of resistivity curves for two layers with contrasts of 3 and $\frac{1}{3}$. The upper bed resistivity is 100 and 300 Ωm for the two cases (to put the two curves on the same ordinate scale), and the thickness is 100 m.

The curve for $\rho_2/\rho_1 = \frac{1}{3}$ is clearly asymptotic to ρ_1 and ρ_2 at the limits of small and large spacing, and its point of maximum slope is approximately at 100 m. Thus we can estimate the depth and the resistivities of the two beds for this simple example.

The other curve gives the upper layer resistivity at small spacing, but it is not so clear what the value of ρ_2 may be. If the spacing were increased to several kilometers, it would be asymptotic to 300 Ωm. The

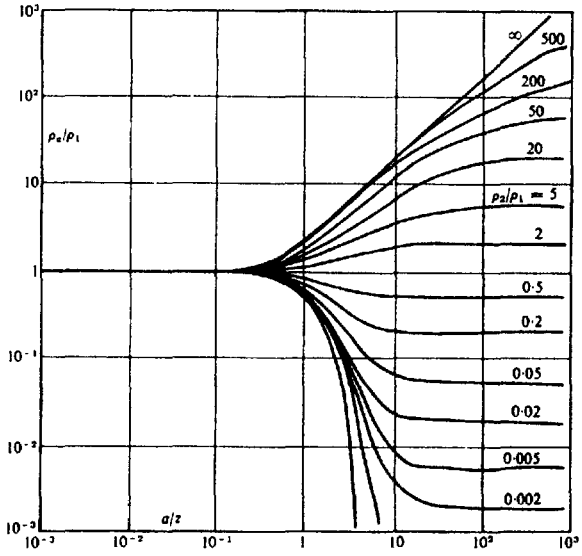

Figure 8.21. Wenner spread – master curves for two horizontal beds. (From Keller and Frischknecht, 1966.)

point of inflexion is not at 100 m but at a larger spacing.

Approximately then, we can get some idea of the unknown parameters ρ_1 and ρ_2 and z from the field curve, provided the resistivity contrast is not too great and particularly if the lower bed is the more conductive of the two.

(g) Curve matching. A much more accurate and dependable method of interpretation in electric sounding involves the comparison of field profiles with characteristic curves. It is quite similar to the interpretation from master curves in magnetotellurics, described in Section 6.2.8b.

The master curves are prepared with dimensionless coordinates. Equations (8.38) to (8.40) can be put in this form by dividing ρ_a by ρ_1. The ratios ρ_a/ρ_1 are then plotted against a/z, L/z, or r/z, that is, the electrode spacing divided by the depth of the upper bed for whatever electrode system is used. The curves are on logarithmic paper, usually six decades each way to provide a large range of both ratios on one sheet. Thus we are plotting ($\log \rho_a - \log \rho_1$) against ($\log a - \log z$). If we make $\rho_1 = 1$ Ωm and $z = 1$ km, all the characteristic curves are preserved in shape. The sets of curves are constructed either for various values of k between ± 1 or for various ratios of ρ_2/ρ_1 between 0 and $+\infty$. A typical set of curves is shown in Figure 8.21.

The characteristic curves are generally drawn on a transparency. To match a field result it is only necessary to slide the master sheet around on the field profile until the latter coincides more or less with one of the master curves (or can be interpolated between adjacent master curves). The respective coordinate axes must be kept parallel. The point where $\rho_a/\rho_1 = a/z = 1$ on the master sheet then determines the values of ρ_1 and z on the field curve axes, while the actual curve fit gives the value of k and hence ρ_2.

(h) Interpretation by asymptotes. In the event that the lower bed has very large resistivity we saw in Section 8.6.3e that the characteristic two-layer curve becomes a straight line for large electrode spacing. In the logarithmic plots this line has a slope of 45° for all of the arrays considered, because we have made ρ_1 and z unity.

The master curves are not necessary in this case. After plotting the field profile on log-log paper, a straight edge is placed horizontally as a best fit along the left-hand portion of the curve. The intersection of this straight edge with the ρ_a axis gives ρ_1. Next the hypotenuse of a 45° triangle is fitted to the sloping part of the curve on the right-hand side of the profile. The interface depth can then be found on the horizontal axis from the intersection of the triangle and the horizontal straight edge. This procedure is illustrated in Figure 8.22.

The asymptote method may also be used even when the maximum spacing has not been large enough to establish that the bottom layer has a very

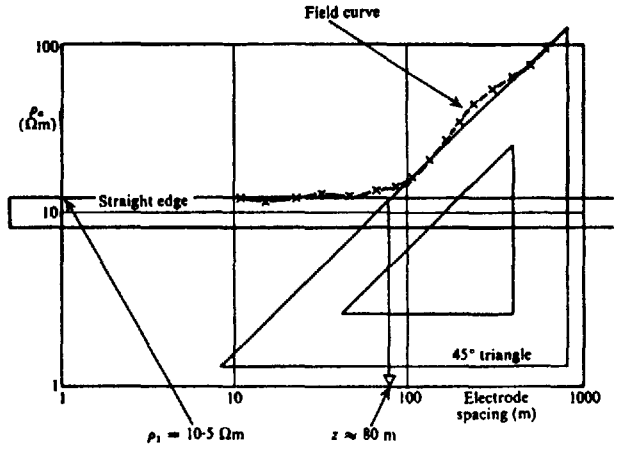

Figure 8.22. Estimate of ρ_1 and z from the 45° asymptote. (After Keller and Frischknecht, 1966.)

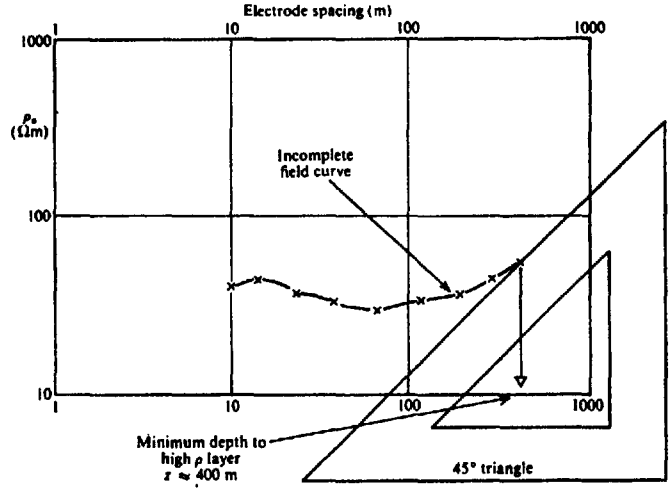

Figure 8.23. Asymptote method of estimating minimum depth.

high resistivity. In this case the 45° triangle is placed to intersect the point of maximum spacing as, for example, in Figure 8.23. In this case the depth estimate can only be a minimum.

8.6.4. Vertical Sounding; Multiple Horizontal Beds

(a) Introduction. When there are more than two horizontal beds present, as is usually the case, the previously mentioned single overburden analysis is first used for relatively small electrode spacing. This gives the depth and resistivity of the upper layer.

Next is is possible to estimate the minimum conductance of all layers above the bottom by drawing the 45° line through the point given for maximum electrode separation, as shown in Figure 8.23. The ratio of spacing to ρ_a for any point on this line will be a conductance representing all the rocks above an insulating layer; in Figure 8.23, for example, it is about 9 S. If the right-hand extreme of the field profile is itself a 45° line on the log-log plot, the bottom layer is highly resistive. In this case the actual, rather than minimum, conductance is determined.

(b) Crude interpretation. The overall shape of the middle portion of the profile will give us some idea of the character of the beds between surface and basement. Several shapes are illustrated in Figure

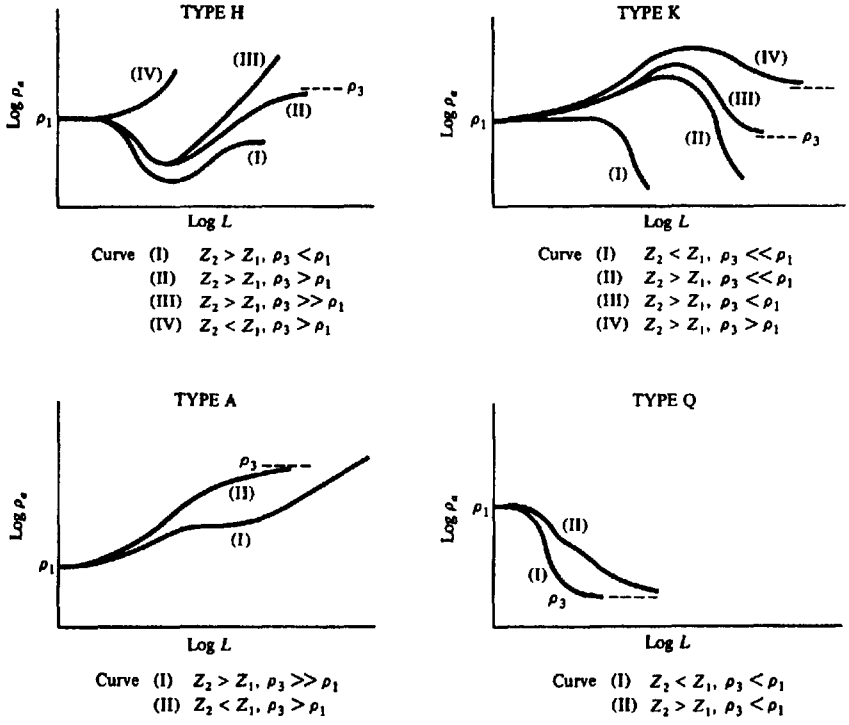

Figure 8.24. Various types of sounding curves over multilayer structures of three or more beds.

8.24. Types H and K have a definite minimum and maximum, indicating a bed, or beds, of anomalously low or high resistivity, respectively, at intermediate depth. Types A and Q show fairly uniform change in resistivity, the first increasing, the second decreasing with depth. Obviously these curves also may be combined. It is generally possible to tell from the shape of the adjacent parts of the profile which layer corresponds to the maximum or minimum on the first two curve types.

Although, in general, the characteristic sounding curves illustrated in Figure 8.24 represent multiple layers, in their crudest form they may be considered to be for two beds over a basement. On this assumption each of the four sets has particular properties that may be roughly classified. For H- and K-type curves $\rho_1 > \rho_2 < \rho_3$ and $\rho_1 < \rho_2 > \rho_3$, respectively, and we may be able to draw some conclusions about the relative values of ρ_1 and ρ_3 if the spread has been extended sufficiently. The A- and Q-type curves correspond to $\rho_1 < \rho_2 < \rho_3$ and $\rho_1 > \rho_2 > \rho_3$, respectively. Some idea of the relative bed thicknesses may be obtained from the horizontal extent of the maxima and minima as well as the flanking portions in all cases.

(c) Use of maximum and minimum points. The coordinates of the extreme points in curves of types H and K, Figure 8.24 (i.e., maximum or minimum ρ_a and electrode separation) may be used with certain characteristic curves for three layers employing a particular electrode spread. Figure 8.25 shows a set for the Schlumberger array in which: (a) $\rho_a(\max)/\rho_1$ is plotted against ρ_2/ρ_1 for various values of z_2/z_1 and (b) the ratio $L(\max)/z_1$ is plotted against z_2/z_1 for various values of ρ_2/ρ_1, $L(\max)$ being the electrode spacing at which ρ_a is a maximum or minimum.

Because we know the value of $\rho_a(\max)/\rho_1$ and $L(\max)/z_1$ (presumably ρ_1 and z_1 can be found from a two-layer curve match on the left of the profile), horizontal lines drawn across the characteristics in Figure 8.25a and b give two sets of possible values of ρ_2/ρ_1 and z_2/z_1, corresponding to the intersections. If we now plot these values of z_2/z_1 versus ρ_2/ρ_1, we get two curves which intersect at

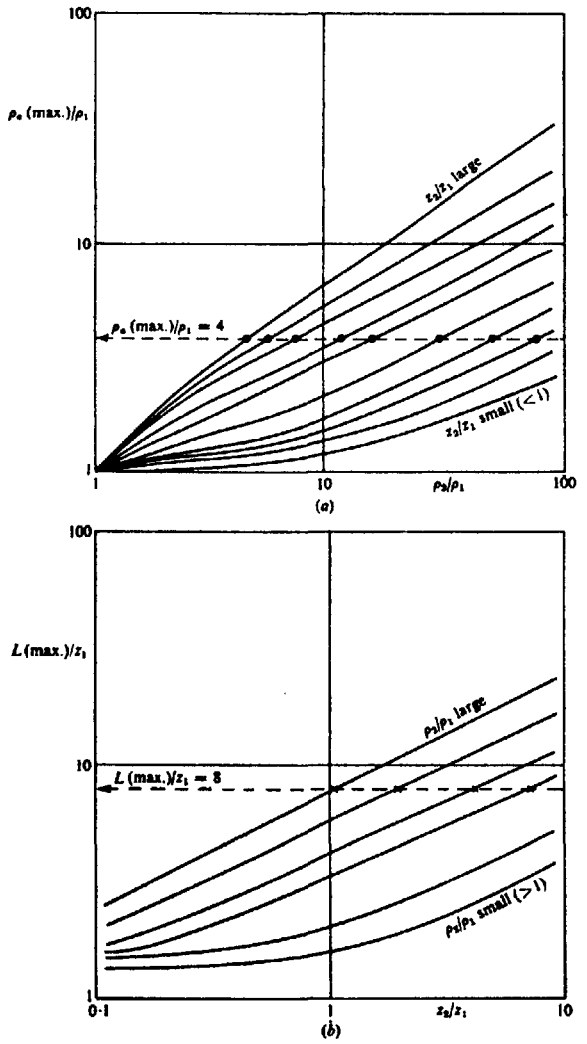

Figure 8.25. Schlumberger array – characteristic curves for three layers with type-K curves (see Fig. 8.24). (After Keller and Frischknecht, 1966.) (a) Plots of ρ_a(max.)/ρ_1 versus ρ_2/ρ_1 for various z_2/z_1 ratios. (b) Plots of L(max.)/z_1 versus z_2/z_1 for various ρ_2/ρ_1 ratios.

one point. This point represents the correct values of z_2 and ρ_2 for the layer in question as shown in Figure 8.26.

(d) Partial curve matching. This technique requires matching of small segments of the field profile with theoretical curves for two or, if possible, three horizontal layers. Generally one would start from the left-hand (small spacing) side of the profile and match successive segments toward the right (large spacing). When a portion of the field curve is reasonably matched in this way, all the layers in this segment are lumped together and assumed to have an effective resistivity ρ_e and depth z_e. This lumped layer is used as a surface layer and the next portion of the field curve is interpreted in a similar way.

It would be quite impractical to slide the field curve on the master randomly in attempting to find a reasonable fit between the segments of the curves. The process requires that we know where to locate the origin (for example, where $\rho_a/\rho_1 = L/z_1 = 1$ on the master two- or three-layer curve) with respect to

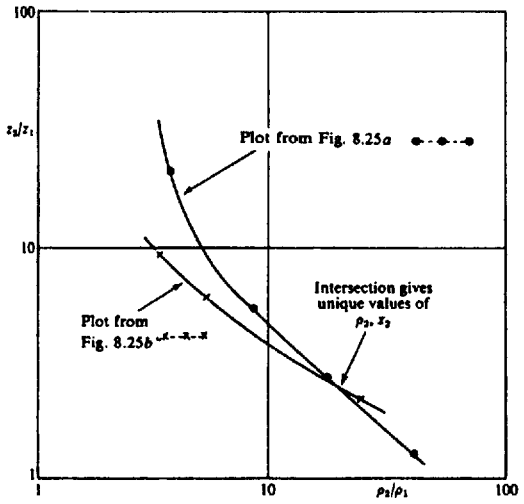

Figure 8.26. Determining second-layer parameters using data from Figure 8.25. (After Keller and Frischknecht, 1966.)

the field curve to obtain the best fit to successive portions of the latter as we progress from left to right. This interim origin is known as the *auxiliary point* or *cross* in the literature (Hummel, 1932; Zohdy, 1965; Bhattacharya and Patra, 1968). To illustrate the significance of these auxiliary points, consider a modification of Figure 5.1 and Equations (5.8) and (5.9). If we change Figure 5.1 so that it represents a vertical stack of beds with resistivities $\rho_1, \rho_2, \ldots, \rho_n$ and thicknesses $z_1, z_2, \ldots, z_n$ from top to bottom, and cross section 1 m^2, then v and $1 - v$ in Equations (5.8) and (5.9) are proportional to the thicknesses.

Analogous to Equations (5.8) and (5.9) we have in the vertical direction a so-called *transverse unit resistance*

$$T = \rho_1 z_1 + \rho_2 z_2 + \cdots + \rho_n z_n = \sum_{i=1}^{n} \rho_i z_i \quad (8.43a)$$

and in the horizontal direction a *longitudinal unit*

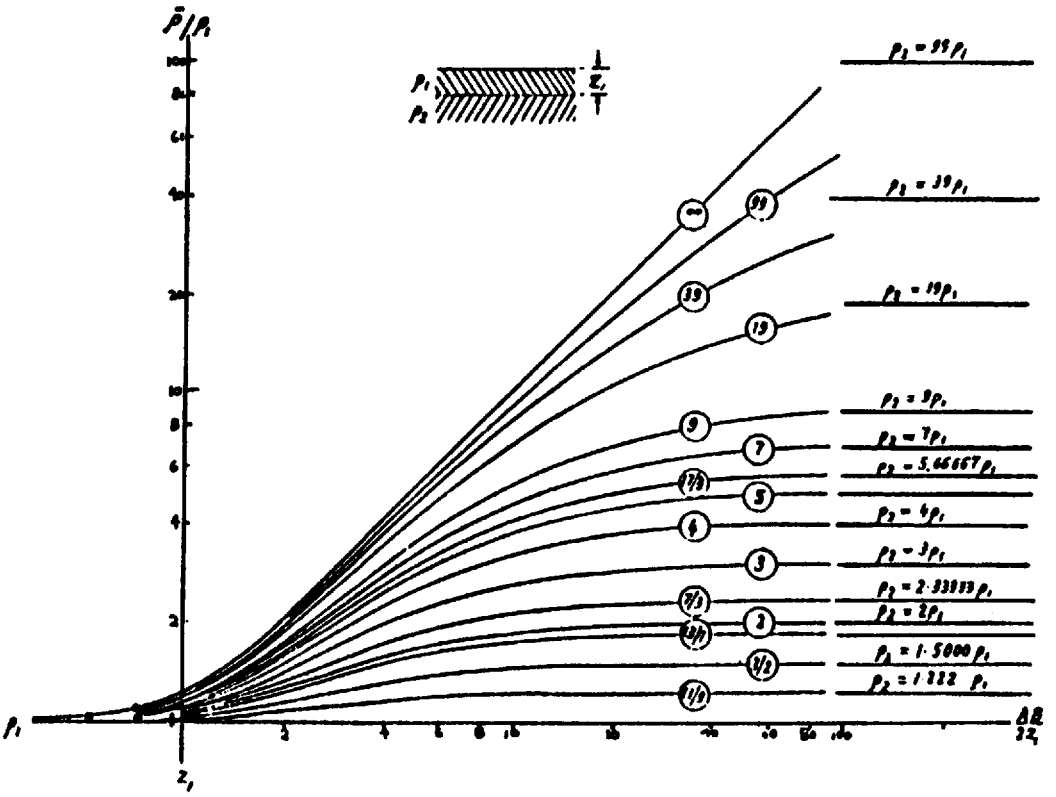

Figure 8.27. Two-layer Schlumberger master curves. (a) Ascending type ($\rho_2 > \rho_1$).

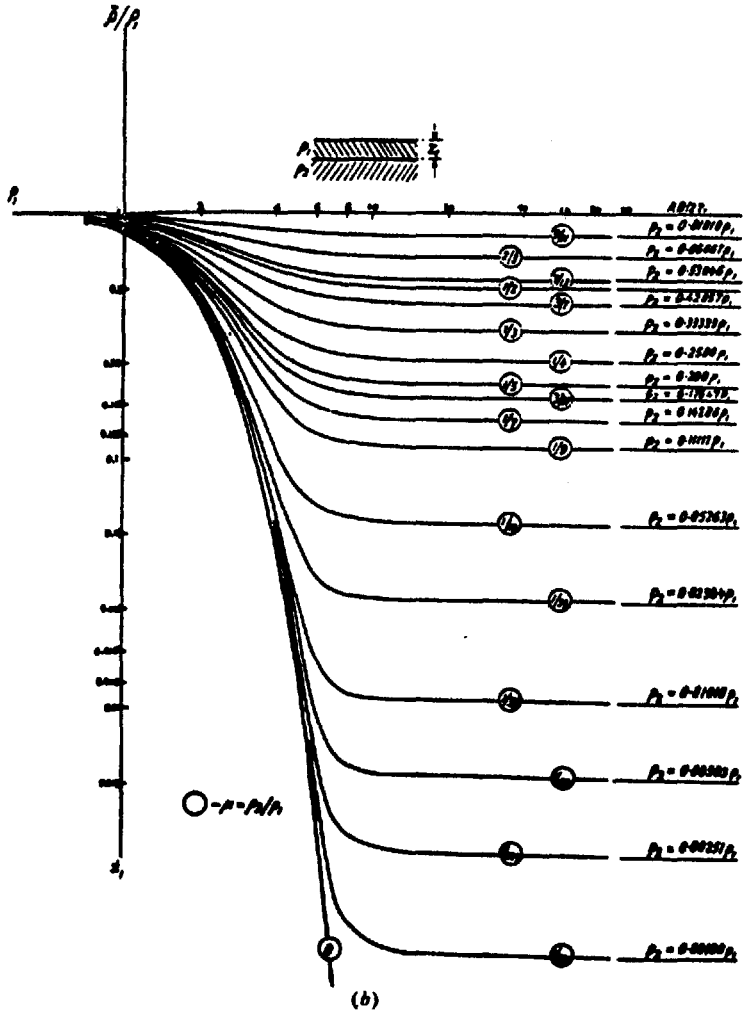

Figure 8.27. (Continued) (b) Descending type ($\rho_2 < \rho_1$).

conductance

$$S = z_1/\rho_1 + z_2/\rho_2 + \cdots + z_n/\rho_n = \sum_{i=1}^{n} z_i/\rho_i \tag{8.43b}$$

The vertical and horizontal resistivities are

$$\rho_v = T/z_e \qquad \rho_h = z_e/S \tag{8.44a}$$

where $z_e = \sum_1^n z_i$.

This column is indistinguishable from a single isotropic layer with resistivity and thickness $\rho_m = (T/S)^{1/2}$, $z_{eq} = z_e\lambda = (TS)^{1/2}$ [see Eq. (8.44b) below]. The quantities T and S are known as the *Dar Zarrouk parameters* and have many interesting properties (Maillet, 1947; Orellana, 1963). For example, the block can be considered anisotropic with an *average square resistivity* ρ_m and *pseudoanisotropy* λ given by [compare with Eqs. (8.24) and (8.25)]

$$\rho_m = (\rho_v\rho_h)^{1/2} \qquad \lambda = (\rho_v/\rho_h)^{1/2} \tag{8.44b}$$

Applying the preceding results to the case of two beds, we change ρ_h to ρ_{e2}, z_e to z_{e2} in Equation (8.44a) and get

$$S = z_{e2}/\rho_{e2} = z_1/\rho_1 + z_2/\rho_2 \tag{8.45}$$

This expression relating the parameters of two individual beds to those of a single equivalent bed allows us to prepare auxiliary charts to complement the master curves, by plotting (ρ_2/ρ_1) versus (z_e/z_1) on log-log scales identical to the master. These are shown in Figure 8.28; the first is used with H- and A-type, the second with K- and Q-type curves. A

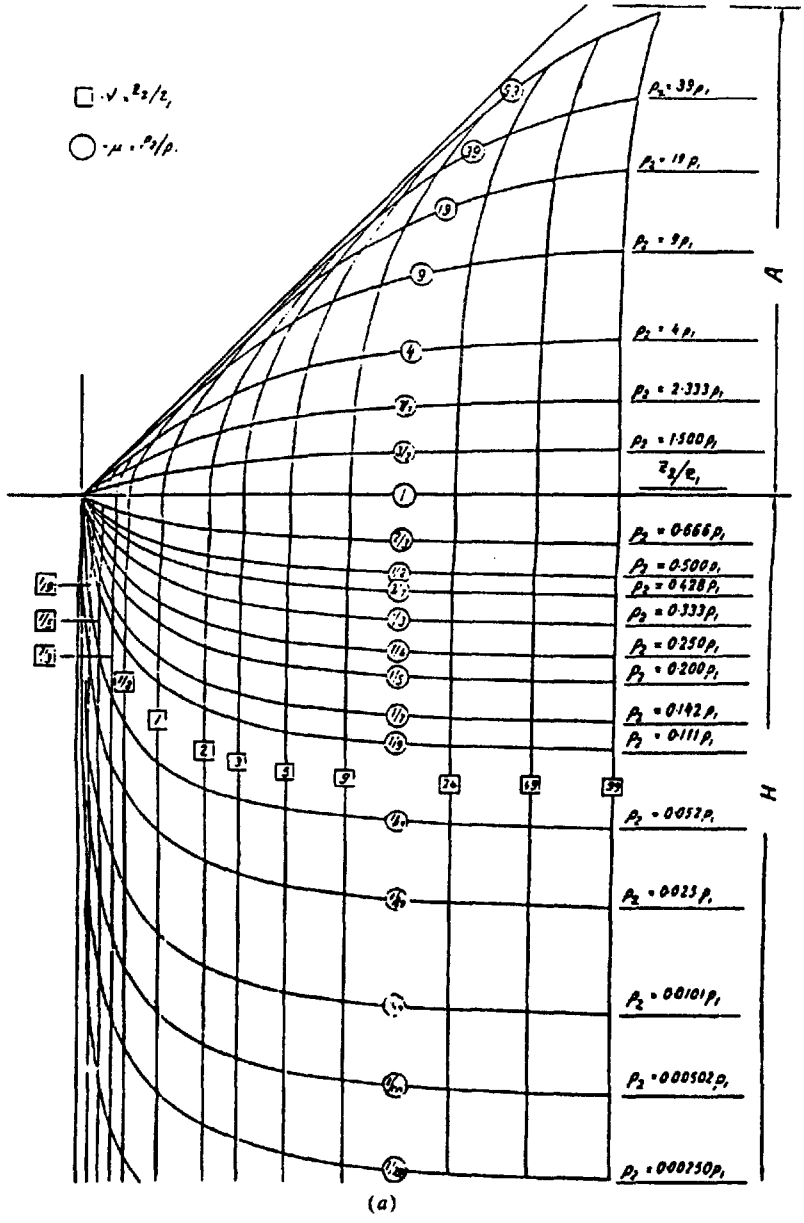

Figure 8.28. Auxiliary-point charts (a) for H- and A-type sounding curves.

pair of Schlumberger two-layer master curves on the ame scale, shown in Figure 8.27, are included for eference. (Note the change in symbols: $\bar{\rho} = \rho_a$, $B = 2L$.)

The procedure for matching successive left-to-ight segments of a field sounding is as follows:

1. The left-hand portion of the field sounding curve, plotted on a transparency of identical log-log scale, is fitted to as many points as possible on the master, maintaining the respective axes parallel. This fit provides the location of the first cross or auxiliary point where the field sheet coincides with $\rho_1 = L = 1$, the origin on the master. Hence we obtain ρ_1, z_1, whereas the best-fit segment gives (ρ_2/ρ_1) or ρ_2. [This segment may be extended beyond the fitted portion along the (ρ_2/ρ_1) line with pencil for a check on the next step.]
2. The sounding curve is transferred to the appropriate auxiliary curve set where the cross is placed at

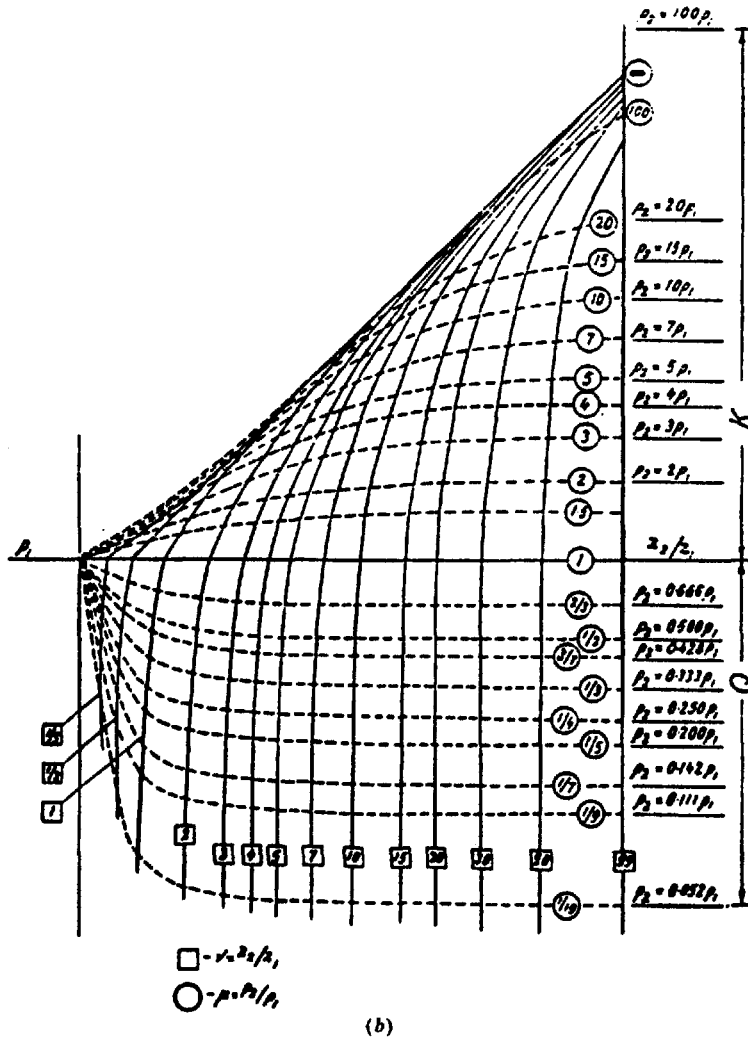

Figure 8.28. (Continued) Auxiliary-point charts (b) for K- and Q-type sounding curves.

the origin and the same (ρ_2/ρ_1) curve of the auxiliary as that in step 1 is drawn in pencil on the sounding.

3. Replacing the sounding curve on the master and maintaining the (ρ_2/ρ_1) line from step 2 on the master origin, a second master segment further to the right is fitted to the sounding curve. The second cross is marked over the master origin, giving ρ_{e2} and z_{e2} where $z_{e2} = z_1 + z_2$ and ρ_{e2} is related to the other parameters by Equation (8.45), that is,

$$z_{e2}/\rho_{e2} = (z_1 + z_2)/\rho_{e2} = z_1/\rho_1 + z_2/\rho_2$$

(Clearly $\rho_{e1} = \rho_1$ and $z_{e1} = z_1$ at the first cross.)

We also obtain (ρ_3/ρ_{e2}) and hence ρ_3 from the fitted segment.

4. The sounding curve is returned to the auxiliary and step 2 is repeated.
5. Repeat step 3 to get ρ_{e3}, z_{e3}, as well as ρ_4 from the third cross.
6. Repeat steps 4 and 5 until the sounding curve is completely fitted.

[A check on the (ρ_e, z_e) values may be taken at any juncture, using the relation in step 3. Also the minimum conductance may be found (Fig. 8.23) and employed for the same purpose.]

If three-layer master curves are available (Compagnie Générale de Géophysique, 1955), it is preferable to use them if the field curve warrants this. The

procedure is similar to the steps 1 to 6, noting the following.

7. The first cross and match gives ρ_1, ρ_2, z_1, z_{e2} (hence z_2), ρ_{e2}.
8. The second cross, equivalent to the third in step 5, locates ρ_{e3}, z_{e3}, from which ρ_3 may be determined by the relation

$$z_{e3}/\rho_{e3} = z_1/\rho_1 + z_2/\rho_2 + z_3/\rho_3$$

z_3, z_{e4}, z_4, and ρ_4 are also obtained.
9. The third cross corresponds to the fifth, if it exists in the two-layer analysis, and so on.

It should be noted that this procedure gives good results only if the bed thicknesses increase rapidly with depth; in fact, each successive layer should be thicker than the total thickness above it ($z_4 > z_{e3}$, etc.). Correction factors for the auxiliary charts (Kunetz, 1966; Keller and Frischknecht, 1966) reduce the effect of this limitation considerably. For example, type-*A* curves require that $z_e' = \lambda(z_1 + z_2)$, that is, the lumped layer is thicker than the sum of the individuals (because $\lambda = (\rho_0/\rho_h)^{1/2} > 1$–see §8.3.6). For type-*K* curves the correction is still greater by a factor η which increases nonlinearly from 1 to 1.5 as λ increases from 1 to 3.

With *Q* curves we find that $z_e' = (z_1 + z_2)/\eta$ and $\rho_e' = \rho_e\eta$; the correction factor varies from 1 to 1.25 in the same sense as both z and ρ. Modifications for *H*-type curves appear to be unnecessary.

An example of partial curve matching is shown in Figure 8.29a from a groundwater sounding in Sri Lanka. Overall resistivity is unusually uniform and high. Subsequent drilling produced a dry well.

The crosses are marked on the sounding curve for both two- and three-layer analysis. The curve is erratic beyond 20 m which probably indicates noisy field readings. In any case, resistivity increases with depth.

The technique of partial curve matching, although rather crude compared to complete analysis of the sounding curve by computing methods, is quite useful in the field to keep abreast of daily measurements and as a control for the more sophisticated approach later.

(e) Complete curve matching. The expression for surface potential over two beds, Equation (8.21), may be expressed in integral form as

$$V = (I\rho_1/2\pi r)\left\{1 + 2r\int_0^\infty K(\lambda)\, J_0(\lambda r)\, d\lambda\right\} \tag{8.46}$$

where $K(\lambda) = k\exp(-2\lambda z)/\{1 - k\exp(-2\lambda z)\}$ and J_0 is the zero order Bessel function. This expression is suitable for solving any number of layers (see Keller and Frischknecht, 1966; Zohdy, 1973). Employing the Schlumberger array (which is most convenient for vertical sounding and also measures potential gradient), we may write the resistivity relation in the form [see Eq. (8.39b)]

$$\rho_a = \rho_1\left\{1 + 2L^2\int_0^\infty K(\lambda)\, J_1(\lambda L)\lambda\, d\lambda\right\} \tag{8.47}$$

where $J_1(\lambda L) = -J_0'(\lambda L)$ is the first order Bessel function. J_0' is the first derivative of J_0 and we have replaced r by L, half the current electrode separation. The product $K(\lambda)J_1(\lambda L)$ is known as the *Stefanescu function*.

The solution of this general expression may be obtained by expanding the integral as an infinite series or by numerical integration, both methods being suitable for computer programming. These and other methods are described in the literature (Ghosh, 1971; Inman, Ryu, and Ward, 1973; Johansen, 1975, 1977). Because an enormous number of theoretical models will fit the field data from an average sounding curve within ±5% (which is quite within the data accuracy; see next section), some optimization technique for determining the limits on the parameters providing the curve match is necessary in practice. This additional feature is included in the methods of Inman, Ryu, and Ward, and Johansen. An example that employs a program somewhat similar to those is shown in Figure 8.29b.

(f) Sounding interpretation errors. Practically there are often erratic variations in field sounding measurements of ρ_a due to local resistivity changes near surface and poor electrode contacts. In addition, anisotropic ground and terrain effects will lead to errors in estimating both z and ρ_1.

An expanding spread, in homogeneous ground, parallel and adjacent to a vertical contact will give a profile that is somewhat similar to that obtained over horizontal layers, particularly if the bed on the other side of the contact has low resistivity (Fig. 8.34c, §8.6.5d). In all depth-probing operations the expanding spread should be carried out in at least two azimuths, a sound preliminary procedure in any case.

An example of pronounced topography effect is shown in Figure 8.30. Apparent resistivities were obtained from an expanding Wenner system over relatively homogeneous dolomite and limestone. The spread, however, is parallel to a 100 ft cliff, which produces a linearly increasing curve for ρ_a versus electrode separation. The bumps in curve *A* are probably the result of local variations in surface resistivity near the cliff edge. Obviously this is an

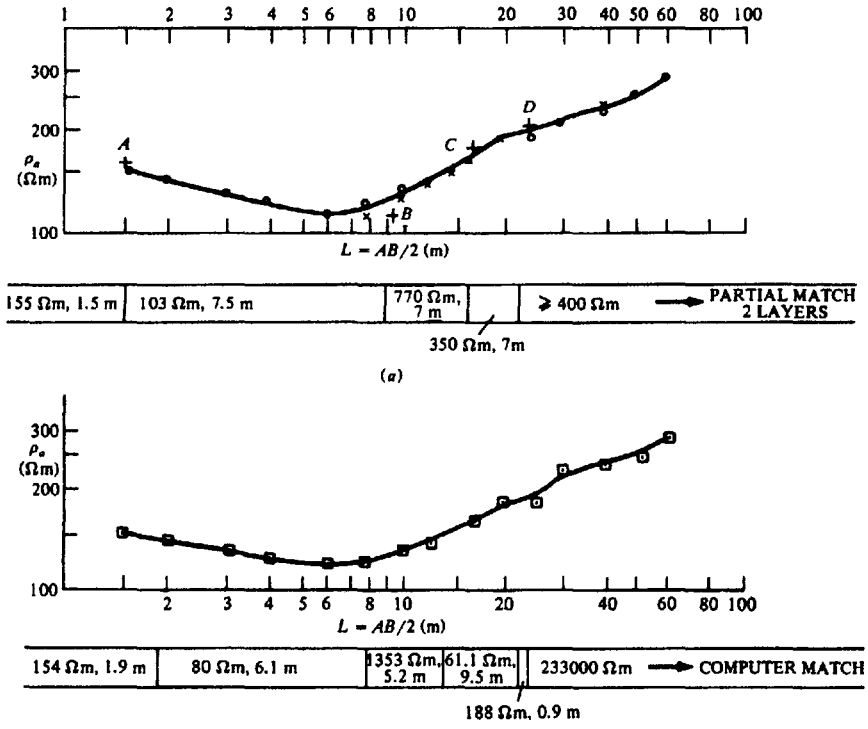

	FINAL PARAMETERS & STANDARD DEVIATION LAYER THICKNESS & RESISTIVITY Z and ρ	Std. devn.
1	Z_1 1.9172 m	0.49198
2	Z_2 6.0628	14.597
3	Z_3 5.1734	423.76
4	Z_4 9.5293	1690.5
5	Z_5 .89508	1120.0
6	ρ_1 153.91 Ωm	3.2000
7	ρ_2 79.962	21.536
8	ρ_3 1353.0	91113.
9	ρ_4 61.104	13379.
10	ρ_5 188.12	0.11483E+06
11	ρ_6 .23329E+06	0.59222E+08

(c)

SPACING	OBS. DATA	CALC. DATA	%ERROR
1.50 m	150 Ωm	148.613 Ωm	0.925
2.00	140	142.376	−1.697
3.00	130	129.463	0.413
4.00	122	120.537	1.199
6.00	115	115.193	−.168
8.00	120	120.083	−.069
10.00	130	129.340	0.508
12.00	135	139.933	−3.654
16.00	160	160.395	−.247
20.00	185	177.681	3.956
25.00	185	194.885	−5.343
30.00	220	208.754	5.112
40.00	230	232.678	−1.164
50.00	250	257.201	−2.880
60.00	290	284.690	1.831

(d)

Figure 8.29. Examples of partial and complete curve matching of field soundings for groundwater, Sri Lanka. (a) Partial curve matching (two layers). (b) Complete curve matching. (c) Computer results for complete curve matching using six layers. (d) Comparison of observed ρ_a and ρ_a calculated from the data in (c).

extreme case, but the curves would be similar if the cliff face were a contact and the void filled with high resistivity rock. In the latter case the result could be erroneously interpreted as a subsurface layer of high resistivity.

The effect of dipping beds is not serious in sounding operations unless the sounding array is normal to strike and particularly if the spread crosses over an outcrop of the dipping bed. Parallel to strike the z values will be those of the point directly below the array, and with a large enough separation of electrodes the response may become similar to that in Figure 8.30. The double-dipole array is said to be more sensitive to dipping beds than Schlumberger

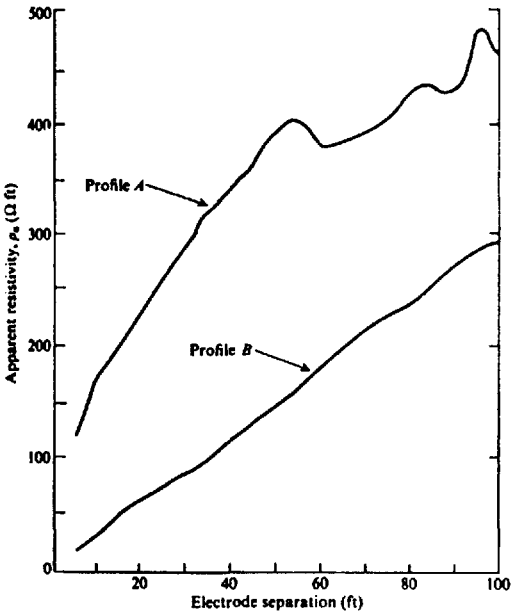

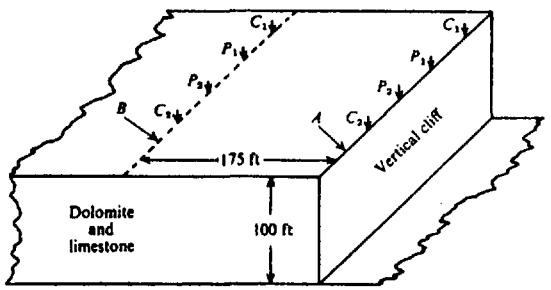

Figure 8.30. Effect of topography on expanding Wenner spread.

and Wenner configurations. Again, to determine the dip it is necessary to measure ρ_a in two orthogonal directions.

Aside from the preceding errors which are related to the field work, ambiguity in sounding interpretation may arise owing to two factors. The first, known as the *principle of equivalence*, may be stated as follows: it is impossible to distinguish between two highly resistive beds of different z and ρ values if the product $z\rho$ is the same, or between two highly conductive beds if the ratio z/ρ is the same. In Figure 8.31a the block of cross section ΔA offers a resistance to vertical current flow given by $R = \rho_2 z_2/\Delta A$; thus layers having an identical product $z\rho$ are equivalent and we cannot determine the two parameters separately. In the conductive bed of Figure 8.31b, the vertical current is deflected almost normal to the vertical stack, making $R = \rho_2 h/z_2 l$. Thus beds having the same ratio ρ/z are equivalent so that again ρ and z cannot be measured separately.

For either of these configurations the bed thickness and resistivity may vary within wide limits with respect to layers above and below it. However, these limits may be found by optimization methods as mentioned in Section 8.6.4e.

Some feeling for the wide limits of equivalence may be obtained from the examples of three-bed equivalent curves displayed in Figure 8.32, parts (a) and (b) being for types A and H, parts (c) and (d) for types K and Q sections analogous to the auxiliary curves in Figure 8.28. The dashed 45° slope lines represent equal S_2/S_1 ratios, whereas the solid-line curves are limiting values of ρ_2/ρ_1 and z_{e2}/z_1 for equivalence within $\pm 5\%$.

To illustrate the application consider the hatched area in the H-type section of Figure 8.32b. An approximate match produced the circle in the shaded square at $\rho_2/\rho_1 = 1/39$, $z_{e2}/z_1 = 3$. The minimum and maximum limits for the equivalence are at the corners of the square. Hence $1.6 < z_{e2}/z_1 < 4.2$,

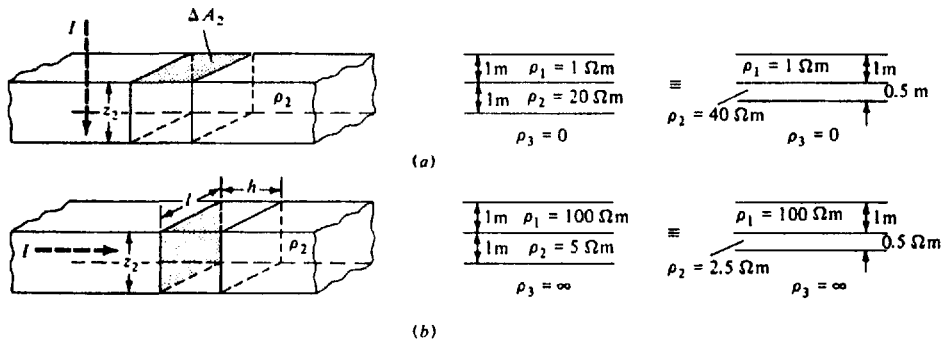

Figure 8.31. The equivalence principle (schematic). (a) $\rho_1 < \rho_2 > \rho_3$, $\rho_2 z_2$ = constant. (b) $\rho_1 > \rho_2 < \rho_3$, ρ_2/z_2 = constant.

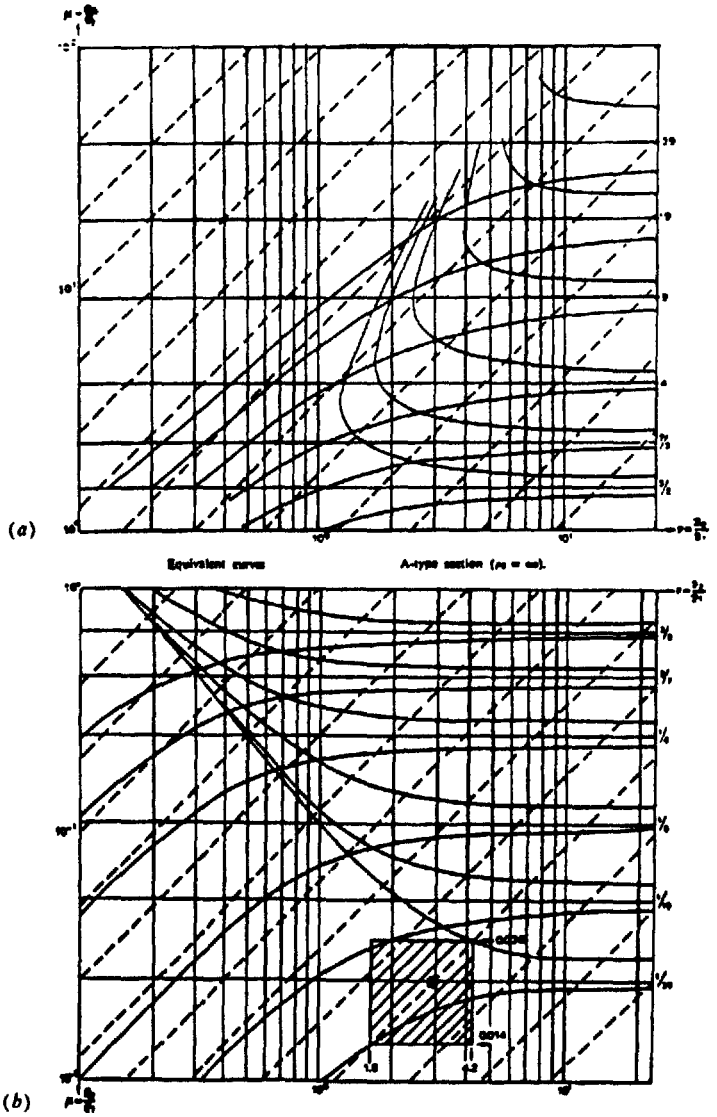

Figure 8.32. Equivalent curves. Solid-line curves are limiting values of $\mu = \rho_2/\rho_1$ and $\nu = z_2/z_1$ for equivalence; dashed lines are lines of equal S_2/S_1 in (a) and (b), equal T_2/T_1 in (c) and (d). (a) A-type section, $\rho_3 = \infty$. (b) H-type section, $\rho_3 = \rho_1$.

$0.014 < \rho_{e2}/\rho_1 < 0.038$. Thus the same field curve section may be matched only within $\pm 45\%$. The limits are still wider in areas of the equivalent curves where the z ratios are smaller and/or ρ ratio estimates larger than this, as is clear from the open sections at the upper left.

The suppression principle states that if a bed is very thin compared to those above and below, its effect on the sounding curve is insignificant unless its resistivity is extremely high or low.

8.6.5. Lateral Mapping; Vertical Contact

(a) General equations. Also called lateral profiling, this technique is of considerable importance in mineral prospecting. It is also used for the measure-

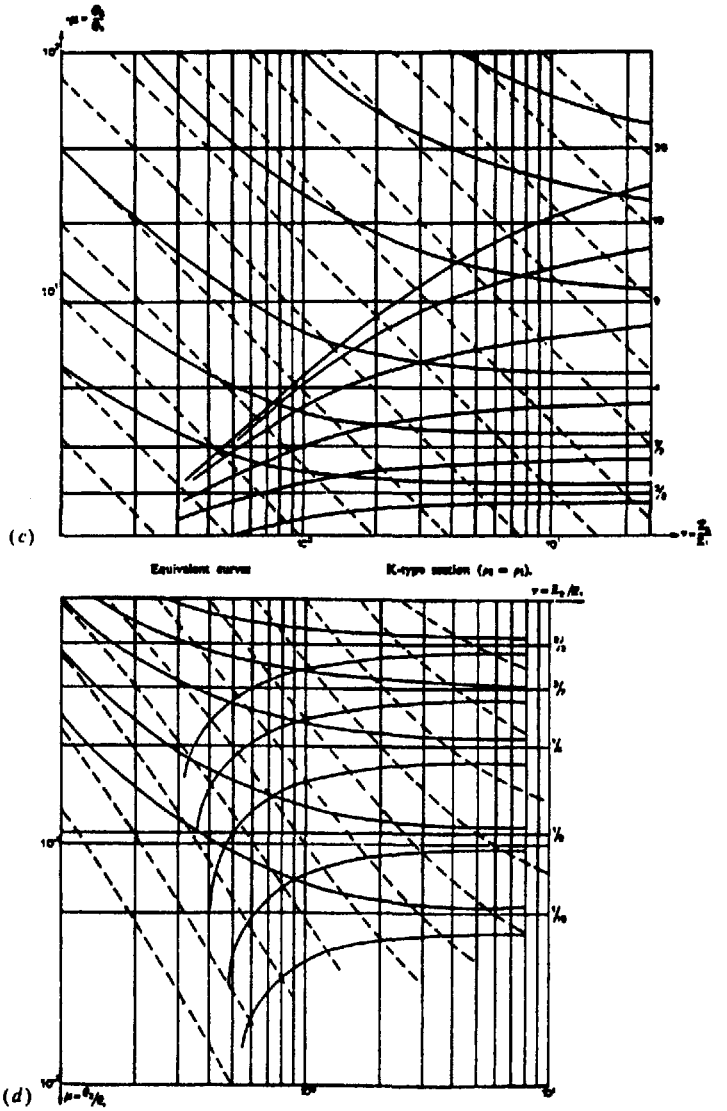

Figure 8.32. (Continued) (c) K-type section, $\rho_3 = \rho_1$. (d) Q-type section $\rho_3 = 0$.

ment of overburden depth in civil engineering work. The mineral exploration intepretation includes location of vertical contacts – faults, dikes, shear zones, and steeply dipping veins – and three-dimensional bodies of anomalous conductivity, such as massive sulfides.

In Section 8.3.3 the variation in potential crossing a plane interface was established for a single current and a single potential electrode system. Equation (8.17) gave the potential with both electrodes in the same medium, Equation (8.18) when they were on opposite sides of the contact.

Any of the electrode arrays may be used for this type of mapping, but the profiles differ considerably from one to another. There is also a practical consideration: the traverse can be made faster and more easily if it is not necessary to move all the electrodes for each station measurement. It turns out also that the profiles are usually easier to understand as well in this case.

For the general case, with spacing r_1, r_2, r_3, and r_4 we have five possible situations, depending on electrode positions with respect to the contact (Fig. 8.33):

(i) All electrodes on left-hand side:

$$V_1 = \frac{I\rho_1}{2\pi}\left\{\left(\frac{1}{r_1} + \frac{k}{2s - r_1}\right) - \left(\frac{1}{r_2} + \frac{k}{2s - 2r_1 - r_2}\right)\right\}$$

$$V_2 = \frac{I\rho_1}{2\pi}\left\{\left(\frac{1}{r_3} + \frac{k}{2s - r_3}\right) - \left(\frac{1}{r_4} + \frac{k}{2s - 2r_3 - r_4}\right)\right\}$$

$$\Delta V = \frac{I\rho_1}{2\pi}\left[\left(\frac{1}{r_1} - \frac{1}{r_2}\right) - \left(\frac{1}{r_3} - \frac{1}{r_4}\right) + k\left\{\left(\frac{1}{2s - r_1} - \frac{1}{2s - 2r_1 - r_2}\right) - \left(\frac{1}{2s - r_3} - \frac{1}{2s - 2r_3 - r_4}\right)\right\}\right] \quad (8.48a)$$

(ii) C_2 on right-hand side (note that k changes sign for a current electrode to the right of the vertical contact and that there is no image of C_2):

$$\Delta V = \frac{I\rho_1}{2\pi}\left[\left(\frac{1}{r_1} - \frac{1}{r_2}\right) - \left(\frac{1}{r_3} - \frac{1}{r_4}\right) + k\left\{\left(\frac{1}{2s - r_1} - \frac{1}{r_2}\right) - \left(\frac{1}{2s - r_3} - \frac{1}{r_4}\right)\right\}\right] \quad (8.48b)$$

(iii) C_2, P_2 on right-hand side:

$$V_1 = \frac{I\rho_1}{2\pi}\left\{\left(\frac{1}{r_1} + \frac{k}{2s - r_1}\right) - \frac{1 + k}{r_2}\right\}$$

$$V_2 = \frac{I\rho_2}{2\pi}\left\{\frac{1 - k}{r_3} - \left(\frac{1}{r_4} - \frac{k}{2r_3 + r_4 - 2s}\right)\right\}$$

Using Equation (8.19) to express ρ_2 in terms of ρ_1, and setting $k^* = (1 + k)/(1 - k)$, we obtain

$$\Delta V = \frac{I\rho_1}{2\pi}\left[\left(\frac{1}{r_1} - \frac{1}{r_2}\right) - k^*\left(\frac{1}{r_3} - \frac{1}{r_4}\right) + k\left\{\left(\frac{1}{2s - r_1} - \frac{1}{r_2}\right) + k^*\left(\frac{1}{r_3} - \frac{1}{2r_3 + r_4 - 2s}\right)\right\}\right] \quad (8.48c)$$

(iv) C_2, P_2, P_1 on right-hand side:

$$V_1 = \frac{I\rho_2}{2\pi}\left\{\left(\frac{1}{r_1} - \frac{1}{r_2}\right) - k\left(\frac{1}{r_1} - \frac{1}{2r_1 + r_2 - 2s}\right)\right\}$$

$$V_2 = \frac{I\rho_2}{2\pi}\left\{\left(\frac{1}{r_3} - \frac{1}{r_4}\right) - k\left(\frac{1}{r_3} - \frac{1}{2r_3 + r_4 - 2s}\right)\right\}$$

$$\therefore \quad \Delta V = \frac{I\rho_1}{2\pi}\left[k^*\left\{\left(\frac{1}{r_1} - \frac{1}{r_2}\right) - \left(\frac{1}{r_3} - \frac{1}{r_4}\right) - k\left\{\left(\frac{1}{r_1} - \frac{1}{2r_1 + r_2 - 2s}\right) - \left(\frac{1}{r_3} - \frac{1}{2r_3 + r_4 - 2s}\right)\right\}\right\}\right] \quad (8.48d)$$

(v) All electrodes on right-hand side:

$$V_1 = \frac{I\rho_2}{2\pi}\left\{\left(\frac{1}{r_1} - \frac{k}{2s + r_1}\right) - \left(\frac{1}{r_2} - \frac{k}{2s + 2r_1 + r_2}\right)\right\}$$

$$V_2 = \frac{I\rho_2}{2\pi}\left\{\left(\frac{1}{r_3} - \frac{k}{2s + r_3}\right) - \left(\frac{1}{r_4} - \frac{k}{2s + 2r_3 + r_4}\right)\right\}$$

$$\therefore \quad \Delta V = \frac{I\rho_1}{2\pi}\left[k^*\left\{\left(\frac{1}{r_1} - \frac{1}{r_2}\right) - \left(\frac{1}{r_3} - \frac{1}{r_4}\right) - k\left\{\left(\frac{1}{2s + r_1} - \frac{1}{2s + 2r_1 + r_2}\right) - \left(\frac{1}{2s + r_3} - \frac{1}{2s + 2r_3 + r_4}\right)\right\}\right\}\right] \quad (8.48e)$$

If we ignore the existence of the contact, we can substitute for $\Delta V/I$ in Equation (8.26) and get ρ_a. This gives

$$\rho_a/\rho_1 = p/p'$$

where $1/p'$ is the quantity in square brackets in Equations (8.48) and p is the quantity in Equation (8.26) evaluated for the particular electrode spacing that holds for Equations (8.48).

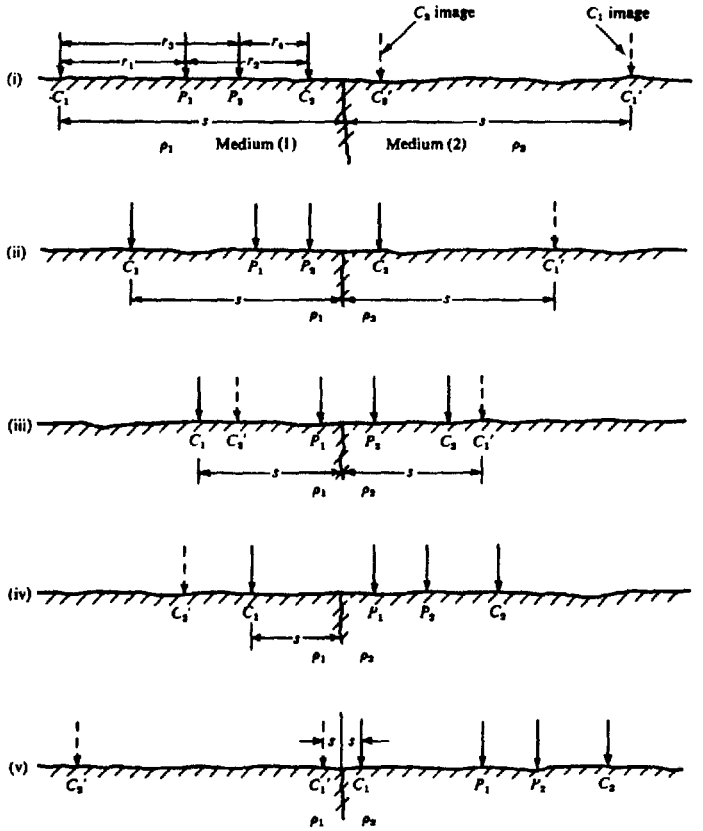

Figure 8.33. General resistivity spread over a vertical contact.

The expressions for ρ_a for the Wenner and Schlumberger arrays are cumbersome in general. We shall consider certain special cases in the following section.

(b) Half-Wenner array. $r_1 = a$, $r_2 = r_3 = r_4 = \infty$. For the preceding configurations, the results are:

(i) $$\rho_a/\rho_1 = 1 + \{ ka/(2s - a)\} \quad (8.49a)$$

(ii), (iii) Same as in (i) (8.49b, c)

(iv) $$\rho_a/\rho_1 = (1 + k) \quad (8.49d)$$

(v) $$\frac{\rho_a}{\rho_1} = k^*\left(1 - \frac{ka}{2s + a}\right) \quad (8.49e)$$

(c) Half-Schlumberger array. $r_1 = L - \ell$, $r_3 = L + \ell$, $r_2 = r_4 = \infty$, $L \gg \ell$.

(i) $$\frac{\rho_a}{\rho_1} \approx 1 - \frac{kL^2}{(2s - L)^2} \quad (8.50a)$$

(ii) Same as in (i) (8.50b)

(iii) $$\frac{\rho_a}{\rho_1} = 1 + \frac{k(L - s)(L - \ell)}{\ell(2s - L + \ell)} \quad (8.50c)$$

(iv) $$\frac{\rho_a}{\rho_1} = 1 + k \quad (8.50d)$$

(v) $$\frac{\rho_a}{\rho_1} \approx k^*\left\{1 - \frac{kL^2}{(2s + L)^2}\right\} \quad (8.50e)$$

(d) Double-dipole array. (Potential electrodes to right of current pair.) $r_1 = r_4 = r$, $r_2 = r - \ell$, $r_3 = r + \ell$, $r \gg \ell$.

(i) All four electrodes on left-hand side:

$$\frac{\rho_a}{\rho_1} \approx 1 - \frac{kr^3}{(2s - r)^3} \quad (8.51a)$$

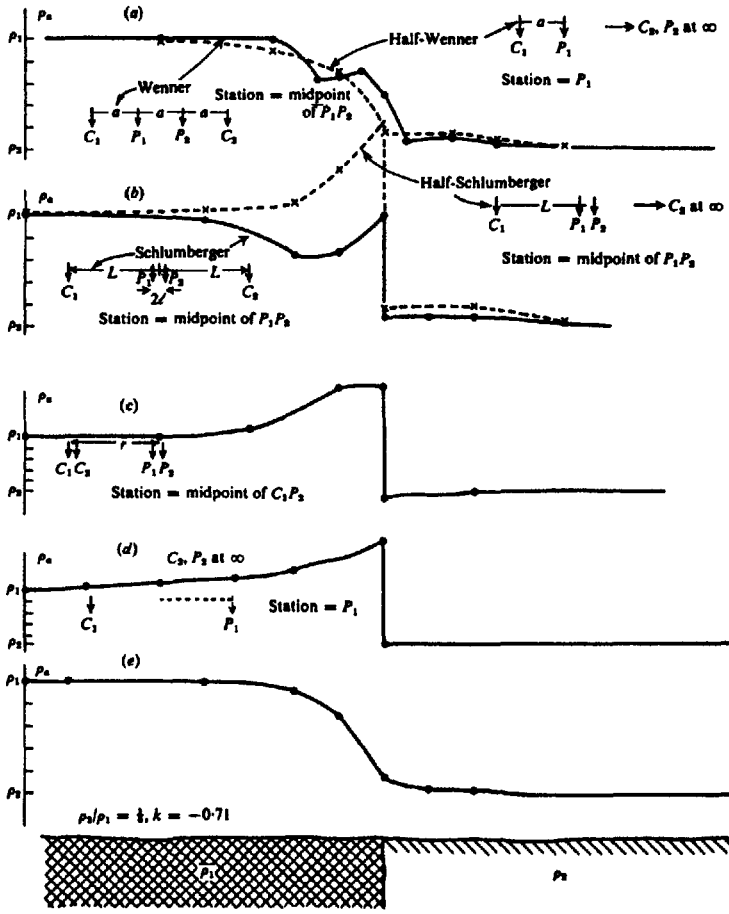

Figure 8.34. Profiles over a vertical contact using different electrode spreads. (a) Wenner spread. (b) Schlumberger spread. (c) Double-dipole spread. (d) Spread with fixed C_1, movable P_1. (e) Schlumberger broadside spread.

(ii) Dipole straddles contact:

$$\frac{\rho_a}{\rho_1} = 1 + k \tag{8.51b}$$

(iii) All four on right-hand side:

$$\frac{\rho_a}{\rho_1} = k^*\left\{1 + \frac{kr^3}{(2s + r)^3}\right\} \tag{8.51c}$$

Profiles for these three electrode systems, plus some other possible arrangements, are shown in Figure 8.34. The profiles are characteristic of the array used. Except for Figure 8.34e, they all have discontinuities in the vicinity of the contact, related to the electrode spacing. In Figure 8.34e the electrodes are aligned parallel to the contact and are moved broadside, so that they all cross it simultaneously. The value of ρ_a/ρ_1 can be obtained in this case by substitution in Equation (8.48a) and (8.48e). With the usual approximation ($L \gg \ell$), we have:

Electrodes in medium (1):

$$\frac{\rho_a}{\rho_1} \approx 1 + k\left\{1 + \left(\frac{2s}{L}\right)^2\right\}^{-3/2}$$

Electrodes in medium (2):

$$\frac{\rho_a}{\rho_1} \approx k^*\left[1 - k\left\{1 + \left(\frac{2s}{L}\right)^2\right\}^{-3/2}\right]$$

This profile is by far the best for interpretation but it

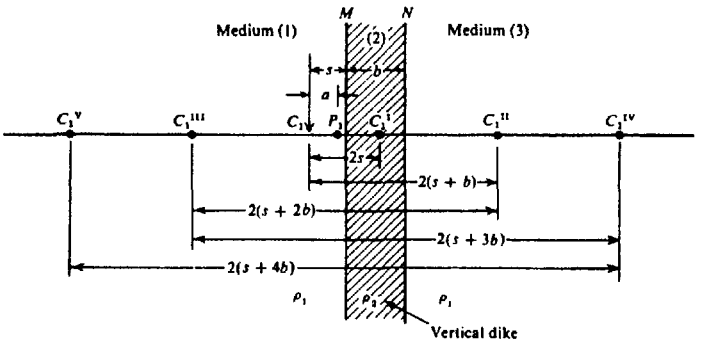

Figure 8.35. Locations of current images near a vertical dike.

is not very practical in the field. In some of the spreads the profile shape varies with the direction of traversing, that is, it depends on which electrode crosses the contact first.

8.6.6. The Vertical Dike

When a dike of anomalous resistivity and finite width is traversed, the profiles are even more affected by the electrode spacing than in the case of the vertical contact. The expressions for potential are as in Section 8.6.5 plus the effect of one or two sets of images caused by reflections in the two boundaries. The development is not fundamentally difficult, but is tedious. We will describe only one configuration in detail, that in which we have one current electrode and one potential electrode, both initially in medium (1) (fig. 8.35).

The current source I at C_1 has an image in the dike at C_1^{I} (provided $s < b$), caused by reflection in boundary M. Its strength is kI and it is located $(2s - a)$ from P_1, the potential electrode.

There is a second image of C_1 reflected in boundary N at C_1^{II}, which is located in medium (3) at a distance $(2b + 2s - a)$ from P_1. This in turn causes an image in medium (1) at C_1^{III}, $(2b + a)$ from P_1. It is reflected in N to produce image C_1^{IV}, at $(4b + 2s - a)$ from P_1. These reflections are repeated indefinitely in M and N to give two infinite series, of which only the set of images in medium (3) have any effect on the potential in medium (1).

When the potential electrode is in medium (2), the image at C_1^{I} does nothing, but both the series in medium (1) and (3) influence the potential. Finally when P_1 is in medium (3), it is perturbed by C_1^{I} and all the images in medium (1). As a result we obtain the following potential expressions, for the different locations of P_1:

Medium (1):

$$V_1 = \frac{I\rho_1}{2\pi}\left\{\frac{1}{a} + \frac{k}{2s-a} + A\sum_{m=0}^{\infty}\frac{(k^2)^m}{2(m+1)b + 2s - a}\right\} \quad (8.52a)$$

Medium (2):

$$V_2 = \frac{I\rho_1}{2\pi}\left\{B\sum_{m=0}^{\infty}\frac{(k^2)^m}{2(m+1)b + 2s - a} + C\sum_{m=0}^{\infty}\frac{(k^2)^m}{2mb + a}\right\} \quad (8.52b)$$

Medium (3):

$$V_3 = \frac{I\rho_1}{2\pi}\left\{D\sum_{m=0}^{\infty}\frac{(k^2)^m}{2mb + a}\right\} \quad (8.52c)$$

A, B, C, and D are constants that are evaluated by applying the boundary condition of Equation (8.7b) at the boundaries M and N. They turn out to be

$$A = -k(1 - k^2) \qquad B = -k(1 + k)$$
$$C = 1 + k \qquad D = 1 - k^2$$

By a similar analysis, we can obtain the potentials when the current electrode is in the dike.

Medium (1):

$$V_1' = \frac{I\rho_1}{2\pi}(1+k) \times \left\{ \sum_{m=0}^{\infty} \frac{k^{2m}}{2mb+a} - k \sum_{m=0}^{\infty} \frac{k^{2m}}{2(m+1)b+2s+a} \right\} \quad (8.53a)$$

Medium (2):

$$V_2' = \frac{I\rho_1(1+k)}{2\pi(1-k)} \times \left[\frac{1}{a} + k^2 \left\{ \sum_{m=0}^{\infty} \frac{k^{2m}}{2(m+1)b+a} + \sum_{m=0}^{\infty} \frac{k^{2m}}{2(m+1)b-a} \right\} - k \left\{ \sum_{m=0}^{\infty} \frac{k^{2m}}{2(m+1)b+2s \pm a} + \sum_{m=0}^{\infty} \frac{k^{2m}}{2mb-(2s \pm a)} \right\} \right] \quad (8.53b)$$

Medium (3):

$$V_3' = \frac{I\rho_1}{2\pi}(1+k) \left\{ \sum_{m=0}^{\infty} \frac{k^{2m}}{2mb+a} - k \sum_{m=0}^{\infty} \frac{k^{2m}}{2mb-(2s-a)} \right\} \quad (8.53c)$$

In these equations the relative positions of the potential and current electrodes must be specified. In Equation (8.53a) the potential electrode is always to the left of the current electrode, whereas in Equation (8.53c) it is always to the right. In Equation (8.53b), however, it may be on either side of the current electrode. When it is on the left, one uses the upper signs for a in the denominators of the last bracket; when on the right, the lower sign.

Finally, when the current electrode is on the right-hand side in medium (3), and P_1 is to the left of C_1, the respective potentials are:

Medium (1):

$$V_1'' = \frac{I\rho_1}{2\pi}(1-k^2) \sum_{m=0}^{\infty} \left(\frac{k^{2m}}{2mb+a} \right) \quad (8.54a)$$

Medium (2):

$$V_2'' = \frac{I\rho_1}{2\pi}(1+k) \left\{ \sum_{m=0}^{\infty} \left(\frac{k^{2m}}{2mb+a} \right) - k \sum_{m=0}^{\infty} \frac{k^{2m}}{2mb-(2s+a)} \right\} \quad (8.54b)$$

Medium (3):

$$V_3'' = \frac{I\rho_1}{2\pi} \left\{ \frac{1}{a} + k \sum_{m=0}^{\infty} \frac{k^{2m}}{2(m-1)b-(2s+a)} - k \sum_{m=0}^{\infty} \frac{k^{2m}}{2mb-(2s+a)} \right\} \quad (8.54c)$$

From these relations one can obtain the value of ρ_a in terms of ρ_1, in the usual way, for complete profiles across the dike. In addition, the expressions can be made more general by assuming a resistivity ρ_3 in medium (3).

The formulas are modified in all cases by differentiating the potentials for a half-Schlumberger array and by using the second derivative for the double dipole.

Profiles obtained with different spreads in traversing a thin dike are shown in Figure 8.36. On the whole the half-Schlumberger curve reproduces the shape of the dike best, particularly for thin dikes. The corresponding dipole profile has two peaks, the gap between being equal to the dipole spacing. This double anomaly could be quite misleading. On the other hand, the half-Wenner spread over a thin dike of high resistivity shows a "conductor" of width greater than the actual dike. The full-Wenner system, however, gives better results, although there are discontinuities near the edges of the dike, as illustrated in Figure 8.36c.

As in the case of the single vertical contact, better profiles would be obtained by moving the array broadside to the structure. In fact, the profiles are considerably better over thin dikes when the traverse is made at an oblique angle, although the anomalies will be wider than the actual dike.

Lateral exploration may also be applied to channels and filled sinks of anomalous resistivity when such features outcrop or lie very close to the surface. The profiles are similar to the dike, although the latter was assumed to have infinite depth in the previous discussions.

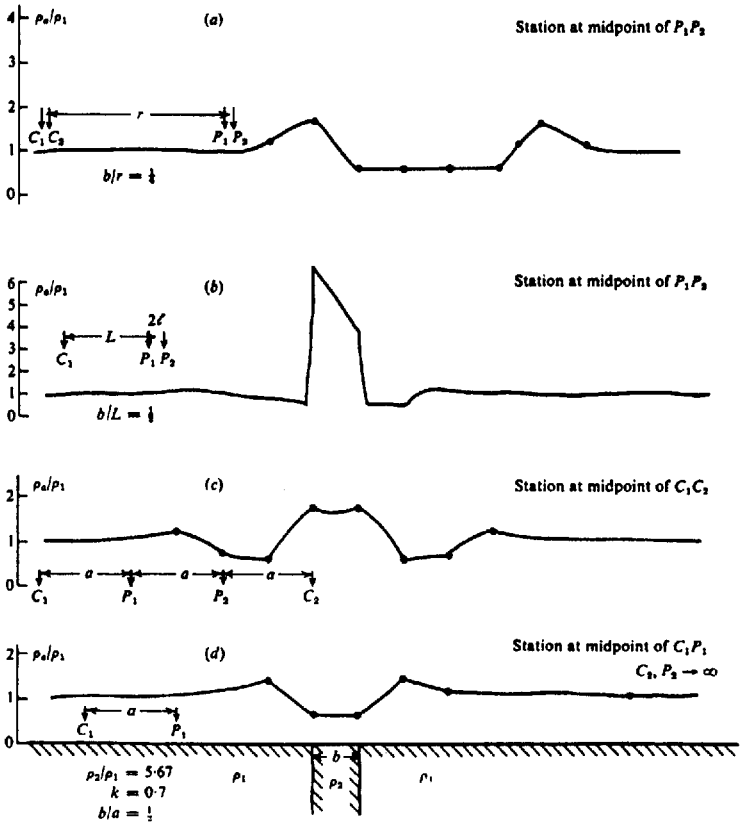

Figure 8.36. Profiles over a thin dike using different electrode spreads. (a) Double-dipole spread. (b) Half-Schlumberger spread. (c) Full-Wenner spread. (d) Half-Wenner spread.

8.6.7. Mapping Three-Dimensional Anomalies

The resistivity method is not particularly sensitive to 3-D anomalies for the same reason that it is ineffective over buried 2-D structures of finite width. This limitation is well illustrated by reference to the buried sphere considered in Section 8.3.5. Using a Schlumberger spread, the apparent resistivity can be calculated by differentiating Equation (8.22) with respect to x [note that $E_0 = \rho_1 I$, $x = r\cos\theta$, and $\rho_a = (1/I)(\partial V/\partial x)$] and assuming that the sphere is a very good conductor so that $\rho_2 = 0$, we obtain

$$\frac{\rho_a}{\rho_1} \approx 1 + \left(\frac{a}{z}\right)^3 \frac{(2x^2/z^2) - 1}{(1 + x^2/z^2)^{5/2}} \qquad (8.55)$$

where x is the distance of the potential electrode from the surface point above the origin and z the depth to the sphere center. When $z = 2a$ the maximum contrast between ρ_a and ρ_1 is only 12%. Thus a sphere 30 m in diameter whose top lies only 15 m below surface probably would not be detected.

A similar limitation exists when the body outcrops, for instance, a hemispherical sink. Unless the traverse passes very close to the rim, the anomaly will be missed. These effects are illustrated in Figure 8.37. Note that when the survey line is over the center of the bowl ($d = 0$), the ratio ρ_a/ρ_1 remains zero until the potential electrodes are out of the sink, because $\Delta V = 0$ for $a \leq 2R$.

It is not surprising that numerical methods like those described in Sections 6.2.7, 6.2.8, and 9.5.3 have been developed for resistivity modeling as well (Coggon, 1971; Lee, 1975; Snyder, 1976; Dey and Morrison, 1979). The models include 2-D and 3-D structures of the usual types. Again, the most striking feature of the resistivity results is the poor response of 3-D targets. Unless they are shallow and the width about the same as the depth, the anomaly

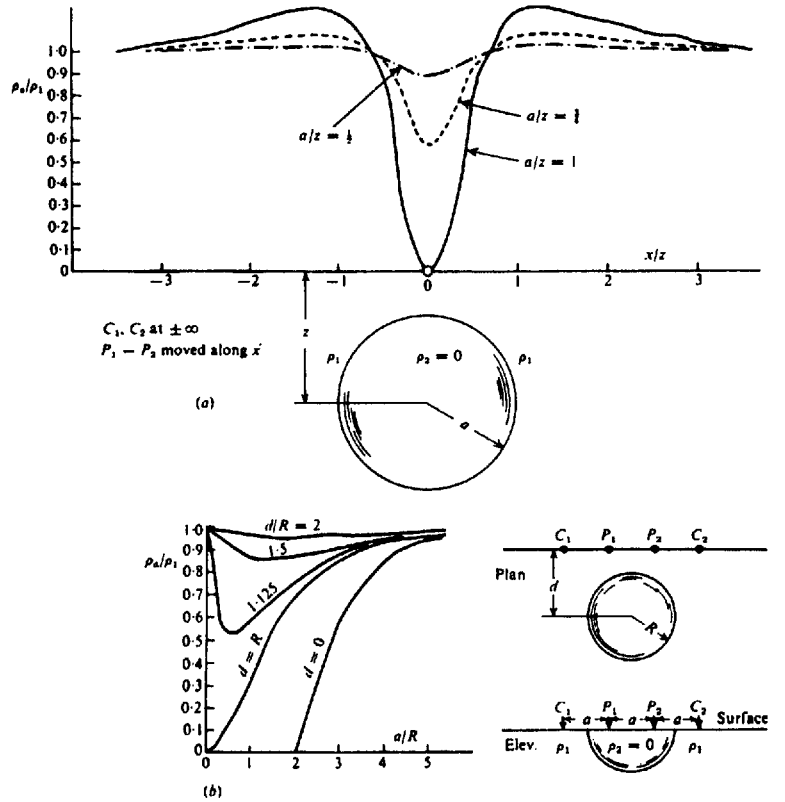

Figure 8.37. Resistivity profiles over three-dimensional conductors. (a) Schlumberger array over buried sphere. (b) Expanding Wenner array over outcropping hemispherical conductor.

is weak. Conductive overburden is also very effective in masking such structures. Figure 8.38 demonstrates these limitations with a display of profiles and pseudosections (§9.5.1) over a vertical block with and without overburden cover.

8.6.8. Measuring Overburden Depth and Resistivity

Obviously the depth of overburden can be found using an expanding spread. However, if the bedrock surface is irregular, many soundings will be necessary, entailing considerable time and expense. Where the overburden has much lower resistivity than bedrock, which is the usual case, good results may be obtained with three traverses, employing different electrode separations.

Obviously one small spread is necessary to measure ρ_1. This is achieved with a separation that is less than half the minimum overburden thickness; it should not be required at every profile station unless ρ_1 varies rapidly. The conventional procedure has been to complete the profile at all stations with a second electrode spacing, which is somewhat larger than the maximum overburden depth. This gives a relation for z from Equation (8.42d):

$$z = c(\rho_1/\rho_a) \times (\text{electrode spacing}) \quad (8.56)$$

where $c = 1.38$, 1.0, 0.5 and the spacing is a, L, r for the Wenner, Schlumberger, and double-dipole arrays, respectively. However, the value obtained is generally much larger than the correct value unless the spacing is large enough to make $\rho_a \simeq \rho_2$. A better estimate may be obtained by taking two readings of ρ_a at two spreads larger than maximum overburden depth. Then the z values obtained from Equation (8.56) are plotted against the corresponding a, L, or r values; the straight line joining the two points, when extended to the ordinate axis, gives the correct depth. Figure 8.39 clarifies this procedure on linear z versus a, L, or r axes. Several additional

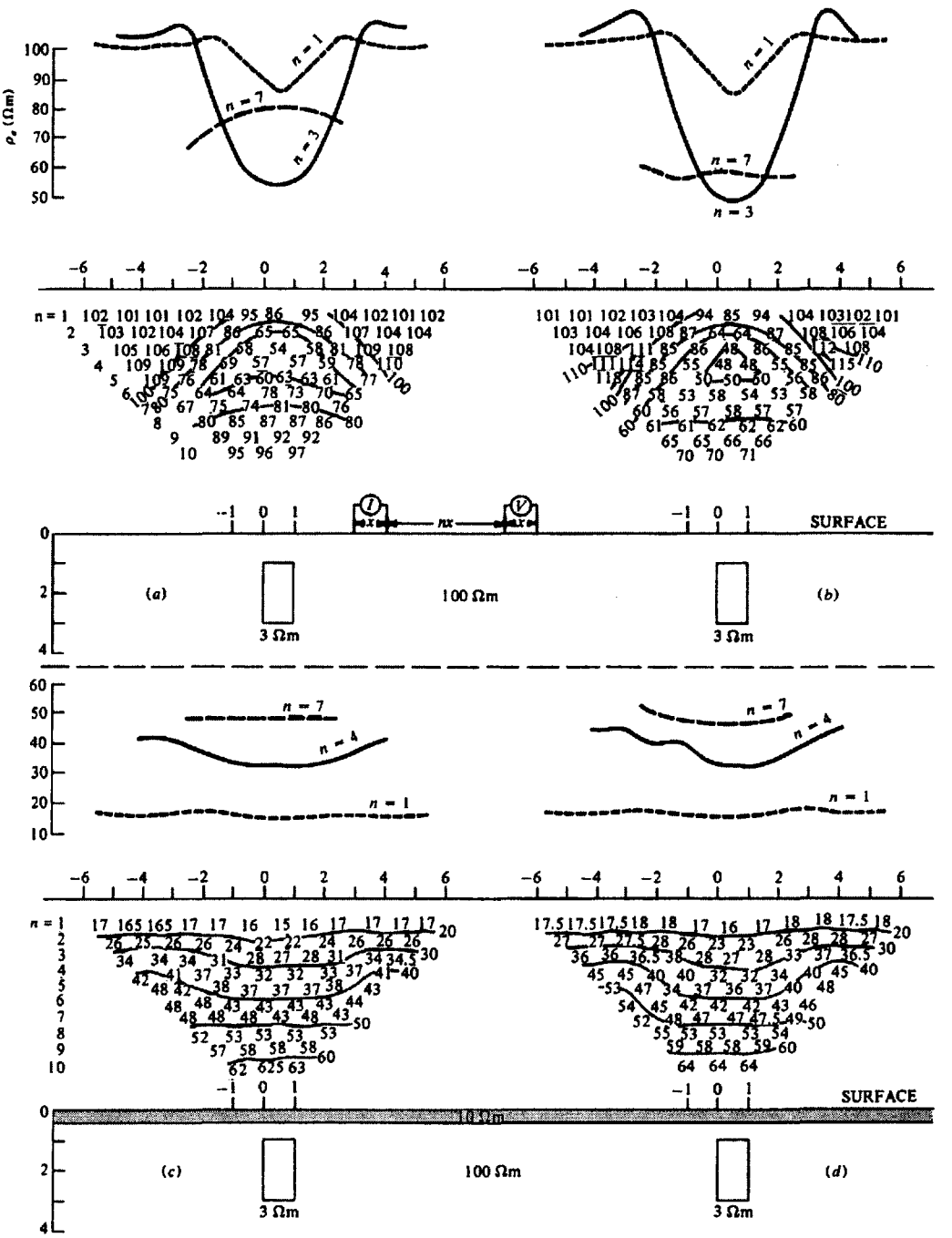

Figure 8.38. Resistivity finite-difference modeling; profiles and pseudodepth plots for the dipole-dipole array of Figure 9.8a. (After Dey and Morrison, 1979.) (a) 3-D block, strike length = 6 units. (b) 2-D block, infinite strike length. (c) and (d) same as (a) and (b) with conductive overburden 0.5 units thick, ρ = 10 Ωm.

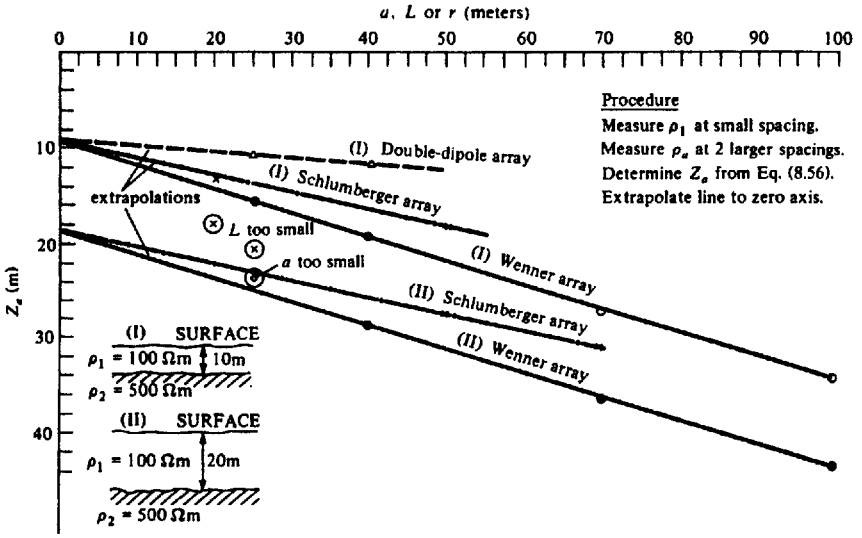

Figure 8.39. Graphical determination of overburden thickness using one small spread to get ρ_1 and two large spreads to get z.

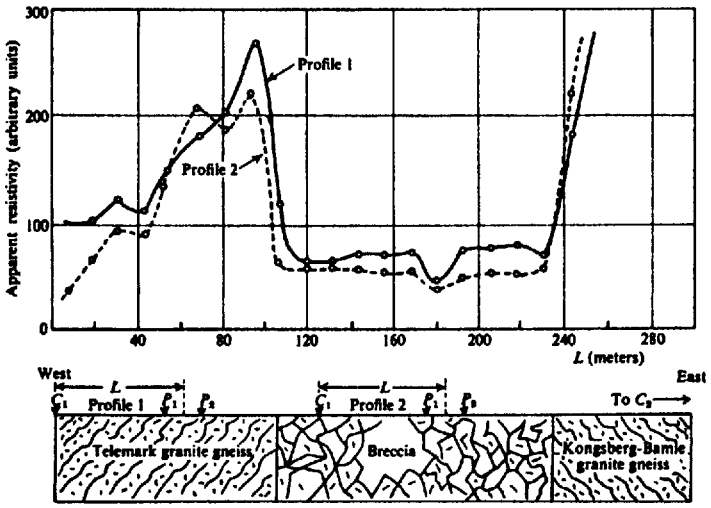

Figure 8.40. Mapping vertical contacts with the half-Schlumberger array, Kongsberg, Norway. (After Van Nostrand and Cook, 1966.)

points are included in the plot to indicate where the straight line extrapolation begins to fail. Because the relation appears to be linear, the usual log-log scale is not suitable. Alternatively the extrapolated z values may be calculated from $z_s = ms + z_c$ where s is the separation, z_s is obtained from Equation (8.56), and z_c is the intercept on the ordinate.

If bedrock resistivity is lower than that of the overburden, it is necessary to use expanding spreads to get quantitative values for the depth, although the electrode separation need not be as large as for $\rho_2 > \rho_1$. When $\rho_2 < \rho_1$, there is no relation between ρ_a and z equivalent to Equation (8.56), as can be seen from Figures 8.21 and 8.27b.

The cumulative-ρ_a plot was formerly used to find depth of overburden and shallow resistivities. Although it has no sound theoretical basis, it works for soundings on thin beds but requires many constant increments of electrode spacing, which are small compared to bed thickness. The data are plotted by

summing successive ρ_a values for the ordinate, that is, if the readings were 100, 200, and 300 Ωm for spacings of 10, 20, and 30 m, one would plot 100, 300, and 600 Ωm versus 10, 20, and 30 m. An attempt is then made to find points where straight-line segments (drawn through as many points as possible) change slope, indicating depth to the interface.

8.7. FIELD EXAMPLES

In recent years most resistivity data related to mineral exploration are included in the results of IP surveys; the resistivity method is not much used as an independent technique in this application. It has, however, been employed to a considerable extent in ground water search and for engineering geology – preparation of dam sites, highway routes, building foundations, and so forth. Consequently the case histories and problems in this section include several examples not directly related to conventional prospecting. Further examples may be found in Chapter 9 of surveys where resistivity data were obtained in conjunction with IP data.

1. Apparent resistivity profiles obtained with a half-Schlumberger, or gradient, array traversing vertical contacts are shown in Figure 8.40. The two profiles correspond to different fixed locations of the current electrode C_1. The potential electrodes, which are close together compared to their separation from C_1, are moved together, whereas the second current electrode is effectively at infinity to the east. The contact with the low resistivity breccia is sharply defined in both profiles, which are quite similar to the theoretical result for the vertical contact shown in Figure 8.34b.

2. Resistivity data obtained in conjunction with an IP survey are shown in Figure 8.41. The area is the Cavendish Township test site, 100 miles northeast of Toronto. Unfortunately no detailed section is available for the subsurface.

The rocks are mainly metasedimentary with small areas of acidic and basic igneous types. The trend is northeast. Sulfides are present throughout the area, at least in trace amounts, and graphite occurs in a band of calcareous-siliceous rocks in the western part of the area.

Figure 8.41a shows apparent resistivities plotted in profile for four separations of the double-dipole electrode system (x = 200 ft, n = 1, 2, 3, 4) on line B; Figure 8.41b shows the usual pseudodepth plot employed in IP work (§9.5.1.) Clearly there is a low-resistivity zone, continuous at depth from 4W to 18W, which is capped by a higher-resistivity bowl near surface, located between 10W and 14W. A variety of EM surveys made on the Cavendish test site agree with the shallow resistivity profiles, because they outline two distinct zones trending NE, located at 8W and 15W.

3. The search for groundwater normally requires resistivity surveys, both for regional mapping and for sounding. Frequently these are combined with gravity and seismic refraction, the former during reconnaissance and the latter to aid in identifying saturated beds containing fresh or salt water and to resolve the equivalence ambiguity between z and ρ by unique determination of bed thickness.

This problem is well illustrated by a groundwater survey carried out in the central Sudan savannah belt near the White Nile (van Overmeeren, 1981). Figure 8.42 displays vertical electric sounding (VES) data from three locations west of the river and includes a schematic of two interpretations of the basement section, assuming either fresh or saline water. Both versions fit the sounding curves, although only VES 13 suggests fresh water. However, the results from seismic refraction plus data from a well drilled earlier in the vicinity favored the shallower basement depths associated with salt water as shown in Figure 8.42d.

4. Resistivity is an important component of multiple-method geophysical surveys for geothermal sources. Geothermal targets are of two types: the more common hot-water systems characteristically have high concentrations of chlorides and if the subsurface temperatures are ~ 180°C or higher they produce hot springs and deposit a sinter; the other type, vapor-dominated geothermals, is low in chlorides and rich in sulfate ions or alternatively in sodium bicarbonate.

The Mud Volcano area in Yellowstone Park, a typical vapor-dominated system, was surveyed in the late 1960s using IP, SP, resistivity lateral mapping, and resistivity soundings (Zohdy, Anderson, and Muffler, 1973). Three profiles of PFE (§9.3.3a), SP, and ρ_a are shown in Figure 8.43 together with a 6.7 km wide geoelectric section of the geothermal anomaly area. The profile line follows the Yellowstone River slightly SW of it. IP and resistivity profiles were carried out with a pole-dipole or half-Schlumberger array (Fig. 8.18) whose dimensions were $(a + b)/2$ = 1,000 ft (300 m). The SP electrode spacing was 400 ft (120 m).

The IP profile is not very significant except for a strong PFE response about 2,000 ft (600 m) wide at the NW boundary of the geothermal area. The high IP background is attributed to widely distributed clay with some pyrite, whereas the anomaly is probably caused by pyrite concentration at depth, because a second profile with spacing $AB/2$ = 600 ft (180 m) (not shown here) had a much reduced IP response in this vicinity.

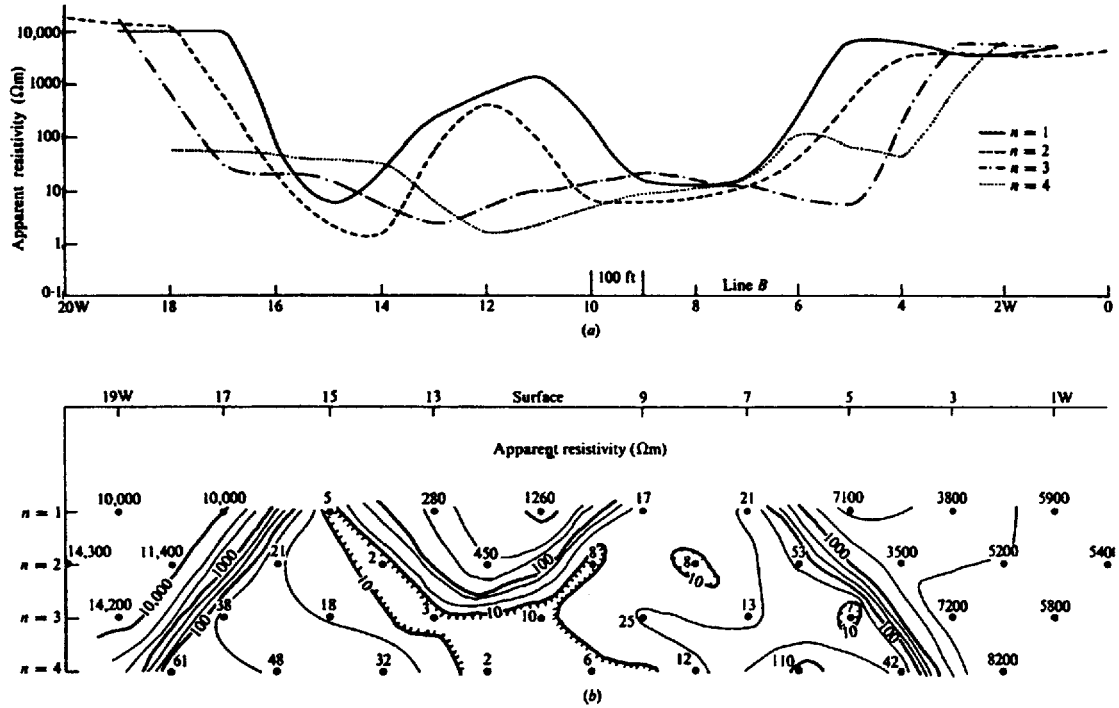

Figure 8.41. Resistivity results, Cavendish Township, Ontario. (a) Resistivity profile using a double-dipole array with n = 1, 2, 3, 4. (b) Pseudodepth plot using the data in (a).

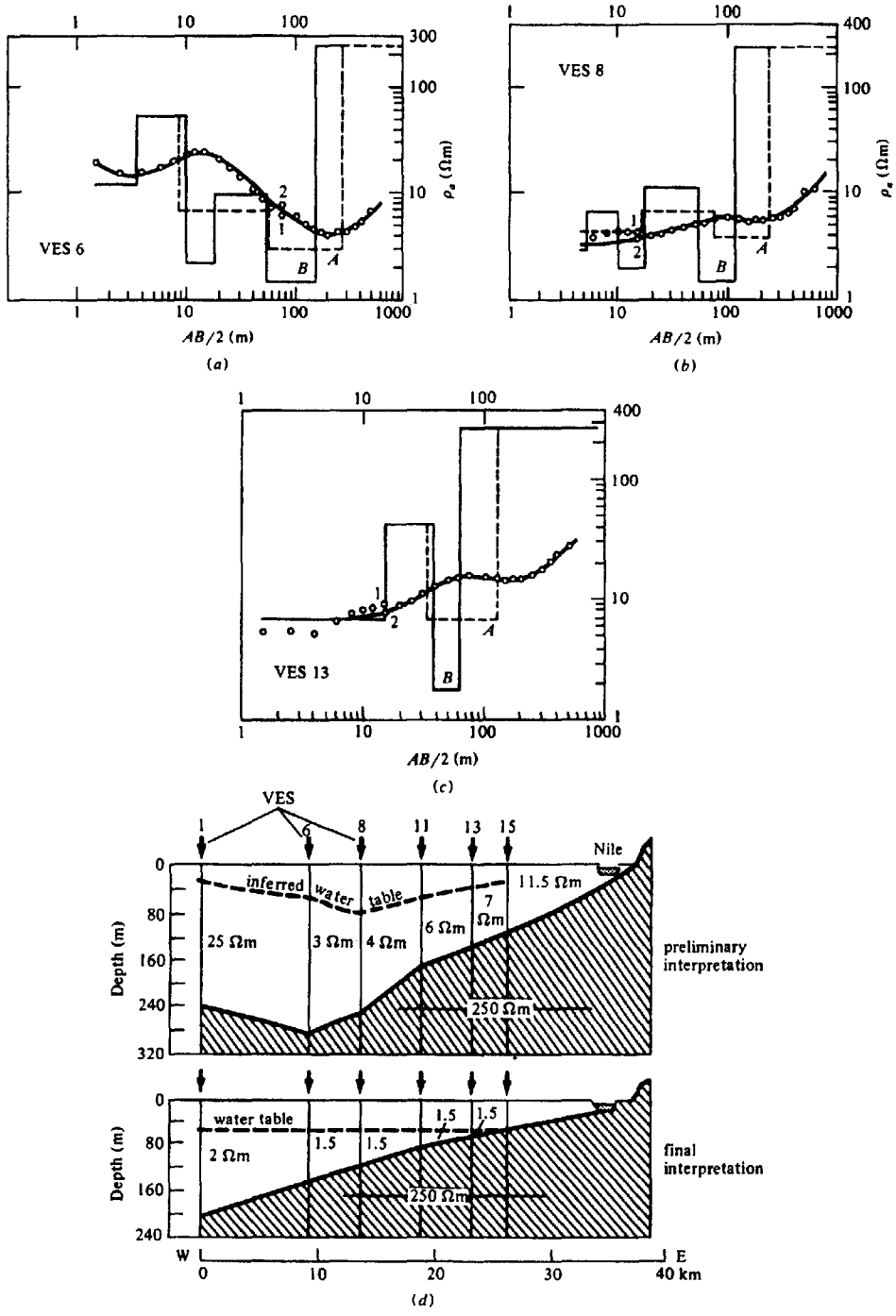

Figure 8.42. Results of vertical electric soundings, Sudan. (After van Overmeeren, 1981.) (a) Sounding VES 6 and two equivalent solutions, both for saline water. (b) Sounding VES 8 and two equivalent solutions. (c) Sounding VES 13 and equivalent solutions for fresh water (A) and saline water (B). (d) Preliminary and final interpretation.

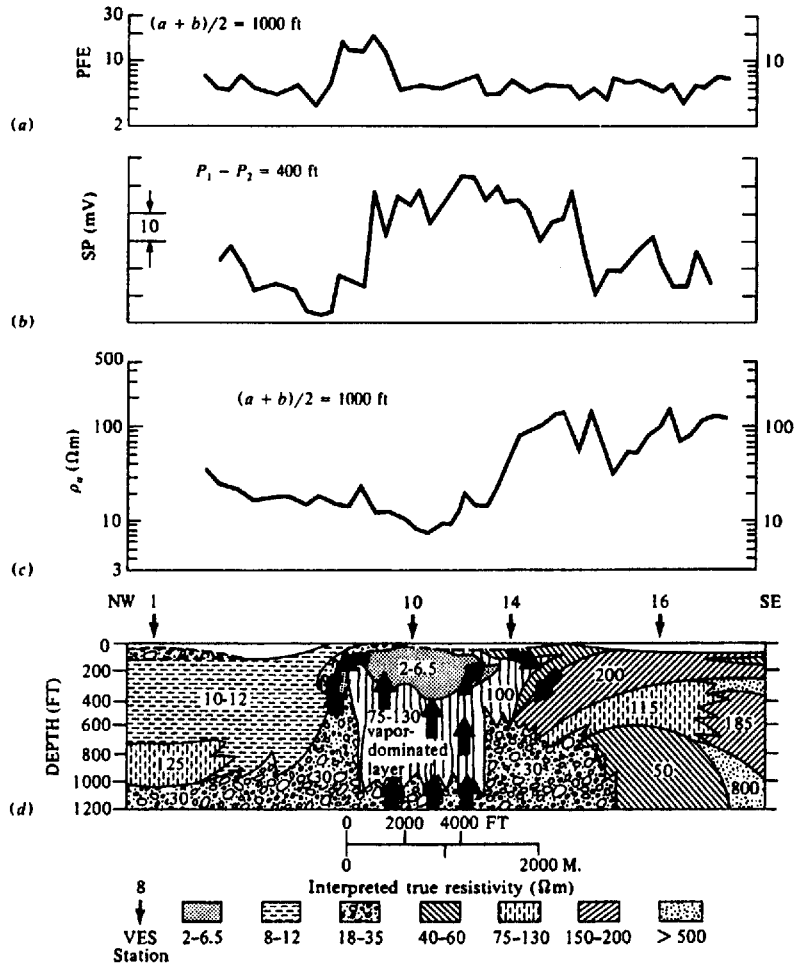

Figure 8.43. IP, SP, and resistivity profiles with geoelectric section, Mud Volcano, Yellowstone National Park geothermal zone. (After Zohdy, Anderson, and Muffler, 1973.)

There is a positive SP anomaly of − 60 mV straddling the target and persisting for some 2,500 ft (760 m) beyond on the SE side. This anomaly is probably due to streaming or electrokinetic potential (§5.2.1b, §6.1.1), but the SE segment is not explained. The resistivity profile outlines the geothermal area best with a well-defined low directly above.

The results of 16 vertical soundings were used to produce the geoelectric section in Figure 8.43. Soundings VES 1, 10, 14, and 16 (see Fig. 8.43d for locations) are displayed in Figure 8.44, with the layer resistivities and thicknesses plotted along the Schlumberger horizontal axes. Interpretation of the sounding curves was done by two methods, one with partial master-curve matching and auxiliary-point diagrams (VES 10, 14) and the other using an automatic technique for the complete curve (VES 16). Both interpretations are shown for VES 1, the first with a 6-bed model, the second with a 19-layer computer model.

5. It is worthwhile to summarize some rough rules for success in exploring for groundwater and geothermal sources:

(i) The most important is to assemble as much geological information as possible, with particular emphasis on any logs from old wells or drill holes in the area.
(ii) Next is to do the same for geochemical and geophysical data.

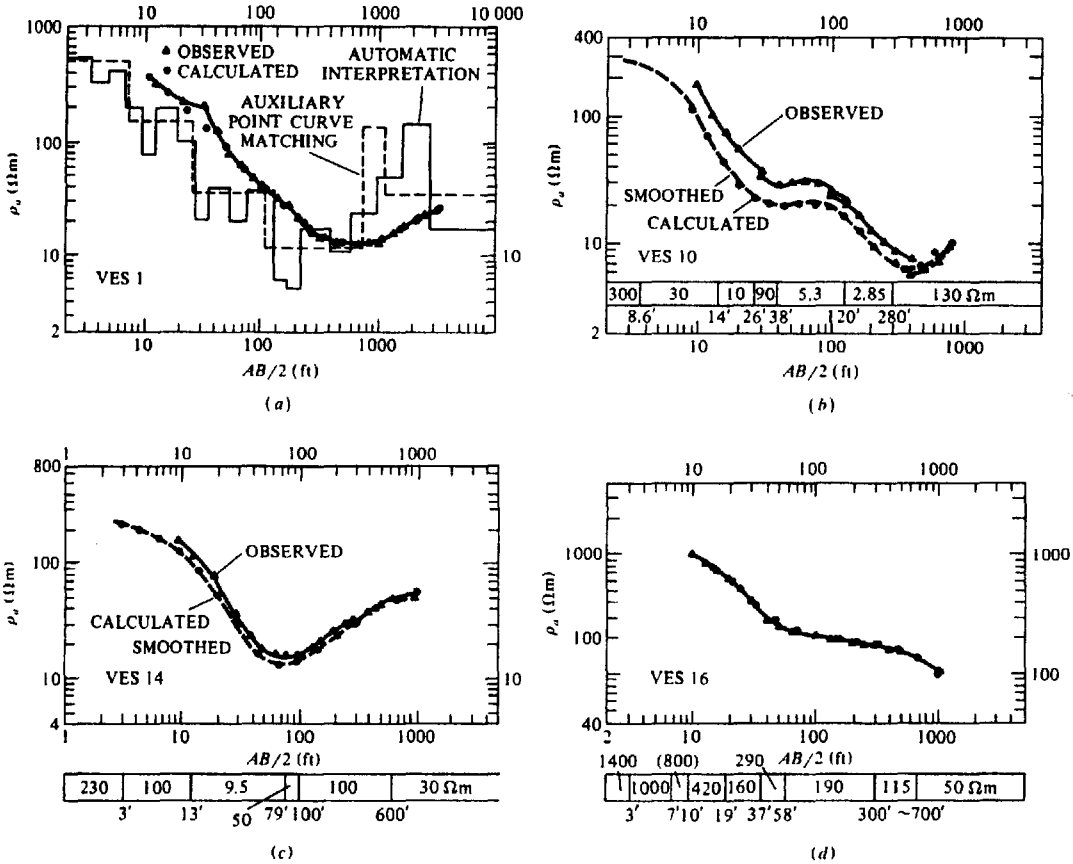

Figure 8.44. Soundings used to obtain geoelectric section in Figure 8.43. ▲ and ○ denote observed and calculated values. (Note the alternative plotting methods used in (a) and (b); see also Figs. 8.29 and 8.42.) (After Zhody, Anderson, and Muffler, 1973.) (a) VES 1 interpreted by partial curve matching (6-layer) and complete curve matching (19-layer). (b) VES 10, partial curve matching (7-layer). (c) VES 14, partial curve matching (6-layer). (d) VES 16, complete curve matching (9-layer).

Table 8.1. *Sounding data.*

Well	Min. ρ_a (Ωm)	Max. ρ_a (Ωm)	Av. ρ_a (Ωm)	Max/Min	Depth (m)	Yield (min.) (gal/min)
R161	55	120	80	2.2	2.5	Producer
R162	14	60	30	4.3	3	Producer
R102	25	60	39	2.4	30	10
R72	20	160	48	8.0	16	60
MH-10	60	100	89	1.7	10	25
Average	35	100	57	3.7	12	—
R163	35	100	57	2.9	30	Dry
R164	110	300	171	2.7	6	Dry
R166	110	210	172	1.9	25	Dry
Average	85	203	133	2.5	20	0

(iii) Survey procedures should be similar to those described in field examples 3 and 4.
(iv) On completion of resistivity profiling, it is desirable to select VES locations at resistivity lows taking into account (i) and (ii).
(v) The shape of the sounding curve is certainly significant. The low-grade data from groundwater surveys given in Table 8.1 serve as an illustration of this.

The data in Table 8.1 are from various locations in Sri Lanka, whose geology is a continuation of the South India Decca platform, mainly Paleozoic and Precambrian with younger coastline sediments. The data in the table are not representative because the ratio of dry-to-producing wells drilled over the past five years (mainly less than 50 m deep) is less than 10%. However, it seems clear from the above and from other groundwater results in West Africa that, for a successful well, the sounding curve should have a fairly well defined minimum at reasonable depth, although, if this minimum is less than a few ohm-meters, the chances are increased that any water will be saline.

Although the same remarks apply to geothermal exploration, the problem is more complex. Depth of exploration is usually greater than that necessary in groundwater search and more geophysical methods are required. The resolution of saline from fresh sources, however, is not a factor.

8.8. PROBLEMS

1. In an investigation to determine the depth of a conducting layer of brine at Malagash, Nova Scotia, the readings in Table 8.2 were taken with a Megger using an expanding Wenner spread. The surface layer was found to have a resistivity of 29 Ωm. Determine the depth and resistivity of the brine layer.

Table 8.2.

Separation (ft)	ρ_a (Ωm)
40	28.5
60	27.1
80	25.3
100	23.5
120	21.7
140	19.8
160	18.0
180	16.3
200	14.5
220	12.9
240	11.3
260	9.9
280	8.7
300	7.8
320	7.1
340	6.7
360	6.5
380	6.4

Table 8.3.

Electrode separation (ft)	Resistivity (Ωm)
5	78.1
10	56.0
15	49.8
20	47.1
25	46.0
30	51.2
35	59.8
40	76.0
45	79.8
50	72.2

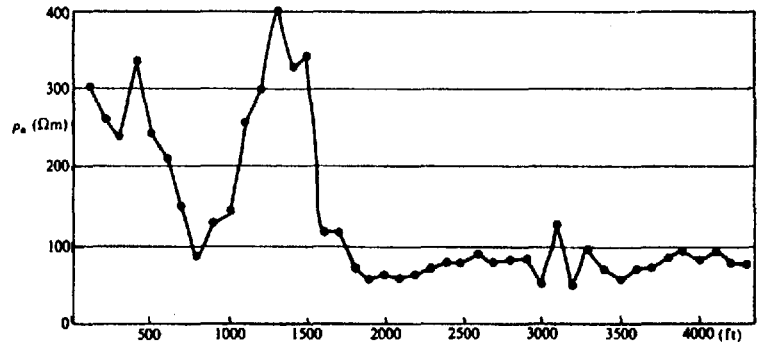

Figure 8.45. Resistivity mapping with Wenner spread over limestone and sandstone section separated by vertical contacts. Station interval 100 ft, a = 100 ft. (After Van Nostrand and Cook, 1966.)

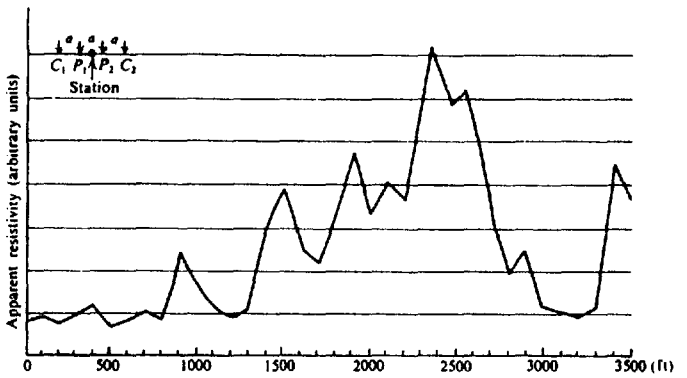

Figure 8.46. Resistivity mapping with Wenner spread over karst topography, Hardin County, Illinois. Station interval = 100 ft, a = 100 ft. (After Van Nostrand and Cook, 1966.)

Table 8.4.

	Line 10 + 00S		Line 0 + 00		Line 10 + 00N	
Station	$\rho_a(n=1)$ (Ωm)	$\rho_a(n=4)$ (Ωm)	$\rho_a(n=1)$ (Ωm)	$\rho_a(n=4)$ (Ωm)	$\rho_a(n=1)$ (Ωm)	$\rho_a(n=4)$ (Ωm)
26W	2,750					
25	2,000					
24	1,700					
23	1,850					
22	2,250	1,450				
21	2,000	700				
20	1,000	450	1,700		500	1,500
19	400	250	3,000		150	1,900
18	250	200	2,150	500	400	2,000
17	200	150	850	300	850	1,600
16	150	200	350	500	1,500	800
15	250	150	250	500	1,700	2,400
14	400	100	250	450	1,200	5,300
13	600	20	200	50	3,800	10,000
12	900	150	150	100	8,900	12,700
11	1,000	350	250	450	9,300	13,500
10	150	200	450	850	9,200	12,700
9	550	50	650	1,100	6,650	12,000
8	4,100	20	1,750	550	2,460	10,900
7	3,600	25	2,350	800	5,750	7,800
6	2,800	100	3,800	1,550	6,600	5,700
5	1,000	350	1,000	850	4,000	5,500
4		700	950	1,250	2,250	5,200
3			1,000	850	4,000	5,500
2			1,100	2,000	7,400	4,300
1			1,600	2,850	7,000	6,500
B.L.			3,200	2,350	6,600	6,800

2. In a resistivity survey performed for highway construction, the readings in Table 8.3 were obtained with an expanding Wenner spread. Plot ρ_a versus a. How many layers are indicated by this curve? Can you use the method of partial curve matching for multiple layers and if so, do the results agree with those obtained by the cumulative ρ plot and from the extrapolation described in Section 8.6.8? Find the depth of overburden by any or all of these methods.
3. Figure 8.45 shows a profile taken with a Wenner spread having a fixed spacing of 100 ft. Station intervals are 100 ft. The geologic section includes sandstone and limestone beds with practically

Table 8.5.

L (m)	ρ_a (Ωm)
1.5	160
2	96
3	70
4	54
6	40
8	33
10	27
12.5	20
15	20
20	22
25	23
30	27
40	30
50	38
60	48
80	67

vertical contacts. Locate these beds and speculate on the source of the small positive anomaly at 3,100 ft.

4. The profile of Figure 8.46 was obtained in exactly the same manner as that of problem 3; this is an area of karst topography in Hardin County, Illinois. The limestone contains numerous sinkholes and channels, most of which are filled with clay. There are occasional empty caverns as well. Make a rough interpretation of the near-surface section from the resistivity profile by locating the clay-filled sinks and/or caverns in the limestone host rock.
5. Apparent resistivities in ohm-meters are given in Table 8.4 for portions of three lines from an area in eastern Nova Scotia where an IP survey was carried out. The topography is generally flat except for the west portion (line 0 + 00 has an elevation change of +250 ft between stations 13 and 20, line 10 + 00N has a change of +100 ft between stations 15 and 20, line 10 + 00S has a change of +75 ft between stations 21 and 26). The rocks are known to be sedimentary in the valley whereas the hills in the vicinity are mainly granitic. Lines are 1,000 ft apart and stations 100 ft. The double-dipole spread (Fig. 9.8a) was used with dipole spacings of $x = 100$ ft; resistivities are given for $n = 1$ and 4 only, i.e., the distances between the inner electrodes were 100 and 400 ft, respectively. Plot these profiles and interpret the results.
6. The readings in Table 8.5 were obtained during a Schlumberger VES program for rural groundwater supply. $L = AB/2$ is half the current electrode spacing. Potential electrode spacing was

Table 8.6.

Stn.	Resistivity $\rho_a(10)$ (Ωm)	Resistivity $\rho_a(30)$ (Ωm)	EM16 Dip (%)	EM16 Quad. (%)
−4SW	—	—	−6	6
−3	—	—	−5	4
−2	135	—	−1	4
−1	—	—	+1	4
0	135	225	0	3
1NE	160	180	−3	1
2	177	220	−4	1
3	—	210	0	0
4	105	190	4	−1
5	—	172	5	−2
6	75	—	3	−2
7	80	150	2	−3
8	80	—	−1	−5
9	87	168	−2	−2
10	87	130	−2	−2
11	90	137	−10	−3
12	100	168	−19	−7
13	150	165	−26	−7
14	300	245	−27	−13
15	460	355	−13	−15
16	250	270	+3	−13
17	204	242	17	−10
18	103	190	24	−12
19	90	197	22	−17
20	60	178	27	−19
21	—	86	28	−17
22	30	68	13	−17
23	32	67	7	−14
24	33	102	3	−14
25	—	60	2	−12
26	30	47	1	−7
27	—	48	−3	−4
28	30	50	−4	+1

increased three times during the sounding: at $L = 8$, 20, and 30 m; the resultant discontinuities have been eliminated by smoothing at these points.

Analyze the sounding using partial and complete curve matching with auxiliary-point curves plus two- and three-bed master curves and by computer, whatever is available. Compare the results.

7. Although resistivity profiling has been carried out routinely for many years in groundwater exploration, it is a rather slow and expensive survey and the possibility of substituting a faster, cheaper technique is attractive.

The readings in Table 8.6 are from part of a Schlumberger profile done with two separations. The purpose was to locate an intrusive ledge of basement rock in a sedimentary section. At the same time a VLF profile was done with an

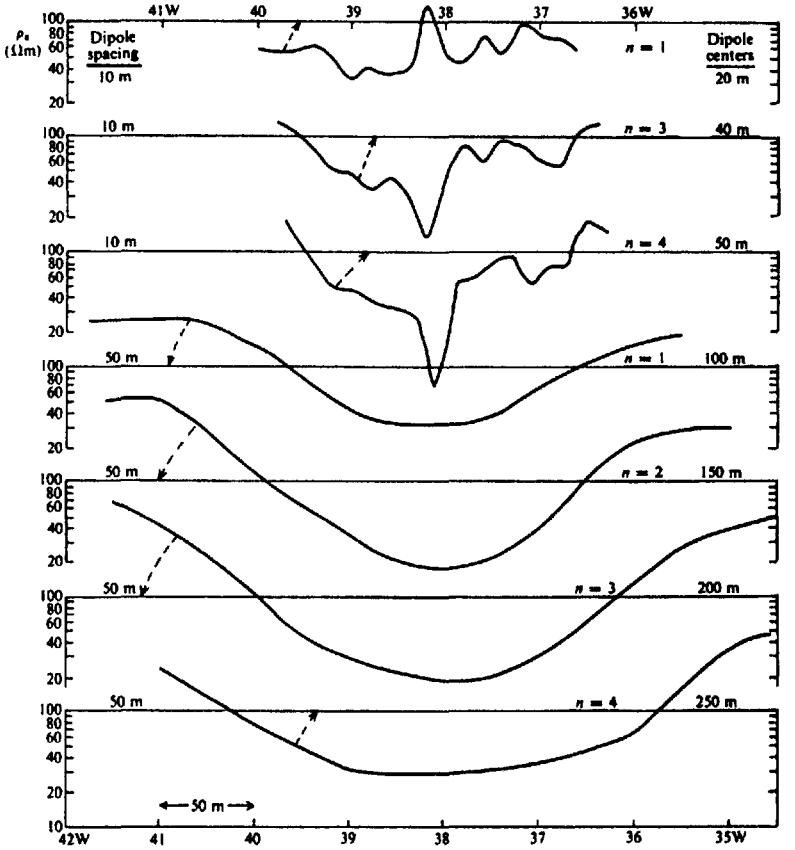

Figure 8.47. Apparent resistivities from IP survey, northeast Brazil.

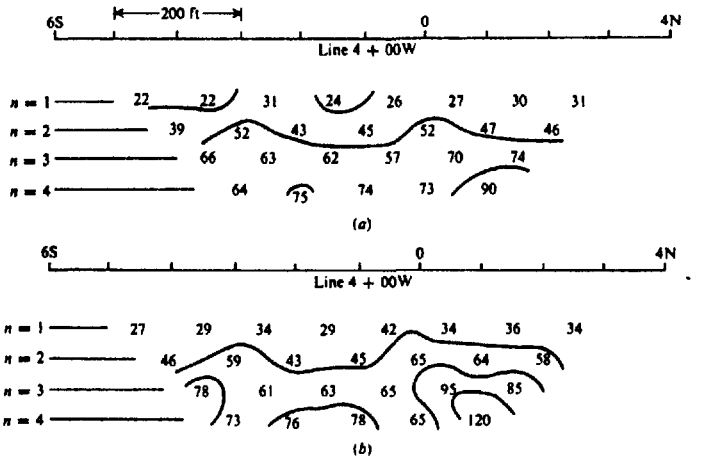

Figure 8.48. Apparent resistivities ($\rho_a/2\pi$ Ωft) from two IP surveys using a double-dipole array with separation 100 ft. (a) Data from frequency-domain IP. (b) Data from time-domain IP.

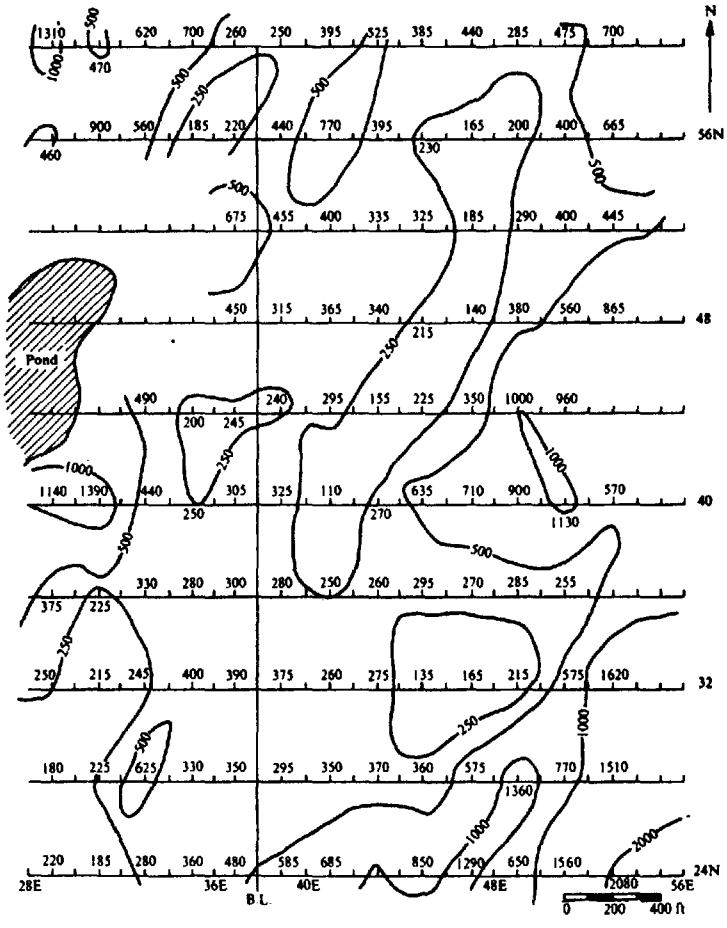

Figure 8.49. Apparent-resistivity contours (Ωft) for a base-metal zone, eastern Nova Scotia.

EM16 instrument (§7.4.2f; §7.8, examples 3, 4) which measured dip and quadrature associated with the secondary vertical EM field. These data are also given in Table 8.6.

Stations are 10 m apart. The resistivity columns are for Schlumberger spreads with $AB/2 = 10$ m, $MN/2 = 2$ m, and with $AB/2 = 30$ m, $MN/2 = 5$ m, respectively. Plot the resistivity and EM16 profiles on the same horizontal scales and compare them as to information derived and correlation.

Now plot the EM16 dip-angle data using the contouring relations given in Section 7.8, example 3. To maintain the proper polarity, the plotting is done from NE to SW (right to left with respect to the other profiles). Also the vertical scale should be chosen roughly the same length as the ρ_a scale to enhance the curve match. In considering the possible correlation between the profiles, why should it exist? Is there any physical relation between the numbered vertical scale for the EM16 and the ρ_a scale of the resistivity profile? Hence what is the fundamental difference remaining between the two types of survey with respect to acquired data? The EM16 survey extended an additional 300 m SW and was performed by one man in 40 min; the resistivity profile occupied four men for nearly 3 h.

8. The resistivity profiles shown in Figure 8.47 are taken from an IP survey. The double-dipole spread was used with two dipole spacings: $x = 10$ m for the top three profiles, 50 m for the remaining four. Distances between the dipole centers are noted on the right-hand column beside the profiles, corresponding to $n = 1, 3$, and 4 for $x = 10$ m, and $n = 1, 2, 3, 4$ for $x = 50$ m.

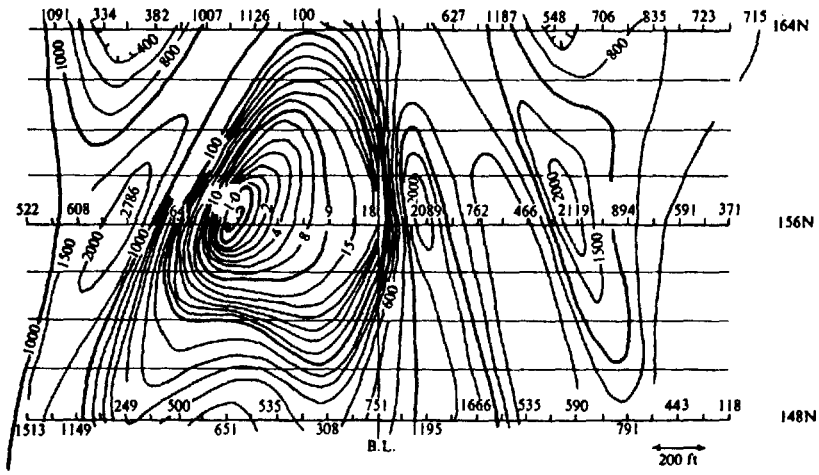

Figure 8.50. Apparent-resistivity contours (Ωm), southern New Brunswick.

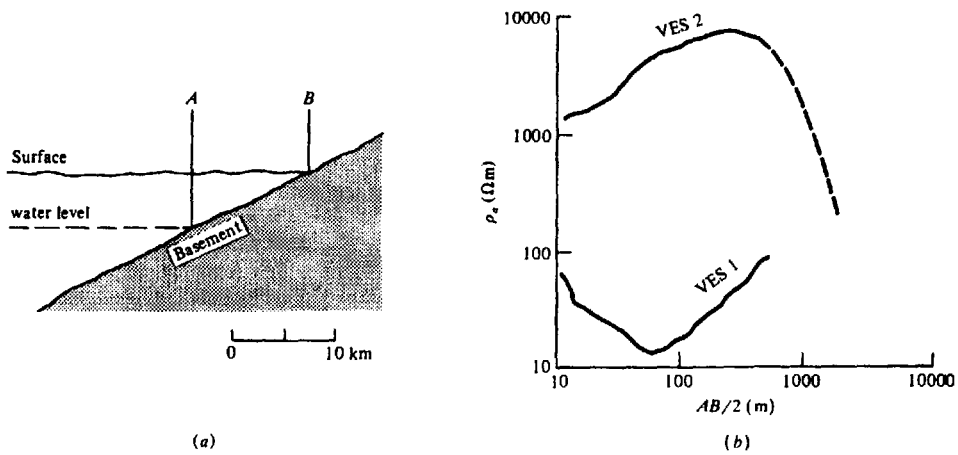

Figure 8.51. Example of "dry wedge" and related electric soundings for groundwater. (a) Vertical section. (b) Vertical sounding over the section.

Apparent resistivities are plotted on a log scale and vary from a maximum of about 700 Ωm (west end of profile for $x = 50$ m, $n = 3$) to a minimum of 7 Ωm (at 38W on the profile for $x = 10$ m, $n = 4$). The profiles represent successively larger depths of penetration from top to bottom of the figure. The overburden is considerably oxidized but is known to be thin, about 1–2 m. What interpretation can be made from these profiles? Would there be any advantage in plotting expanding spreads, that is, depth sounding profiles, for fixed station locations?

9. Two depth sections of apparent resistivity are shown in Figure 8.48 for an area in northern Quebec. Both employed the same double-dipole electrode system with $x = 100$ ft and $n = 1, 2, 3, 4$. One was done with a time-domain, the other with a frequency-domain, IP set. The traverse is in the vicinity of an old mining operation in which zinc, copper, lead, and some silver were recovered. Compare the results obtained by the two methods by plotting the profiles for $n = 1$ to 4. Can you explain the difference? Are there any obvious interesting features in these plots? The survey was done during winter because of swampy terrain.
10. Figure 8.49 shows apparent resistivity contours obtained from an IP survey in eastern Nova Scotia. The electrode arrangement was double-dipole with $x = 200$ ft and $n = 1$. The rocks in

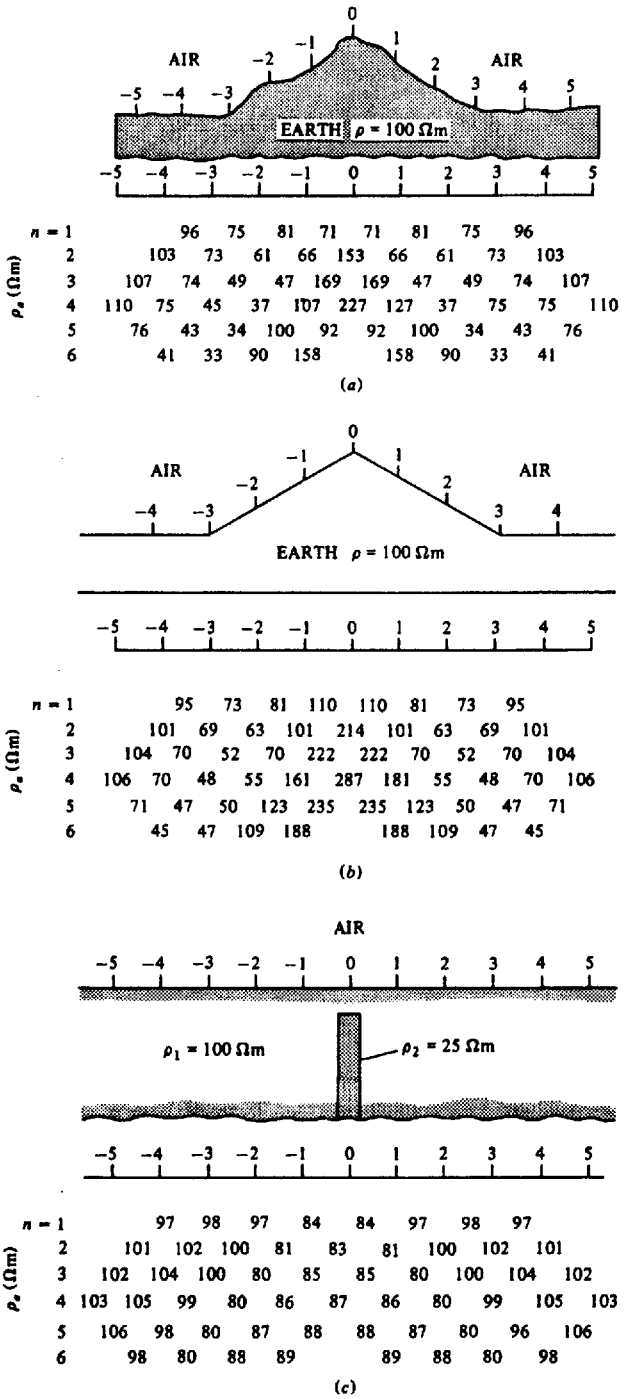

Figure 8.52. Effect of terrain on dipole-dipole resistivity survey. (a) Pseudodepth plot of ρ_a over 2-D ridge. (b) Model results for a 30° ridge. (c) Results over a buried vertical conductive dike.

the area are generally volcanics, although in the section shown there are no outcrops; the overburden is not expected to be anywhere more than 25 ft deep and usually is less than 15 ft. There is a large-scale geochemical anomaly (Cu, Pb, Zn) associated with the area. Drainage is to the south whereas the glaciation direction is approximately northeast. With these data make an interpretation of the zone.

11. The contours of apparent resistivity illustrated in Figure 8.50 were developed from an IP survey in southern New Brunswick. The predominant geological feature in this area is a stock-like basic intrustive of gabbro-norite in an anticlinal structure of metasediments – argillite, slate, quartzitic mica schist, and gneiss. Note that the only lines actually surveyed are 148, 156, and 164N. Would you consider this coverage sufficient to interpolate contours of this type? Take off profiles from lines 156N and 160N and make an interpretation.
12. A problem encountered occasionally in groundwater search over large basin regions is called the "dry wedge." This is an area located above a relatively shallow section of inclined basement. As the name indicates, a well that reaches the impermeable basement above the water level in overlying sediments will be dry.

    The section shown in Figure 8.51a is a schematic of this situation from a groundwater program in West Africa. The dry wedge is between *A* and *B*. The two soundings shown in Figure 8.51b were carried out in the area. Interpret the geologic section below each and determine roughly where they were located in Figure 8.51a. What prior information about the region would be necessary to eliminate this difficulty?
13. The apparent-resistivity pseudodepth plot displayed in Figure 8.52a is from a dipole-dipole survey over the surface section above it. This was a 2-D feature that approximated a 30° ridge. The survey crew was supplied with a set of model cards for terrain corrections, of which Figure 8.52b was the closest match.

    Correct the data for topography and replot them. Compare the results with the dike anomaly in Figure 8.52c. Discuss any obvious differences between your corrected plot and Figure 8.52c.

REFERENCES

Bewley, L. V. 1963. *Two-Dimensional Fields in Electrical Engineering*. New York: Dover.

Bhattacharya, P. K., and Patra, H. P. 1968. *Direct Current Electrical Sounding*. Amsterdam: Elsevier.

Bhattacharyya, B. B., and Sen, M. K. 1981. Depth of investigation of colinear electrode arrays over homogeneous anisotropic half-space in direct current methods. *Geophysics* 46, 768–80.

Coggon, J. H. 1971. Electromagnetic and electrical modeling by the finite element method. *Geophysics* 36, 132–55.

Compagnie Générale de Géophysique. 1955. Abaque de sondage électrique. *Geophys. Prosp.* 3, Supp. no. 3.

Dey, A., and Morrison, H. F. 1979. Resistivity modeling for arbitrarily shaped three-dimensional structures. *Geophysics* 44, 753–80.

Dobrin, M. 1960. *Introduction to Geophysical Prospecting*. New York: McGraw-Hill.

Fox, R. C., Hohmann, G. W., Killpack, T. J., and Rijo, L. 1980. Topographic effects in resistivity and induced polarization surveys. *Geophysics* 45, 75–93.

Ghosh, D. P. 1971. The application of linear filter theory to the direct interpretation of geoelectric resistivity sounding measurements. *Geophys. Prosp.* 19, 192–217.

Holcombe, H. T., and Jiracek, G. R. 1984. Three-dimensional terrain corrections in resistivity surveys. *Geophysics* 49, 439–52.

Hummel, J. N. 1932. A theoretical study of apparent resistivity in surface potential methods. *Trans. A.I.M.E. Geophys. Prosp.* 97, 392–422.

Inman, J. R., Ryu, J., and Ward, S. H. 1973. Resistivity inversion. *Geophysics* 38, 1088–1108.

Johansen, H. K. 1975. Interactive computer-graphic-display-terminal system for interpretation of resistivity soundings. *Geophys. Prosp.* 23, 449–58.

Johansen, H. K. 1977. A man/computer interpretation system for resistivity soundings over a horizontally stratified earth. *Geophys. Prosp.* 25, 667–91.

Keller, G. V., and Frischknecht, F. C. 1966. *Electrical Methods in Geophysical Prospecting*. London: Pergamon.

Kunetz, G. 1966. *Principles of Direct Current Resistivity Prospecting*. Berlin-Nikolasee: Gebruder Borntraeger.

Lee, T. 1975. An integral equation and its solution for some two- and three-dimensional problems in resistivity and induced polarization. *Geophys. Jour. Roy. Astron. Soc.* 42, 81–95.

Maillet, R. 1947. The fundamental equations of electrical prospecting. *Geophysics* 12, 529–56.

Orellana, E. 1963. Properties and drawing of the so-called Dar Zarrouk curves. *Geophysics* 28, 99–110.

Snyder, D. D. 1976. A method for modeling the resistivity and IP response of two-dimensional bodies. *Geophysics* 41, 997–1015.

Van Nostrand, R. G., and Cook, K. L. 1966. Interpretation of resistivity data. U.S.G.S. Prof. Paper No. 499.

van Overmeeren, R. A. 1981. A combination of electrical resistivity, seismic refraction, and gravity measurements for groundwater exploration in Sudan. *Geophysics* 46, 1304–13.

Zohdy, A. A. R. 1965. The auxiliary point method of electrical sounding interpretation and its relation to the Dar Zarrouk parameters. *Geophysics* 30, 644–60.

Zohdy, A. A. R. 1973. Automatic interpretation of resistivity sounding curves using modified Dar Zarrouk functions. U.S.G.S. Report USGS-GD-74-017, PB-232703.

Zohdy, A. A. R., Anderson, L. A., and Muffler, L. J. P. 1973. Resistivity, self-potential and induced polarization surveys of a vapor-dominated geothermal system. *Geophysics* 38, 1130–44.